Report Title: "Sulfur Tolerant Pd/Cu and Pd/Au Alloy Membranes for H_2 Separation with High Pressure CO_2 for Sequestration"

Type of Report: Final Scientific Technical Report

Reporting Period Start Date: 1 October 2004

Reporting Period End Date: 30 September 2008

Principal Author(s): Yi Hua Ma, Natalie Pomerantz (PhD candidate), Chao-Huang Chen (PhD candidate)

Date Report was Issued: January 2009

DOE Award Number: DE-FG26-04NT42194

Name and Address of Submitting Organization:
Worcester Polytechnic Institute
100 Institute Road
Worcester, MA 01609-2280

Name and Address of Significant Subcontractors/Sub-recipients:
Oak Ridge National Laboratory
Attn: E. Andrew Payzant
P.O. Box 2008
Oak Ridge, TN 37831

Disclaimer

Abstract

The effect of H_2S poisoning on Pd, Pd/Cu, and Pd/Au alloy composite membranes prepared by the electroless deposition method on porous Inconel supports was investigated to provide a fundamental understanding of the durability and preparation of sulfur tolerant membranes. X-ray photoelectron spectroscopy (XPS) studies showed that the exposure of pure Pd to 50 ppm H_2S/H_2 mixtures caused bulk sulfide formation at lower temperatures and surface sulfide formation at higher temperatures. Lower temperatures, longer exposure times, and higher H_2S concentrations resulted in a higher degree of sulfidation. In a Pd membrane, the bulk sulfide formation caused a drastic irrecoverable H_2 permeance decline and an irreparable loss in selectivity.

Pd/Cu and Pd/Au alloy membranes exhibited permeance declines due to surface sulfide formation upon exposure to 50 ppm H_2S/H_2 gas mixtures. However in contrast to the pure Pd membrane, the permeances of the Pd/Cu and Pd/Au alloy membranes were mostly recovered in pure H_2 and the selectivity of the Pd alloy layers remained essentially intact throughout the characterization in H_2, He and H_2S/H_2 mixtures which lasted several thousand hours. The amount of irreversible sulfur poisoning decreased with increasing temperature due to the exothermicity of H_2S adsorption. Longer exposure times increased the amount of irreversible poisoning of the Pd/Cu membrane but not the Pd/Au membrane.

Pd/Au coupon studies of the galvanic displacement method showed that higher Au^{3+} concentrations, lower pH values, higher bath temperatures and stirring the bath at a rate of 200 rpm yielded faster displacement rates, more uniform depositions, and a higher Au content within the layers. While 400ºC was found to be sufficient to form a Pd/Au alloy on the surface, high temperature X-ray diffraction (HTXRD) studies showed that even after annealing between 500 – 600ºC, the Pd/Cu alloys could have part or all of the surface in the less sulfur resistant β phase.

Table of Contents

Table of Figures

Table of Tables

Executive Summary

The interactions between H_2S and Pd and Pd alloys and characterization of the long-term stability of Pd and Pd alloy composite membranes in H_2, He and H_2S/H_2 mixtures were investigated. The tubular supports used for the permeation experiments consisted of 0.1 μm media grade Inconel (length: 6 cm, outer diameter: 1.25 cm, thickness: 0.16 cm) and the supports (coupons) used for the surface and phase analysis consisted of 0.5 μm media grade 316L porous stainless steel (PSS, 1 cm x 1 cm x 1 mm). The samples were oxidized for 12 hours between 700 - 800ºC to form an intermetallic diffusion barrier between the support and the membrane layer. The tubular supports were graded with an Al_2O_3 slurry and plated with a porous Pd/Ag intermetallic diffusion barrier. Pd was plated on the supports with the electroless deposition method followed by plating either Cu with the electroless deposition method or Au by the galvanic displacement method.

Pure Pd coupons were annealed in mixtures of approximately 50 ppm H_2S/H_2 for 2 - 96 hours between the temperatures of 350 - 500ºC. Annealing at lower temperatures resulted in bulk sulfide Pd_4S formation. The stresses released due to the change in the lattice structure and the lattice constant caused drastic changes in the morphology as well as the formation of numerous cracks and pinholes which would render a Pd membrane unusable. Lower annealing temperatures and longer periods of exposure time resulted in a higher degree of sulfidation and a thickening of the bulk sulfide layer. Increasing the concentration of H_2S to approximately 200 ppm resulted in a higher degree of sulfidation of Pd. At higher temperatures, the exposure of the Pd coupons to the 50 ppm H_2S/H_2 mixture resulted in sulfur adsorbing on the Pd surface and forming surface sulfide bonds with Pd. In addition, less sulfur chemisorbed with increasing temperature due to an increase in the rate of H_2S desorption and surface sulfides becoming less stable. A Pd composite membrane with no detectable leaks was tested at 400ºC in a 50 ppm H_2S/H_2 mixture. Upon the onset of the exposure to the mixture, the permeance of the membrane first had a sharp decline and then a more gradual decline. Pure H_2 was reintroduced but the H_2 permeance was not recovered, indicating that the poisoning of the pure Pd membrane was irreversible. Following the exposure to the 50 ppm H_2S/H_2 mixture, the

ideal H_2/He separation factor dropped from infinity to 3 due to the bulk sulfide scale which penetrated at least 5 μm deep into the Pd layer.

Pd/Cu composite membranes with a Cu gradient in the top layer were characterized in H_2 and He for several thousand hours between the temperatures of 250 - 500ºC. The membranes made with an oxide and an additional Pd/Ag intermetallic diffusion barrier had the most stability in H_2 permeance at 500ºC. Due to the Al_2O_3 grading of the support preventing the penetration of Pd into the support pores, the membrane fabricated with the Pd/Ag barrier had a permeance which was much higher than that of the membrane with only the oxide intermetallic diffusion barrier (18.0 and 10.8 $m^3/m^2*h*bar^{0.5}$ at 450ºC).

The Pd/Cu membranes were then tested for several thousand hours in H_2, He and 45 – 55 ppm H_2S/H_2 mixtures in the temperature range of 350 - 500ºC. Upon exposure to the H_2S/H_2 mixture at 500ºC, the Pd/Cu membranes lost approximately 80% of the hydrogen permeance due to the formation of surface sulfides and blocking H_2 adsorption sites, with the amount of permeance loss increasing with decreasing temperature. Reintroducing pure H_2 recovered part of the hydrogen permeance, showing that part of the H_2S poisoning was reversible. The amount of irreversible poisoning increased with increasing time of H_2S exposure and with decreasing temperature of exposure, due to the exothermic nature of H_2S adsorption. The He leak of the Pd/Cu membranes decreased following the poisoning experiments, possibly due to sulfur segregating to the grain boundaries of the Pd/Cu deposits.

Coupons were plated with Pd and Cu such that the total Cu concentration was in the Pd rich FCC phase of the Pd-Cu phase diagram. The coupons were annealed between the temperatures of 500 – 600ºC in pure H_2 and the phase transformations monitored with the XRD. After lengthy annealing times and high annealing temperatures, the less sulfur tolerant β phase was detected on the surface of the samples, indicating that even though EDS analysis detected a Cu concentration conducive to the Pd rich FCC phase on the Pd/Cu alloy membranes tested in this work, the membranes could have part or all of their surfaces in the β phase, decreasing the sulfur resistance.

A coupon study of the Au galvanic displacement plating method on electrolessly deposited Pd layers was conducted. The surface condition of the Pd layers was found to be important for the displacement reaction, and pre-immersion of the Pd layer in a HCl

solution prior to the displacement plating resulted in a larger amount of deposited Au. A higher concentration of HCl and longer immersion time resulted in a larger amount of deposited Au. Higher Au^{3+} concentrations, lower pH values, and higher bath temperatures yielded faster displacement rates and a higher Au content within the layers. Stirring the displacement bath was found to increase the uniformity of the Au deposit and improve the morphology of the Au layer. A stirring rate equal to or higher than 200 rpm was found to yield uniform Au deposits. An annealing study of Pd/Au bi-layers in H_2 atmospheres showed that the degree of Pd/Au inter-diffusion and the formation of the Pd/Au alloy phase depended on both temperature and time. An annealing temperature as low as 400ºC was found to be sufficient to form a Pd/Au alloy on the surface, but annealing temperatures above 500ºC were required to further homogenize the layer. However, annealing temperatures above 500ºC resulted in significant grain coarsening and pinhole formation in the deposit.

Two Pd/Au membranes of approximately 3 – 5 wt% Au and 5 – 8 wt% Au were characterized for 1000 and 500 hours respectively in the temperature range of 250 - 450ºC. The H_2 permeances calculated according to Sieverts' Law were between 50 – 100% higher than those of freestanding Pd films of the same thicknesses and the activation energies were lower than those of pure Pd films. The permeances of both membranes remained stable for the duration of the testing period but the ideal H_2/He separation factors of the 3 – 5 wt% Au and 5 – 8 wt% Au membranes decreased from 850 to 780 at 400ºC and from 790 to 330 at 450ºC respectively.

A Pd/Au membrane of approximately 10 wt% Au was characterized in H_2, He and approximately 50 ppm H_2S/H_2 between the temperatures of 350°C to 500°C. Upon exposure to the H_2S/H_2 mixture, the Pd/Au membrane exhibited a sharp permeance decline indicative of surface sulfide formation. The permeance was almost fully recovered in pure H_2, indicating that the poisoning was reversible. At higher temperatures, the percentage of recovered permeance in pure H_2 was higher but the percentage of permeance loss during the H_2S exposure was lower. A longer H_2S exposure time did not increase the permeance decline, but slowed down the permeance recovery rate. Also, the helium leak after the H_2S exposures did not increase significantly which resulted in an unaltered ideal H_2/He separation factor following the characterization

(exposure to) in the H_2S/H_2 mixture. The activation energy for hydrogen permeation after the H_2S exposure slightly increased indicating a slight change in the membrane properties.

Introduction

Hydrogen selective Pd membranes can improve the efficiency and cost effectiveness of the coal gasification process by recovering high purity hydrogen from the syngas. Also, the high pressure CO_2 in the retentate reduces the cost of carbon capture required for carbon sequestration by lessening the amount of energy required for the pressurizing stage [1]. Asymmetric composite Pd and Pd-alloy membranes deposited on porous metal supports are especially well-suited for industrial applications due to the strength and structural integrity of the metal supports and the simplicity of module construction. In addition, similar coefficients of thermal expansion between the Pd layer and the support ensure stability during temperature cycling. Electroless deposition is an advantageous method of depositing the Pd due to the hardness of the deposited film, the ease of scale-up, and the uniform deposition on complex shapes. The resultant hydrogen selective layer has good adhesion to the support and is thin, ensuring a high hydrogen permeance and low Pd cost.

However, the use of Pd membranes is not without disadvantages. Small quantities of H_2S present in the gas stream poison the Pd membrane and can drastically reduce the hydrogen permeance and cause irreparable damage to the membrane. At 350ºC, a concentration of 4 ppm H_2S/H_2 was sufficient to reduce the H_2 permeance of a Pd foil by 70% [2]. At 320ºC, a 20 ppm H_2S/H_2 mixture was sufficient to convert a Pd foil to a Pd_4S scale [3]. Pd_4S scale formation was shown to drastically reduce the selectivity of a Pd membrane due to the change in lattice parameter [4, 5], causing irreversible structural damage to the membrane.

Pd/Cu alloys have generated much research, not only because they are relatively inexpensive in comparison to other Pd alloys and do not exhibit hydrogen embrittlement even at room temperature [6], but also because Pd/Cu alloys are more resistant to H_2S poisoning than pure Pd when the Cu composition is in the FCC region of the Pd/Cu phase diagram (see Figure 1). In a transient test experiment, Morreale *et al.* [7] showed that FCC Pd/Cu alloy foils exhibited permeance declines varying between 0 – 10% when exposed to 1000 ppm H_2S/H_2 while BCC Pd/Cu alloys showed hydrogen permeance

declines of up to 99%. McKinley and Nitro [2] observed that BCC Pd/Cu foils had a 95% hydrogen permeance decline at 350ºC when exposed to 4 ppm H_2S/H_2. Mundschau *et al.* [3] saw that FCC Pd/Cu alloys only had a 20% permeance decline when exposed to 20 ppm H_2S. Kulprathipanja *et al*. [5] found an almost linear correlation at 450ºC, regardless of Cu content in the FCC phase, between the percent inhibition of H_2 permeation and H_2S feed concentration. They observed that Pd/Cu alloys had a 100% permeance decline at a feed concentration of 300 ppm H_2S/H_2 while Pd membranes exhibited a 100% permeance decline at 100 ppm H_2S/H_2. Clearly, the advantages of the FCC Pd/Cu alloy membranes over the BCC Pd/Cu alloy and the pure Pd membranes have been shown regarding H_2S tolerance.

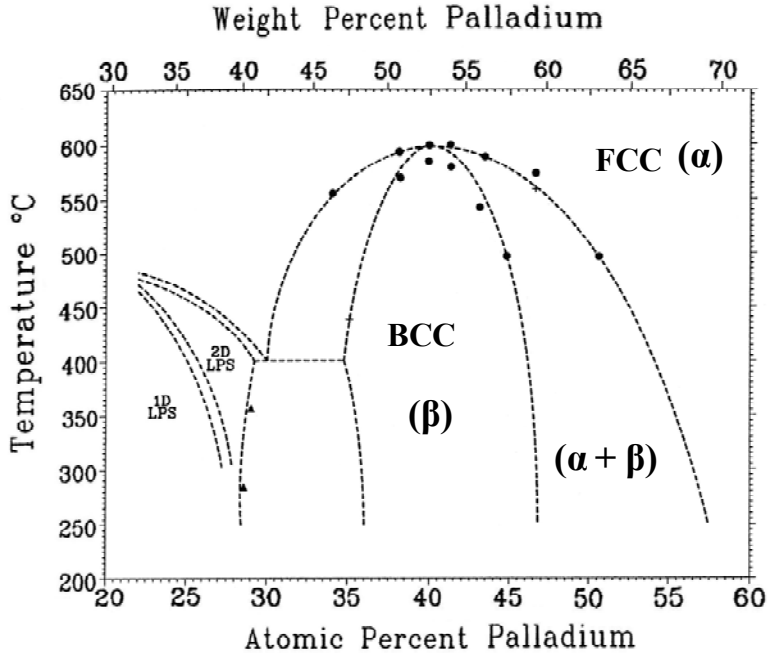

Figure 1. Pd-Cu phase diagram [8].

The disadvantage of FCC Pd/Cu membranes is their low permeance in comparison to Pd and other Pd alloys [9-11]. However, since H_2S poisoning happens on and near the surface of the membrane, an FCC alloy on the top layer of the Pd membrane would protect the surface of the membrane without greatly reducing the permeance. In addition, a thin top FCC layer would preclude the need to form a homogeneous alloy which, in the absence of a co-deposition bath, required temperatures as high as 600°C

[12] in order for the Pd and Cu layers to completely diffuse into each other during a short amount of time (12 hours).

Pd/Au alloys were considered to be one of the most suitable materials for fabricating hydrogen separation membranes due to its multi-beneficial characteristics. Firstly, Pd/Au alloy membranes showed higher H_2 permeability than pure Pd membranes [10, 11] due to their higher H_2 solubility [13]. Knapton [10] found that Pd/Au alloys showed 1.1 times higher hydrogen permeability than pure Pd within 5 – 20 wt% Au range at 350ºC. Others observed even higher H_2 permeance at other temperatures. Grayznov [11] reported that the Pd/Au alloy membranes with the same Au content range showed double the hydrogen permeance of pure Pd membranes at 500ºC. Secondly, Pd/Au alloys were found to show high chemical stability and sulfur resistance. McKinley and Nitro [2] reported that a $Pd_{60}Au_{40}$ alloy showed the best sulfur resistance compared to pure Pd and other alloys, such as $Pd_{73}Ag_{27}$ or $Pd_{60}Cu_{40}$ by observing a 10% H_2 flux decline in the presence of 4.5 ppm H_2S and a 56% H_2 flux decline in the presence of 20 ppm H_2S at 350^{o}C. Way *et al.* [14] also reported high sulfur resistance of Pd/Au alloy membranes with 5 wt% to 45 wt% Au content by observing a 38% H_2 permeance decline of the $Pd_{85}Au_{15}$ alloy membrane in the presence of 5 ppm H_2S at 400^{o}C. Although Au is higher cost compared to Cu or Ag, the higher H_2 permeability and better sulfur resistance of the Pd/Au membranes compensate for the slightly higher cost and make H_2 separation efficient and practical.

The main objective of this work was to fabricate composite Pd membranes with a thin top Pd/Cu layer with the electroless deposition method, and Pd/Au membranes with the galvanic displacement method, to investigate the performance of the Pd alloy membranes in H_2, He and ~50 ppm H_2S/H_2 at membrane operating temperatures, to study the regenerative properties of the membranes and to understand the poisoning mechanism with the goal of fabricating stable, sulfur tolerant membranes.

Experimental

Sample Preparation

The supports used in this study were provided by Mott Metallurgical, Inc. Coupons consisted of 316 L PSS (porous stainless steel) with a 0.5 μm media grade (dimensions: 1 cm x 1 cm x 0.1 cm). The tubular membrane supports consisted of a porous Inconel alloy with a 0.1 μm media grade (dimensions: length - 6 cm, outer diameter - 1.25 cm, thickness - 0.16 cm). All supports were cleaned to remove impurities with an alkaline solution. The cleaned supports were oxidized at either 700°C or 800°C for 12 hours in order to form an oxide intermetallic diffusion barrier [15] between the support metals and the H_2 selective Pd layer. In the case of membrane N_02, 0.5 μm of Ru was deposited as an intermetallic diffusion barrier due to its high Tamman temperature.

To block the larger pores of the support before plating the dense Pd layer, the support was attached to a vacuum and immersed in an Al_2O_3 slurry for 10 seconds. The slurry consisted of 1 g/l of Al_2O_3 with an average particle size of 1 μm, 0.05 g/l of Al_2O_3 with an average particle size of 0.2 – 0.5 μm and 0.5 ml/l of 1 M HCl. The support was dried at 140ºC for 12 hours. To seal the slurry within the pores of the support, the support was activated once under vacuum and plated with Pd for 10 minutes. A Pd/Ag barrier was deposited which further bridged the larger pores of the support and also functioned as an intermetallic diffusion barrier between the support metals and the hydrogen selective layer [16]. After activating the support 3 times, Pd was plated for 30 minutes, Ag for 60 minutes, Pd for 60 minutes, Ag for 60 minutes and Pd for 60 minutes. The resulting Pd/Ag barrier layer was lightly sanded with 1200 grit SiC paper and cleaned before plating the dense Pd layer. Further details on the Pd/Ag barrier layer fabrication can be found in Ma *et al.* [17]

The supports were sensitized and activated with Pd nuclei according to the procedure outlined previously [18]. Prior to plating, the activated supports were dipped in 1 M HCl for 30 seconds and then DI water. The plating bath compositions are listed in Table 1 and the plating procedure was detailed in Mardilovich *et al.* [18]. Following the

plating, the He permeance was measured and if the membrane had a He flow rate of less than 0.03 sccm at ΔP = 1 bar, the membrane was deemed dense and characterized, otherwise the membrane was re-plated with Pd. The Cu plating bath, shown in Table 1, was adapted from Ma *et al.* [19]. Cu was plated for 30 – 60 minutes, in accordance with the desired thickness. After electroless depositions of Cu, the membranes were immediately immersed in 0.01 M HCl to neutralize any residual plating solution followed by rinsing with DI water and ethanol to facilitate drying in order to prevent oxidation of the Cu layer.

To inhibit leak growth, the Pd layer of N_09 was annealed at 550ºC in He for 12 hours, mechanically treated with 600 grit SiC sandpaper, and then re-plated with Pd. The annealing/polishing/replating step was repeated and then Cu was plated.

Table 1. Plating bath compositions and conditions.

	Pd bath	Cu bath	Ag bath	Au bath
$Pd(NH_3)_4Cl_2 \cdot H_2O$ (g/l)	4			
$CuSO_4 \cdot 5H_2O$ (g/l)		25		
$AgNO_3$ (g/l)			0.519	
$NaAu(Cl)_4 \cdot 2H_2O$ (mM)				2 – 12
$Na_2EDTA \cdot 2H_2O$ (g/l)	40.1	47.5	40.1	
NH_4OH (28 %) (ml/l)	198		198	
H_2NNH_2 (1 M) (ml/l)	5.6		5.8	
H_2CO (37 %) (ml/l)		25		
EDA (ppm)		112		
$K_4Fe(CN)_6 \cdot 3H_2O$ (ppm)		35		
$(C_2H_5)_2NCS_2Na \cdot 3H_2O$ (ppm)		5		
pH	10 – 11	12.0	10 – 11	2 – 4
Temperature (°C)	60	25	60	25 – 60

Au plating was carried out with the galvanic displacement method [20,21], which was also considered as an electroless plating procedure [22]. The reaction for the plating of Au by the displacement of Pd can be described by the following:

$$2Au^{3+} + 3Pd^{0} = 2Au^{0} + 3Pd^{2+} \quad (1)$$

For the displacement reaction to take place spontaneously, a higher reduction potential (E_0) of Au complexing ions than that of Pd complexing ions in the plating bath is required. In the present study, a $NaAu(Cl)_4 \bullet 2H_2O$ solution was used for the displacement bath, and the reduction potentials of Au and Pd in the bath were as followed:

$$Au(Cl)^- + 3e^- = Au^0 + 4Cl^-, E_0 = 1.0v \quad (2)$$

$$Pd(Cl)^- + 2e^- = Pd^0 + 4Cl^-, E_0 = 0.62v \quad (3)$$

Several factors could affect the displacement plating reaction including the reduction potential between support and the desired metal, metal concentration, bath pH, bath temperature, and surface roughness of the support [20-22].

Membrane Permeation Testing

The experimental shell and tube set-up for testing the hydrogen permeance and selectivity during H_2S poisoning experiments is shown in Figure 2. The permeation set-up consisted of a Watlow ceramic tube furnace and a 316L SS shell casing. Hydrogen or helium flow to the membrane was controlled with a pressure regulator. A ballast volume of 500 ml was used to ease the transition between H_2 and He gases. The He sweep was a low pressure line on the tube side which prevented the membrane from oxidizing during start up/shut down conditions and flushed the permeate side of the membrane during the transition between H_2 to He atmospheres. The He sweep was not used during permeation experiments. The flow of the H_2S/H_2 mixture was regulated with a mass flow controller and the permeate and retentate flow rates were measured with digital mass flow meters. Pressure gauges were attached to the permeate and feed lines to measure the transmembrane pressure. Omega type K thermocouples monitored the temperature of the permeate flow inside the tube and the temperature between the shell casing and the furnace. The concentration of H_2S was measured with the SRI 8610C gas chromatograph

(GC) equipped with a flame photometric detector (FPD) with a measurement accuracy down to 200 ppb H_2S. The H_2S/H_2 mixtures were made by Airgas and had an analytical accuracy of ± 2 %.

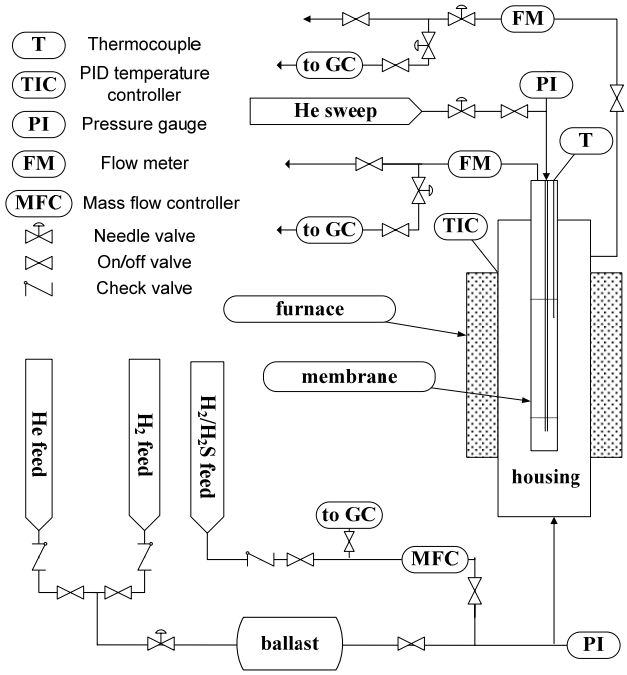

Figure 2. Schematic diagram of the apparatus used for membrane testing.

Sample Characterization

Sample characterizations were carried out with the Amray 1610 Turbo scanning electron microscope (SEM) equipped with a Princeton Gamma-Tech Avalon energy dispersive X-ray light element detector and a RBA-1610 5MC type Robinson retractable backscattered electron detector for qualitative and quantitative analysis. The spatial resolution for SEM-EDS (energy dispersive spectroscopy) lay between 0.8 – 1.2 μm and the penetration depth was about 1 μm for the samples investigated. The phase identification analysis of coupons was performed with a Rigaku Geigerflex X-Ray diffractometer (XRD) equipped with a CuK_α radiation source (λ=1.54 Å), and a curved crystal monochromator.

The near surface elemental analysis available at the Center of Materials Science and Engineering (CMSE) at the Massachusetts Institute of Technology (MIT) was performed with a Kratos AXIS Ultra X-ray Photoelectron Spectrometer (XPS) using a monochromatized aluminum source operated at 150 W, with an analysis area of approximately 300 x 700 μm and a maximum information depth of approximately 10 nm. The pass energy used for high energy resolution spectra was 20 eV. CasaXPS software [23], equipped with a Scofield-cross-section-based sensitivity factor library, was used for the peak-fitting and quantitative analysis. All spectra were calibrated using the adventitious carbon C 1s peak at 285.0 eV and a Shirley-type background was subtracted from the spectra.

High-temperature X-ray Diffraction (HTXRD) measurements were carried out at the High Temperature Materials Laboratory (HTML) at Oak Ridge National Laboratories (ORNL) with the PANalytical X'Pert Pro MPD using Cu Kα radiation. The samples were loaded into an Anton Paar XRK900 reaction chamber and annealed in pure H_2. The quantitative analysis carried out with the software X'Pert Highscore Plus. The weight fractions were calculated by the DCM method [24].

Results and Discussion

Pure Pd studies

Surface studies of poisoned Pd surfaces

In order to observe the Pd – H_2S interactions at membrane operating conditions and to assess the possible effects on membrane performance, a coupon study was performed to investigate the surface morphology, composition and crystal structure change after the H_2S exposure. Coupons were oxidized at 700 - 800ºC for 12 hours and plated with approximately 6 - 9 μm of Pd.

To assess the effect of the temperature of H_2S poisoning, the Pd samples were exposed to either a 54.8 ppm H_2S/H_2 mixture or pure H_2 for 24 hours for the temperature range of 350ºC to 500ºC. Figure 3a shows the EDS spectra of the annealed coupons. The top spectrum was taken from the Pd sample annealed at 350ºC in 54.8 ppm H_2S/H_2 and exhibited a very large sulfur presence with an S/Pd atomic ratio of 0.14. The corresponding XRD pattern in Figure 3b shows the presence of both Pd and the bulk sulfide Pd_4S. In contrast, the coupons annealed at 400, 450 and 500ºC in 54.8 ppm H_2S/H_2 had no detectable sulfur (bottom EDS spectrum in Figure 3a) and their XRD patterns were similar to the XRD patterns of the Pd coupons annealed in pure H_2 (Figure 3b).

Figure 4a shows the uniform granular morphology of the deposited Pd annealed in hydrogen. However, the Pd_4S scale formation (Figure 4b) caused a smooth coral-like structure to form on top of the Pd clusters of the coupon annealed at 350ºC in 54.8 ppm H_2S/H_2. While Pd has a FCC structure with a lattice parameter of 3.9 Å, Pd_4S has a tetragonal structure with the lattice constants of 5.1 Å and 5.6 Å. The lattice reordering due to the formation of the bulk Pd sulfide caused the drastic change in the morphology. Therefore, the bulk sulfide formation in a membrane would cause such irreparable damage to the selectivity that the membrane would only have Knudsen selectivity towards hydrogen [5].

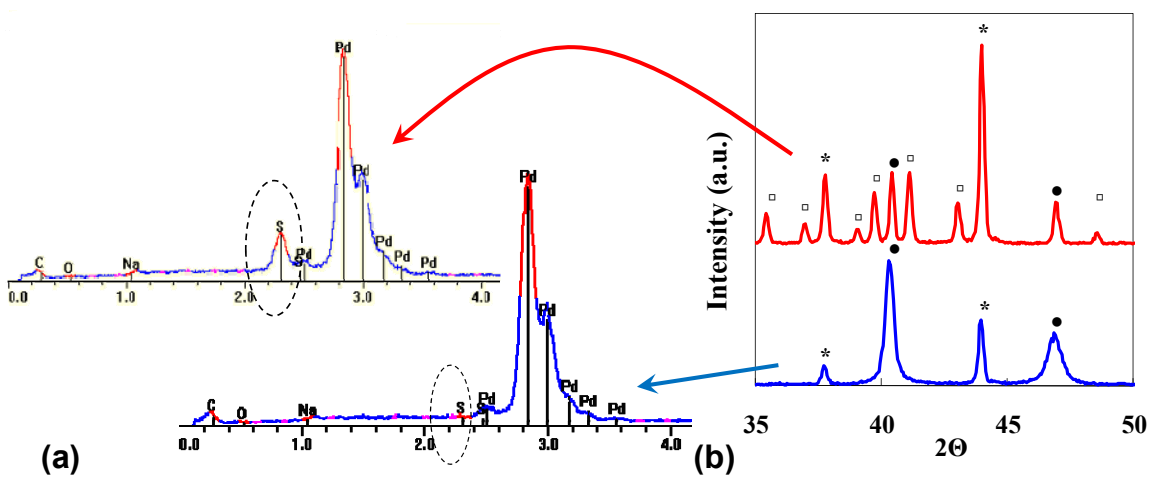

Figure 3. (a) EDS spectrum for the Pd coupon annealed at 350ºC in 54.8 ppm H_2S/H_2 (top) and for the remaining annealed Pd coupons (bottom). (b) Corresponding XRD patterns: (*) - Al sample holder, (●) - Pd, (▫) - Pd_4S.

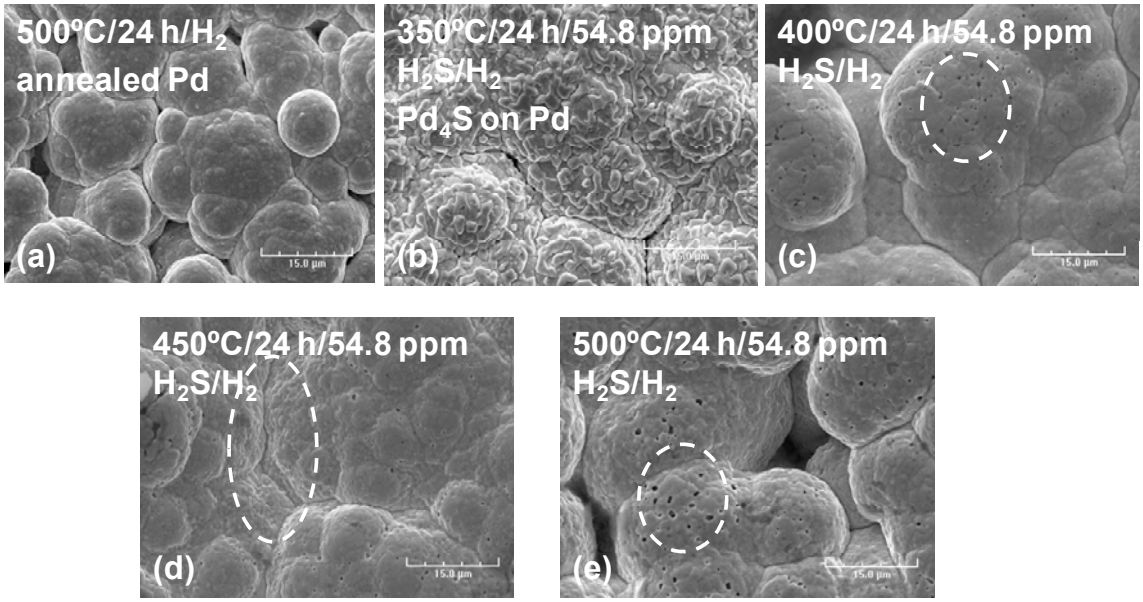

Figure 4. SEI micrographs of surfaces of the annealed Pd coupons.

While the coupon annealed at 350ºC showed a drastic change in the morphology, the Pd coupons annealed in 54.8 ppm H_2S/H_2 at 400, 450, and 500ºC had less extreme

changes in the morphology. Instead of a uniform granular morphology, the morphology of the annealed coupons was chunkier (circled in Figure 4d) and pores formed at the cluster boundaries (circled in Figure 4c and Figure 4e). Since neither EDS nor XRD could detect the presence of sulfur or a bulk palladium sulfide (Figure 3), it appeared that the formation of surface sulfides caused by the dissociative chemisorption of H_2S caused the change in the morphology and the pore formation. The pores and morphology change were both probably caused by the restructuring of the Pd surface atoms as they bonded with the sulfur. The performance of a Pd membrane with adsorbed sulfur would deteriorate due to a decrease in the permeance caused by the adsorbed sulfur preventing the H_2 adsorption, and a decrease in the selectivity caused by the pore formation.

To characterize the nature of the adsorbed sulfur on the Pd surface, XPS was used. Figure 5 shows the XPS survey spectra for the annealed samples. The top spectrum was for the Pd sample annealed at 500ºC for 24 hours in H_2. The spectrum exhibits the characteristic Pd peaks which are the most prominent, the Auger KLL peak for oxygen, a carbon 1s peak, and a nitrogen 1s peak. The latter three were most likely from the acetone and ethanol used to clean the samples prior to the XPS characterization. The spectra for the samples annealed at 500ºC (middle spectrum) and 350ºC (bottom spectrum) in 54.8 ppm H_2S/H_2 were similar to the spectra of the samples annealed in pure H_2 with the exception of the presence of the 2s and 2p sulfur peaks. The presence of the sulfur peaks showed that sulfur had indeed adsorbed on the Pd surfaces following the exposure to the H_2S/H_2 mixture. Similar results were seen with the Pd samples annealed at 400 and 450ºC in 54.8 ppm H_2S/H_2.

Figure 6 shows the high resolution XPS scans of the $3d_{5/2}$ and $3d_{3/2}$ Pd orbitals. The dotted lines show the placement and shape of the Pd peaks from the samples annealed in H_2. The Pd samples annealed in 54.8 ppm H_2S/H_2 at 400, 450 and 500ºC exhibited peaks which had maximums that had shifted to higher binding energies than the value of the Pd – Pd chemistry. Also, the peak shapes had broadened.

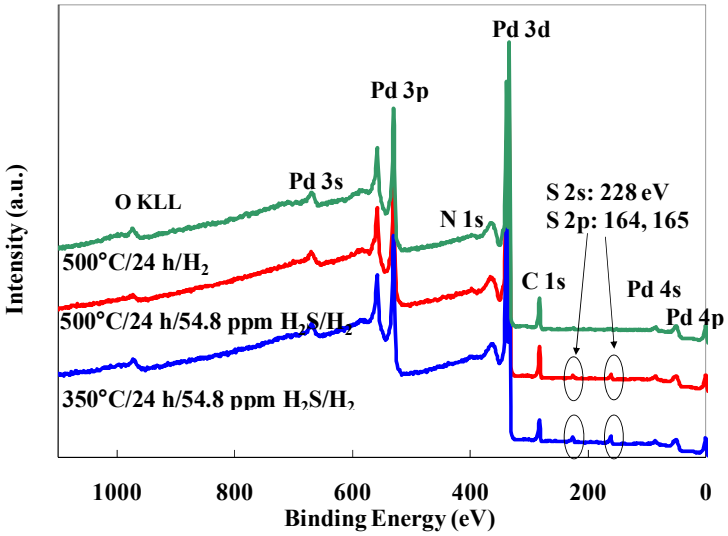

Figure 5. XPS survey spectra of the annealed Pd samples.

Peak broadening and shift of the peak maximum to higher binding energies than that of the Pd – Pd peak maximum (dotted lines) at 400, 450 and 500ºC showed that Pd – S bonds had formed on the surface, indicating that H_2S had undergone dissociative chemisorption and formed a surface sulfide with the Pd. Bulk sulfides had not formed as evidenced by the broad peaks between 400 - 500ºC that indicated the presence of the Pd – Pd chemistry near the surface as well as the Pd – S chemistry. However, at 350ºC the 3d Pd peaks were not as broad and the maximum was at the corresponding binding energy of the Pd – S peak maximum. The only chemistry detected at 350ºC was the Pd – S chemistry of the bulk Pd_4S, previously detected by XRD and EDS. The values of the Pd – Pd and Pd – S chemistries were confirmed with the literature [25-27].

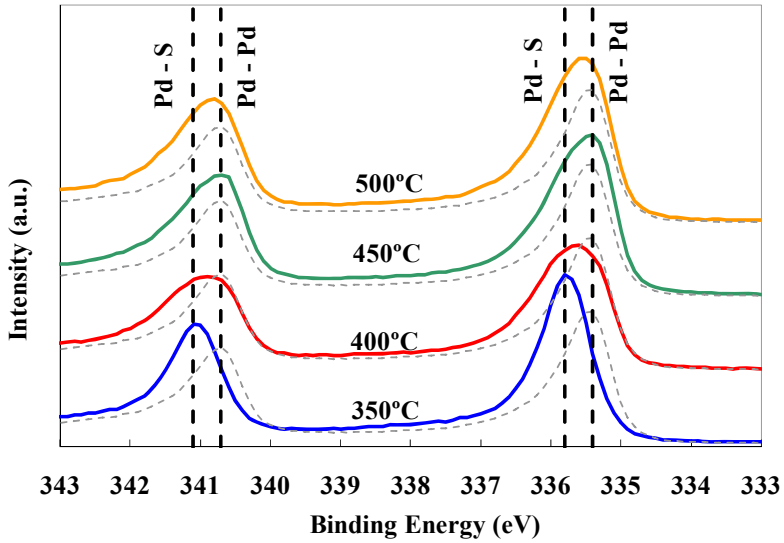

Figure 6. High resolution XPS scan of the $3d_{3/2}$ and $3d_{5/2}$ peaks. The solid and dotted lines correspond to the samples annealed in 54.8 ppm H_2S/H_2 and pure H_2, respectively.

The high resolution XPS scans were used to calculate the respective amounts of the Pd – Pd and Pd – S chemistries. Figure 7a shows the peak fitting of the sample annealed at 400ºC in 54.8 ppm H_2S/H_2. The standards used for the Pd – S and Pd – Pd chemistry shapes were from the samples annealed at 350ºC in 54.8 ppm H_2S/H_2 (shown in Figure 7b) and 500ºC in pure H_2 respectively. The areas of the two standards combined to give the measured signal from both Pd – Pd and Pd – S chemistries with the ratio of the peak areas equaling the ratio of each respective chemistry.

As can be seen in Figure 7a, there was a slight difference between the fitted curve and the measured data where the peaks had trails towards the higher binding energy values. The difference was due to the fact that the Pd – S peaks had trails which could not be fitted exactly. The effect on the quantitative analysis would be that the actual amount of the Pd – S chemistry in relation to the Pd – Pd chemistry would be slightly higher than what was calculated.

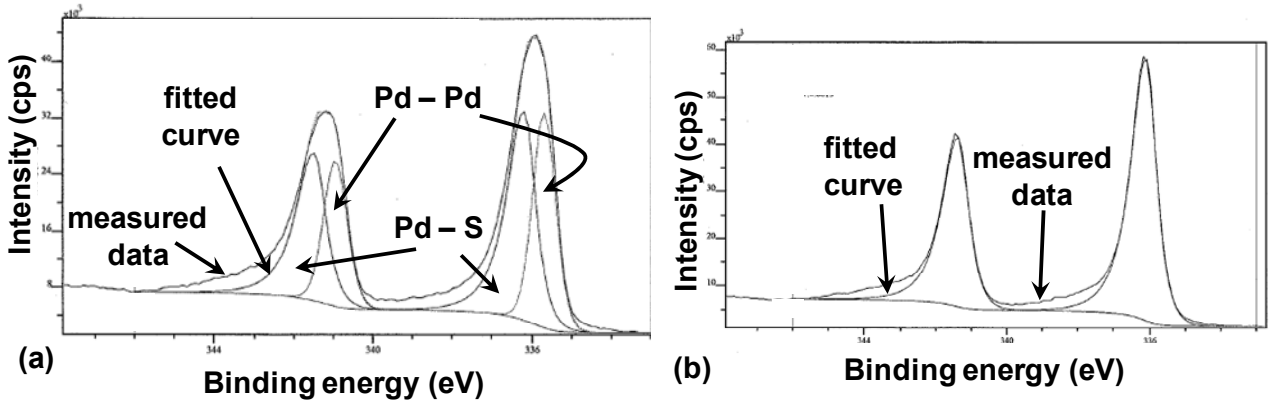

Figure 7. Peak fitting of the high resolution XPS data from the Pd coupons annealed at (a)400ºC in 54.8 ppm H_2S/H_2 for 24 hours and (b)350ºC in 54.8 ppm H_2S/H_2 for 24 hours.

The S/Pd atomic ratio was calculated from the survey scans of the Pd samples at each temperature (shown in Figure 5) and the amount of the Pd – S and Pd – Pd chemistries were calculated from the high-resolution scans (shown in Figure 6) of the Pd samples at each temperature. Figure 8 shows the amount of adsorbed sulfur on the Pd surface as a function of temperature. The S/Pd atomic ratio (y-axis on the left) was calculated from an average of three survey scans taken from different locations on each sample. The error bars corresponded to minimum and maximum values of the measurements which were averaged. The fraction of the Pd – S chemistry is shown on the y-axis on the right.

As can be seen, both the amount of sulfur adsorbed and consequently, the amount of sulfur which bonded with Pd, increased with decreasing temperature. Sulfur adsorption is an exothermic reaction and higher temperatures would cause less sulfur to adsorb [28]. A similar trend was seen with bulk Pd sulfides in previous works [29, 30] indicating that bulk sulfides would only form at lower temperatures. Indeed, at 350ºC, the S/Pd atomic ratio was close to 0.25, which corresponded to the atomic ratio of Pd_4S. At 400, 450 and 500ºC, only surface sulfides formed from the dissociative chemisorption of H_2S.

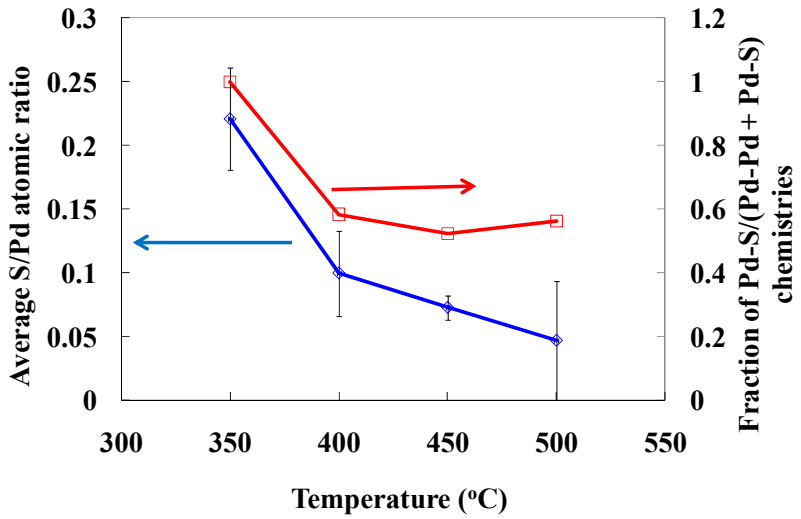

Figure 8. Dependence of the amount of adsorbed sulfur on temperature.

Further work needs to be completed with XPS on the Pd/Cu and Pd/Au systems, however, the importance of the XPS studies on pure Pd can not be discounted since prior research has shown that the presence of H_2S caused Pd atoms to migrate to the top atomic layer of Pd/Cu alloys due to the greater stability of adsorbed sulfur on pure Pd [31]. The effect of recovery in pure H_2 on Pd/Cu and Pd/Au alloys will also be investigated with XPS to better understand the recovery mechanism.

Another set of experiments to test the effect of temperature on H_2S poisoning of pure Pd samples was conducted, and the resultant XRD patterns are shown in Figure 9. The XRD pattern of the Pd coupon before the H_2S exposure (as shown in Figure 9(a)) showed the peaks at 2θ of 40.35°, 47.05°, 68.55°, and 82.5° representing the FCC phase in the planes of (1 1 1), (2 0 0), (2 2 0) and (3 1 1), while those after the H_2S exposure at the temperatures of 350°C to 450°C (as shown in Figure 9(b), (c), and (d)) showed that numerous new peaks appeared along with the Pd peaks. These new peaks were identified as the tetragonal Pd_4S phase.

The formation of the Pd_4S phase indicated that the chemical reaction (sulfidation) between Pd and H_2S occurred during the H_2S exposure and the adsorbed sulfur diffused into the Pd layer forming a bulk sulfide. In addition, the intensity of the Pd_4S peaks decreased as the exposure temperature was increased and became negligible at 500°C, indicating that the sulfidation was temperature dependent. The lesser degree of Pd

sulfidation at higher temperatures resulted from the fact that the formation of Pd_4S was less favorable at higher temperatures according to the Gibb's free energy expression for Pd_4S formation proposed by Niwa [32], which predicted that a higher H_2S concentration was required to form Pd_4S at higher temperatures.

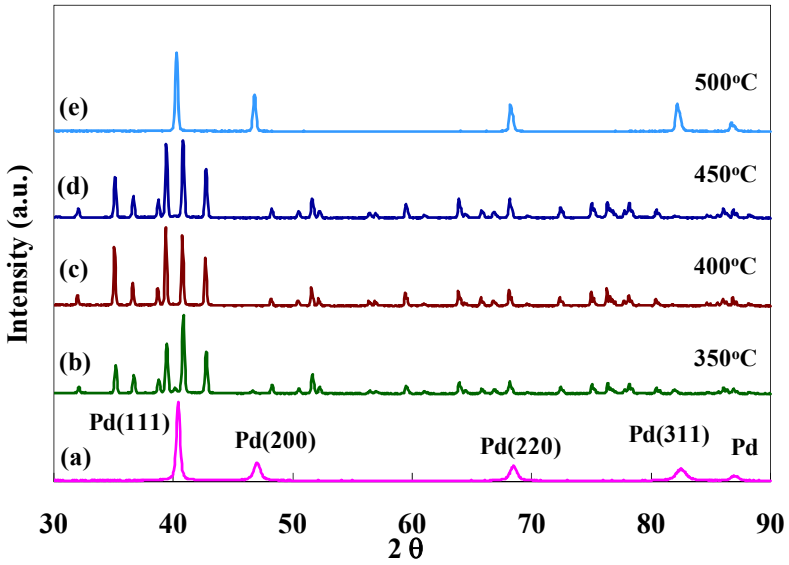

Figure 9. XRD patterns of pure Pd that was (a) as-deposited, (b) exposed to a 54.8 ppm H_2S/H_2 gas mixture for 24 h at 350°C, (c) at 400°C, (d) at 450°C, and (e) at 500°C.

Figure 10 shows the corresponding SEM micrographs of the Pd coupons before and after exposure to the H_2S at different temperatures. The H_2S exposure caused significant morphology changes including numerous pinholes (pores). The formation of pinholes was considered to be the result of the incorporation of sulfur into the Pd lattice, causing stress in the Pd lattice. In addition, the large differences in lattice structure and lattice constant between the pure Pd and Pd_4S phases previously discussed also accounted for the huge stress in the Pd lattice. Several researchers have observed a similar phenomenon. Oudar [33] observed the rupture of iron, nickel and their alloys after exposure to sulfur compounds and described the phenomenon as embrittlement caused by the segregation of adsorbed sulfur on the internal surfaces (such as grain boundaries). Mundschau *et al.* [3] observed a similar surface morphology with numerous pinholes in

pure Pd membrane after exposure to a 20 ppm H_2S/H_2 mixture at 320°C for over 120 hours.

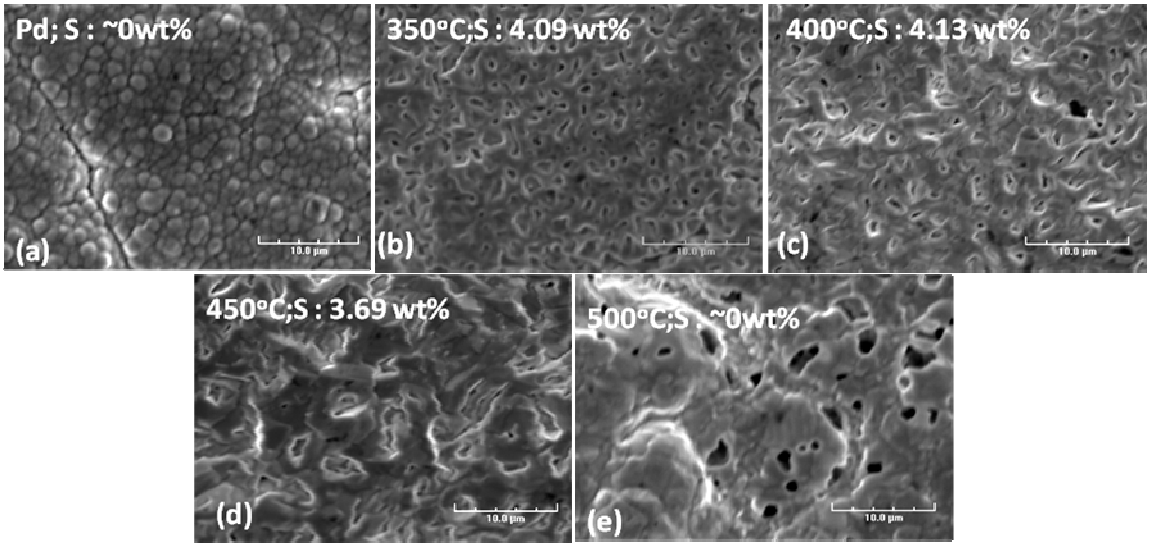

Figure 10. SEM micrographs (3 kX) of Pd that was (a) as-deposited, (b) exposed to a 54.8 ppm H_2S/H_2 gas mixture for 24 h at 350°C, (c) at 400°C, (d) at 450°C, and (e) at 500°C.

As seen in Figure 10, the number of pinholes decreased as the temperature was increased which also indicated that sulfidation decreased at higher temperatures. From the EDS analysis, sulfur content was detected (about 4 wt%) and the S/Pd atomic ratio was about 0.14 on the samples that were exposed to H_2S at 350°C to 450°C, while no sulfur was detected on the sample that was exposed to H_2S at 500°C. The lower S/Pd atomic ratio observed with the EDS than the atomic ratio of Pd_4S (S/Pd = 0.25) was because the pure Pd layer underneath the Pd_4S scale was also detected by the EDS resulting in a lower S/Pd atomic ratio. Furthermore, the negligible sulfur content on the sample exposed at 500°C might have resulted from the fact that the amount of sulfur was under the detection limit of the EDS since the morphology change suggested a certain degree of sulfidation.

A difference was observed in the conditions required for bulk sulfide formation and the actual Pd_4S morphology when comparing the results of the two sets of experiments which tested the effect of temperature. While the results from the first set

only yielded bulk sulfide formation at 350°C, the results from the second set yielded bulk sulfide formation until 450°C. The reason for the discrepancy might be from a temperature gradient in the furnace which depending on the sample placement, might have resulted in inaccurate annealing temperatures. Moreover, failing to flush out the furnace properly with inert gas before reducing the temperature would result in residual H_2S still exposed to the samples below the desired annealing temperature. Also, contaminants in the plating solution could have changed the properties of the Pd layers and caused the two different sets of results. Further confirmation is required to see which set of experiments is more accurate. Nevertheless, the two sets of experiments show that higher temperatures resulted in less sulfidation.

Figure 11 and Figure 12 are the XRD patterns and SEM micrographs of the pure Pd coupons after exposure to 54.8 ppm H_2S/H_2 for different periods of time. The intensity of the Pd peaks in the XRD patterns (as shown in Figure 11) decreased as the H_2S exposure time increased, while that of Pd_4S peaks increased as the exposure time increased. The exposure time of 2 hours showed no Pd_4S peaks in the XRD pattern, while the 24 hours exposure time resulted in the disappearance of the Pd peaks, indicating that the sulfidation of Pd and the formation of Pd_4S increased as the exposure time increased and that the amount of Pd_4S formed was a function of the amount of sulfur adsorbed.

Corresponding SEM pictures showed the morphology changes as the exposure time was increased. The 2 hours exposure (as shown in Figure 12(a)) showed a similar morphology to that of the as-deposited Pd except for the larger grain size due to the grain coarsening at elevated temperatures. No sulfur was detected by EDS. As the exposure time was increased to more than 4 hours (as shown in Figure 12(b), (c), (d), and (e)), the deformation of the surface morphology with droplet-shaped grains was observed and finally numerous pinholes were observed after 24 hours exposure. Although the sulfur content detected by EDS was roughly the same for the samples that were exposed to H_2S from 4 to 24 hours, the progression of the morphology change still implied that the degree of sulfidation increased with time.

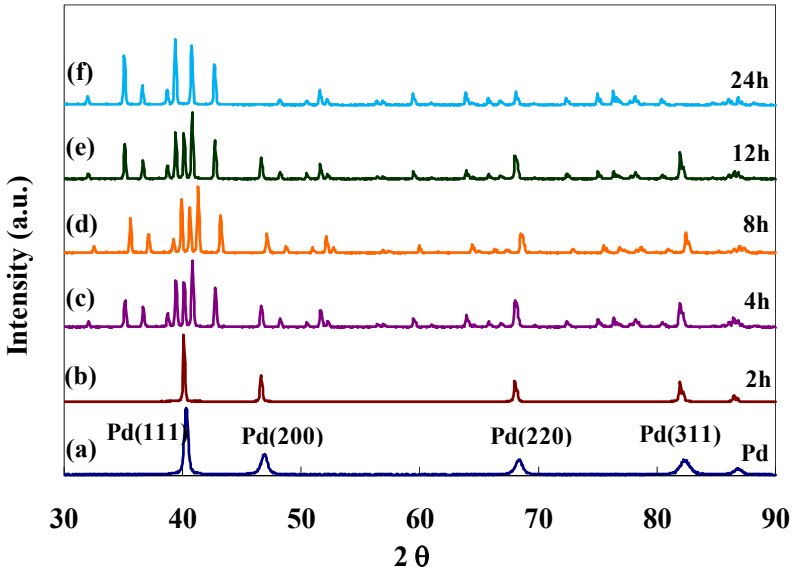

Figure 11. XRD patterns of pure Pd that was (a) as-deposited, (b) exposed to a 54.8 ppm H_2S/H_2 gas mixture at 400°C for 2 hours, (c) for 4 hours, (d) for 8 hours, (e) for 12 hours, and (f) for 24 hours.

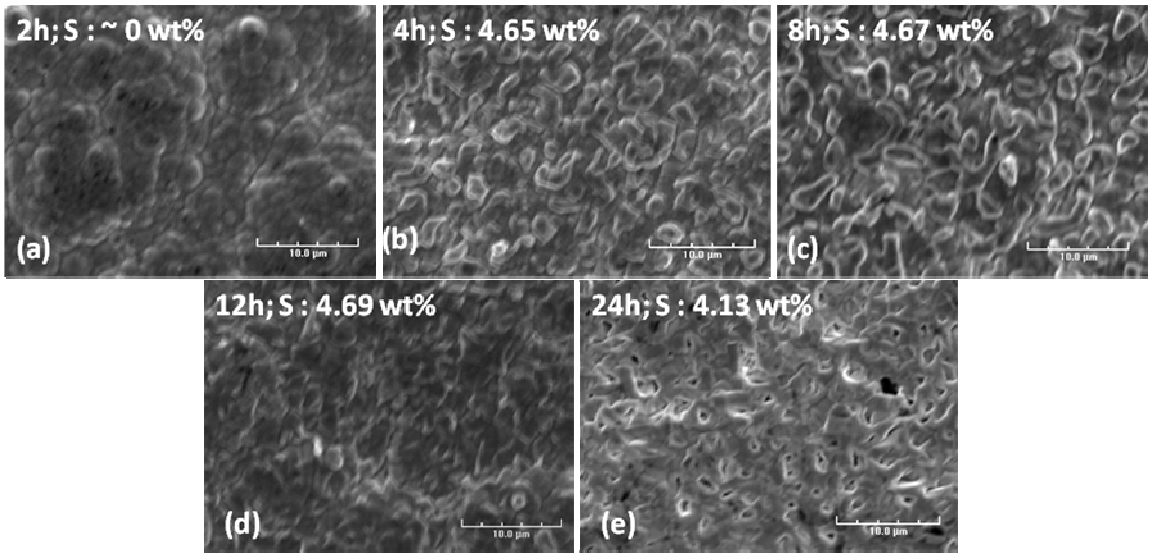

Figure 12. SEM micrographs (3 kX) of pure Pd that was (a) exposed to a 54.8 ppm H_2S/H_2 gas mixture at 400°C for 2 hours, (b) for 4 hours, (c) for 8 hours, (d) for 12 hours, and (e) for 24 hours.

Figure 13 and Figure 14 are the X-ray diffraction patterns and SEM micrographs of the pure Pd coupons after exposure to H_2S/H_2 mixtures of higher concentrations. The Pd coupons were exposed to 54.8 ppm and 213 ppm H_2S/H_2 at 350°C for 24 hours. The intensity of Pd peaks in the XRD patterns (as shown in Figure 13) decreased as the H_2S concentration increased, while the intensity of the Pd_4S peaks increased as the concentration increased. Corresponding SEM micrographs with EDS analyses showed that larger pores formed and slightly more sulfur was present on the sample exposed to the 213 ppm H_2S/H_2 mixture, showing the higher degree of sulfidation. The results suggested that the degree of sulfidation depended on the H_2S concentration. Kulprathipanja *et al.* [5] have also reported that the degree of sulfur poisoning was dependent on H_2S concentration with the Pd/Cu alloy membranes exposed to 100 to 1000 ppm H_2S/H_2 gas mixtures.

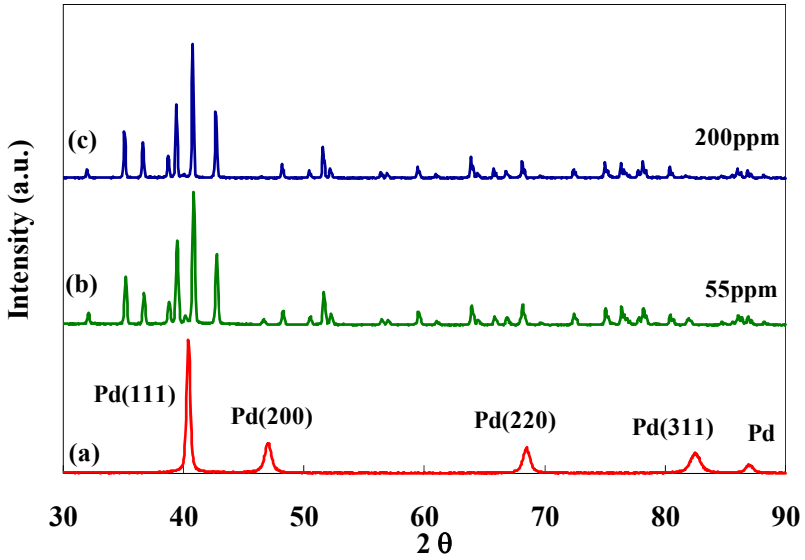

Figure 13. XRD patterns of pure Pd that was (a) as-deposited, (b) exposed to a 54.8 ppm H_2S/H_2 gas mixture, and (c) exposed to a 213 ppm H_2S/H_2 gas mixture at 350°C for 24 hours.

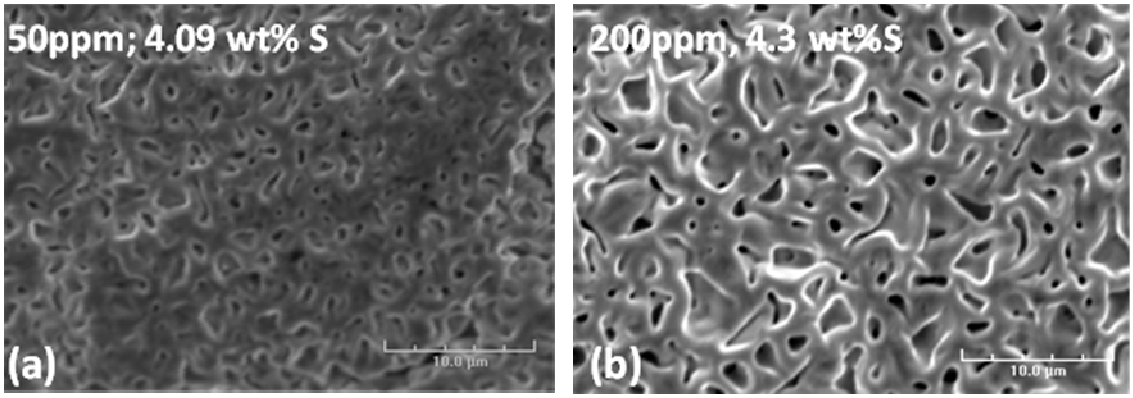

Figure 14. SEM micrographs (3 kX) of pure Pd that was (a) exposed to a 54.8 ppm H_2S/H_2 gas mixture and (b) exposed to a 213 ppm H_2S/H_2 gas mixture at 350°C for 24 hours.

Pure Pd membrane testing in H_2S

The pure Pd membrane, C_06, was prepared by oxidizing the support, grading the support with an alumina slurry, depositing a porous Pd/Ag barrier and then a dense Pd layer. The resultant thickness was 13.8 μm. C_06 was then characterized for its gas permeation characteristics in pure H_2 and He for 120 hours prior to the H_2S characterization and showed a stable permeance of 12.5 $m^3/(m^2*h*atm^{0.5})$ at 250°C, 19.7 $m^3/(m^2*h*atm^{0.5})$ at 350°C, 24.0 $m^3/(m^2*h*atm^{0.5})$ at 400°C, and 28.3 $m^3/(m^2*h*atm^{0.5})$ at 450°C. These values were close to those of free-standing pure Pd foils. The activation energy for the H_2 permeation of C_06 was estimated to be 11.7 kJ/mol and the ideal H_2/He separation factor was infinite after 120 hours of characterization at the elevated temperatures.

C_06 was then characterized for sulfur tolerance by switching the gas feed to a 54.8 ppm H_2S/H_2 gas mixture at 400°C. The resultant H_2 permeance history before and after the H_2S exposure is shown in Figure 15. The permeance dropped instantaneously after the introduction of the 54.8 ppm H_2S/H_2 mixture at 400°C (the period after the first dashed line shown in Figure 15), and continued to decline for over 24 hours before the permeance reached a steady state value. The two stages of permeance decline indicated two possible poisoning mechanisms, the instantaneous permeance drop at the beginning

might have resulted from the sulfur adsorption and the blocking of the sites for hydrogen dissociation which was a rapid process, while the slow and long decline of the permeance afterwards could have resulted from the continuous reaction between the Pd and the adsorbed sulfur to form a bulk sulfide which was a long process. Similarly, Mundschau *et al.* [3] also observed two stages of H_2 permeance decline on a pure Pd membrane upon exposure to a 20 ppm H_2S/H_2 mixture at 320°C for over 120 hours. Furthermore, when pure H_2 was re-introduced (the period after the second dashed line shown in Figure 15), the H_2 permeance remained at the same value, showing no recovery, indicating that an irreversible reaction occurred between Pd and H_2S during the H_2S exposure. In addition, the He leak after the H_2S exposure was more than 10 ml/min, resulting in a decrease in the infinite ideal H_2/He separation factor to 3.

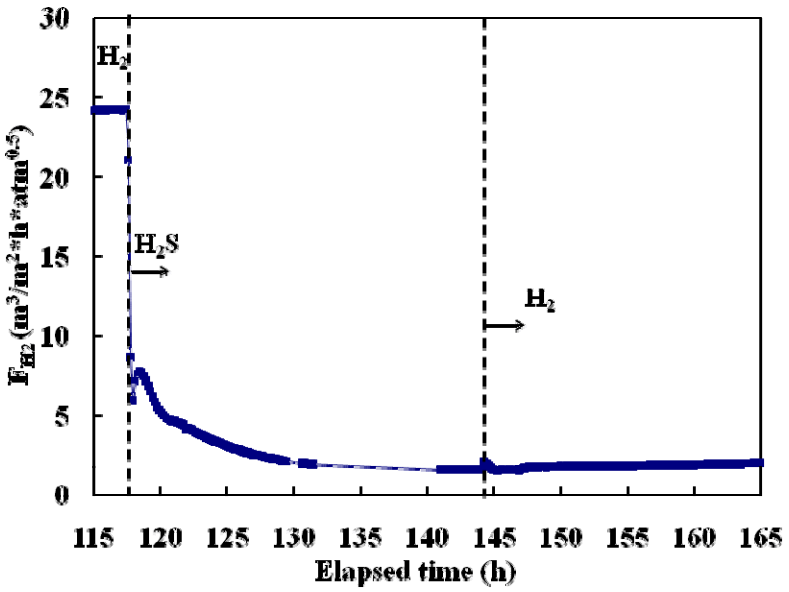

Figure 15. Effect of H_2S on H_2 permeance at 400°C of C_06.

The surface and cross sectional SEM micrographs of C_06 after the H_2S exposure provided the evidence of deterioration of the Pd structure, shown in Figure 16. Pinholes were observed on the surface SEM micrographs shown in Figure 16(a) and the morphology was similar to the result of the coupon study of the H_2S exposure at 400oC shown in Figure 10(c). The S/Pd atomic ratio determined by EDS was also about 0.14, which was very close to the result from the coupon study described earlier. The cross

sectional SEM micrograph shown in Figure 16(b) also showed several pores in the Pd layer near the surface and the EDS line scan shown in Figure 16(c) showed an average of 3 wt% S from the surface to 5 μm below (the inset in Figure 16(c)), indicating that the adsorbed sulfur diffused into the Pd layer (up to 5 μm in depth) forming Pd sulfide and caused pore formation in the Pd layer. The carbon composition was not shown in the line scan in order to eliminate the interference from the carbon signal. Several researchers have also observed ruptures and failures of Pd membranes after exposure to H_2S. Mundschau et al. [3] observed a similar surface morphology with numerous pinholes in a pure Pd membrane after the exposure to a 20 ppm H_2S at 320^oC for over 120 hours. Edlund and Pledger [34] observed the rupture of a Pd composite membrane ($Pd/SiO_2/V$) after testing in the 1.5% H_2S/H_2 mixture at 700^oC. Kajiwara et al. [4] observed cracks in Pd membranes after exposing a Pd/porous alumina composite membrane to a 6200 ppm H_2S/H_2 at 400ºC. Kulprathipanja et al. [5] found numerous pores on the pure Pd membranes after exposure to a 115 ppm H_2S/H_2 mixture at 500^oC for 20 hours.

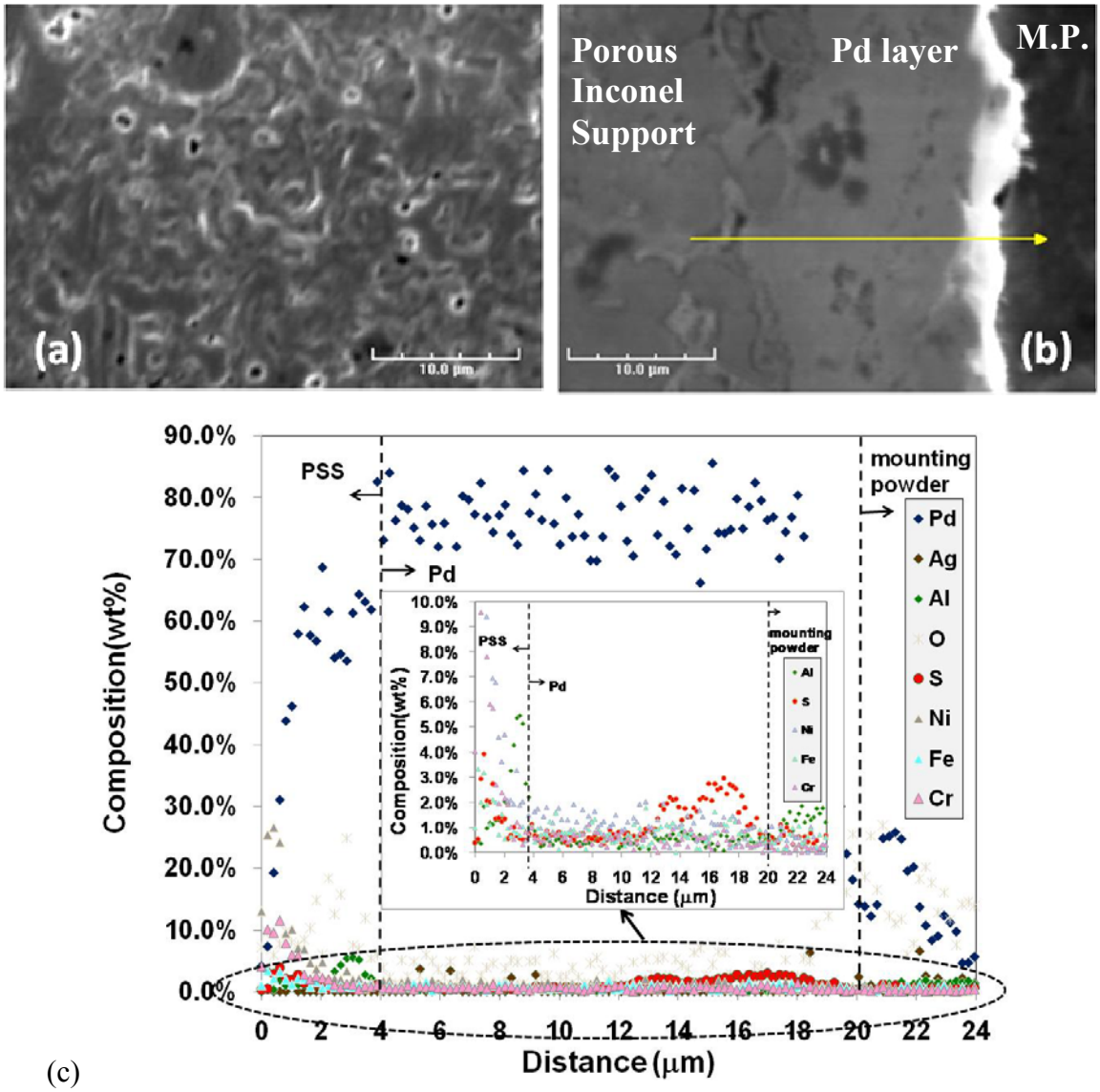

Figure 16. (a) Surface SEM micrograph, (b) cross sectional SEM micrograph, and (c) corresponding EDS line (The insert was emphasizing in the region below 10 wt%) of C_06 after the exposure to a 54.8 ppm H_2S/ H_2 gas mixture at 400°C (M.P. represented mounting powder, which was phenolic powder in the present study).

Pd/Cu studies

Pd/Cu alloy formation

Several Pd/Cu coupons were prepared to determine the annealing time sufficient to produce an FCC alloy on the top layer. Coupons were oxidized at 800ºC for 12 hours and plated with Pd and Cu. Figure 17 shows the XRD patterns of the annealed coupons, their Pd and Cu thicknesses, and the annealing times and temperatures. The Pd/Cu coupon annealed for 120 hours at 500ºC in H_2 had a total Cu composition of 34 wt%. Following the annealing, the XRD pattern showed peaks at 41.36° and 43.02° corresponding to the FCC and BCC phases respectively. No peaks for Pd or Cu were present, signifying that an alloy at least as thick as the penetration depth (5 μm) had formed. The lattice parameters for the BCC and FCC phases were determined from the XRD pattern to be 2.98 Å and 3.78 Å respectively, in agreement with the literature. The lattice parameter for the BCC phase was reported to be between 2.95 and 2.98 Å while the lattice parameter for the FCC phase in the mixed FCC-BCC region in Figure 1 was reported to be between 3.75 - 3.78 Å [8].

Figure 17 also shows the patterns of two coupons with thicker Pd layers and lower Cu compositions than the previous coupon described. The coupons had 18 and 11 wt% Cu and were annealed for 10 and 5 hours at 500ºC in H_2 respectively. Following the annealing, the only Pd/Cu alloy peaks present were those of the FCC phase. The BCC peak at 43.02° was not present, indicating that the FCC alloy had formed on the top layers of both coupons even after a short annealing time. The lattice parameters for the FCC phase of the 18 and 11 wt% Cu coupons were 3.82 and 3.83 Å respectively, in agreement with values reported (3.82 – 3.86 Å) for an FCC alloy to the right of the mixed phase region shown in Figure 1 [8].

In order to verify the presence of a Cu gradient and confirm that the Cu concentration did not reach more than 30 wt% at the top layers of the coupon samples after annealing, the cross sections were analyzed. Figure 18a and Figure 18b show the

cross sections of the annealed Pd/Cu layers on the PSS supports and the corresponding EDS line scans. The 1 – 3 μm dark layer in between the PSS and the Pd/Cu layer was the oxide intermetallic diffusion barrier. The arrows correspond to the direction of the EDS line scans and the dotted lines mark the interfaces of the membrane with the resin and the support.

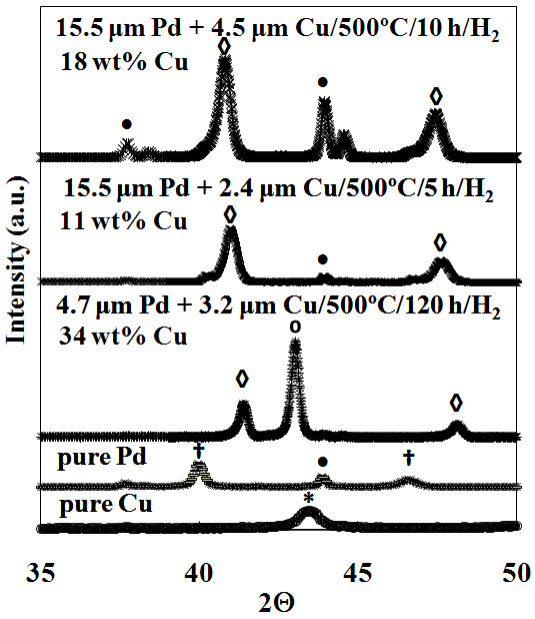

Figure 17. XRD patterns of Pd/Cu coupons annealed in this study. (◊) – FCC phase, (°) – BCC phase, (•) – Al sample holder, (†) – Pd, (*) – Cu. Pd/Cu gravimetric thickness estimate/temperature annealed/time annealed/annealing atmosphere.

In Figure 18a, the Pd/Cu layer consisted of primarily Pd until at a distance of 9 μm from the interface between the support and Pd layers where the Cu gradient became noticeable and the Cu concentration increased towards the surface of the membrane. The Cu concentration in the Pd/Cu alloy was 20 wt% near the surface of the layer. Similarly, in Figure 18b, the Cu concentration started to increase at a distance of 8 μm until a final

composition of 15 wt% near the surface of the Pd/Cu layer. Both Cu compositions near the surface were below the weight composition of the FCC – BCC phase transition.

The XRD patterns in Figure 17 coupled with the line scans in Figure 18 show that relatively short annealing times at 500ºC in H_2 were required to form a Pd-Cu FCC alloy on the top layer of the coupons. The EDS line scans showed the presence of a Cu gradient near the surface, indicating that a homogeneous alloy had not formed throughout the membrane.

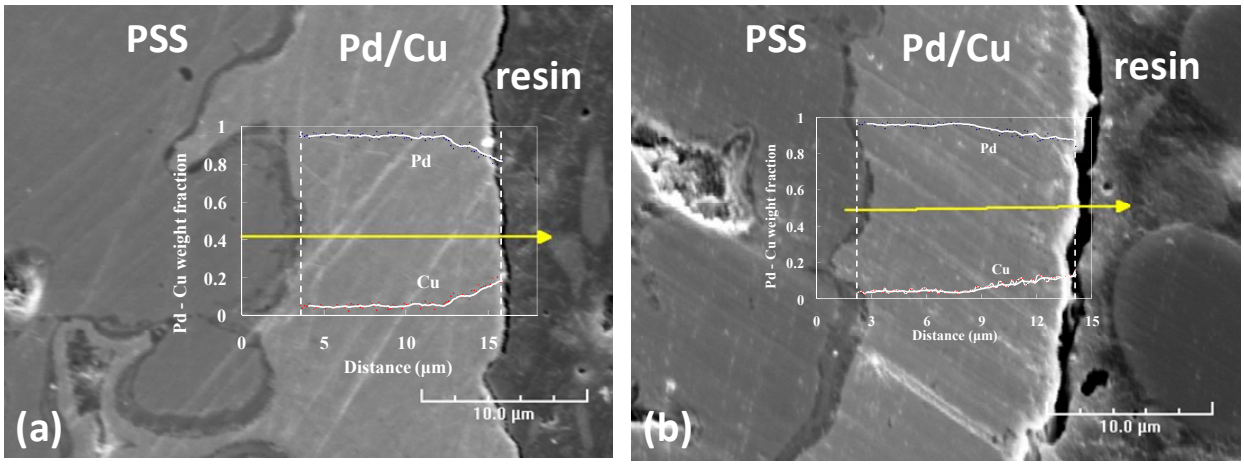

Figure 18. SEI cross sectional micrographs and corresponding EDS line scans of the Pd/Cu coupons annealed in H_2 at 500ºC (a) 15.5 µm Pd + 2.4 µm Cu, annealed for 5 hours and (b) 15.5 µm Pd + 4.5 µm Cu, annealed for 10 hours.

Pd/Cu membrane fabrication and characterization

A summary of the membranes tested in this work and the fabrication methods are listed in Table 2. With the exception of N_09, the membranes were pre-annealed at 500ºC in H_2 for 5 – 10 h and characterized in pure H_2 and He before the testing in H_2S. N_02, N_03 and N_09 were characterized for over 1700, 2300 and 1400 hours respectively between the temperatures of 250 - 500°C. N_08 was characterized for 1200 hours between the temperatures of 250 - 450°C. All three membranes followed the

Sieverts' Law in the temperature ranges tested indicating that one dimensional diffusion through the Pd/Cu hydrogen selective layer was the rate determining step of hydrogen permeation through the composite membrane. The permeance at 450ºC for each membrane before the long-term testing is listed in Table 2 and the Sieverts' Law regression is shown in Figure 19.

Table 2. Pd/Cu membranes tested in this work.

membrane	intermetallic diffusion barrier	grading	Pd/Ag barrier (μm)	Pd layer (μm)	Cu layer (μm)	wt% Cu[a]	$F_{450ºC}$ ($m^3/m^2*h*bar^{0.5}$)[b]
N_02	0.5 μm Ru	none	none	10.8	3.4	19	13.2
N_03	air/700ºC/12 h	none	none	12.5	1.5	8	10.8
N_08	air/700ºC/12 h	Al_2O_3	5.1	7.6	3.8	27	18.0
N_09[c]	air/700ºC/12 h	Al_2O_3	4.3	9.1	1.6	12	13.0[d]

[a]Pd/Ag barrier not included in calculation.

[b]Permeance before long-term testing.

[c]Annealed and polished prior to testing.

[d]Calculated by interpolation from the Arrhenius equation.

Since increasing the Cu concentration in the FCC phase lowers the permeance of a Pd/Cu membrane [35], one would expect that a membrane of higher Cu content and similar thickness would have a smaller permeance. The Cu composition of N_02 was more than double that of N_03, and the membranes had similar thicknesses. Although neither membrane was homogeneous, N_02 should have had a permeance less than that of N_03. However, the permeance of N_02 was higher than that of N_03. The reason for this discrepancy could be due to the inaccuracy in determining the thickness and Cu concentration of the membrane layers with the gravimetric method.

The Cu composition of N_08 was higher than that of N_02. Even so, the H_2 permeance of N_08 was higher than that of either N_02 or N_03 because of the Al_2O_3 grading layer and Pd/Ag barrier, which prevented Pd from deeply penetrating into the pores of the support. The permeance of N_09 should have been the highest of the four membranes tested due to the lower Cu content and the presence of the Al_2O_3 grading and Pd/Ag barrier. However, N_09 had defects in the Pd layer near the area of the weld between the porous and non-porous parts of the support which necessitated repair by

repeated platings. The majority of the membrane surface was not plated during the repair and therefore the thickness of the repaired layer was not taken into account with the overall gravimetric thickness of N_09. It is possible that the thicker Pd layer in the repaired areas reduced the overall permeance.

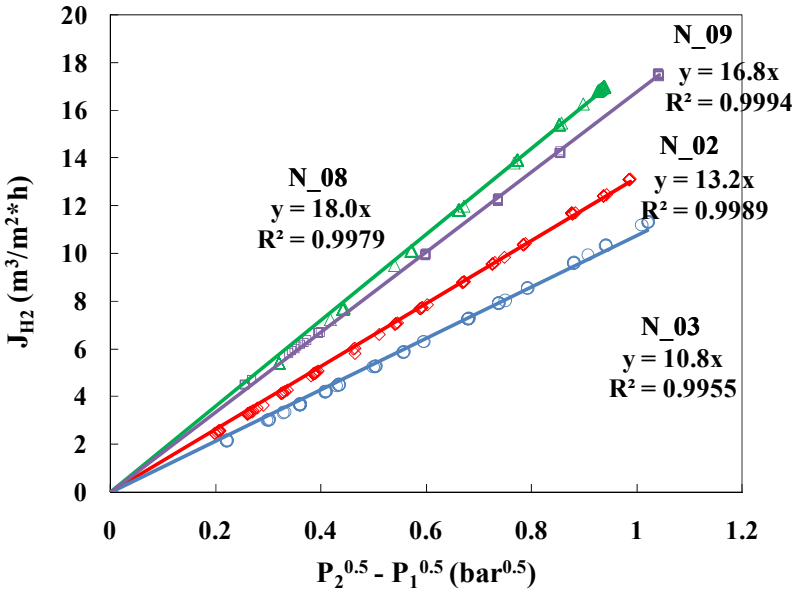

Figure 19. Sieverts' Law regression at 450°C for N_02, N_03 and N_08 and at 500°C for N_09, before the long-term testimg.

Figure 20 shows the high temperature testing of N_02, N_03 and N_09 at 500ºC. N_03 had a stable permeance for over 1150 hours at 500ºC after an initial decrease of permeance of 26% (from 12 to 8.9 $m^3/m^2*h*bar^{0.5}$). N_09 had a stable permeance for 600 hours after which the permeance increased from 16.8 to 19.8 $m^3/m^2*h*bar^{0.5}$. N_02 exhibited steady intermetallic diffusion of the support metals into the hydrogen selective layer at 500°C and the permeance decreased from 15.0 to 3.3 $m^3/m^2*h*bar^{0.5}$, showing that the 0.5 µm Ru was not an effective barrier. The oxide layer coupled with the Pd/Ag intermetallic diffusion barrier present in N_09 appeared to be a more effective barrier than the oxide layer alone on N_03 since N_09 did not exhibit any permeance decrease at 500°C.

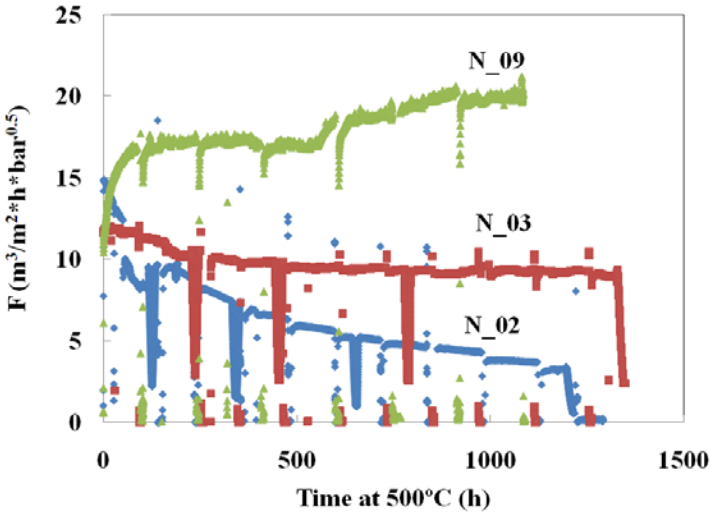

Figure 20. Permeance as a function of time during the long-term, high temperature testing.

Figure 21 shows the Arrhenius plot of the permeance as a function of temperature for all of the membranes tested in this work, following the long-term testing in H_2 and He. The activation energy for N_09 was calculated from the regression of permeances calculated by Sieverts' Law at 250, 350 and 500ºC. In order to determine the activation energy of permeation for N_02, N_03 and N_08, the permeance was calculated according to the linear regression for Sieverts' Law (as shown in Figure 19) at 500ºC for N_02 and N_03 and at 450ºC for N_08. The temperature was ramped in hydrogen at a rate of 0.5ºC/min to 250ºC with the permeance calculated upon the assumption of Sieverts' Law from each measurement of flux and pressure (ΔP = 1 atm) instead of a linear regression. When 250ºC was reached, the respective permeances of N_02, N_03 and N_08 were calculated in accordance with the Sieverts' Law regression (such as seen in Figure 19) to verify that the measurements were at a pseudo steady state throughout the ramping, thus ensuring the accuracy of the permeance calculations during the temperature ramping. The activation energy was then calculated from the regression of the permeance measurements taken during the temperature ramping.

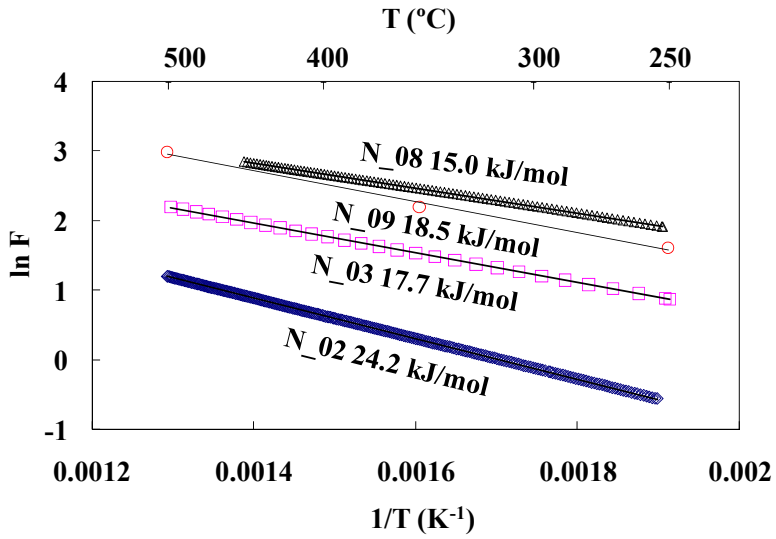

Figure 21. Activation energies of the membranes after the long-term testing.[*]

The activation energies for N_03, N_08, and N_09 were close to 15 kJ/mol, the activation energy of Pd membranes [36]. The unusually high activation energy for N_02 of 24.2 kJ/mol was caused by intermetallic diffusion because support metals in the hydrogen selective layer both decreased the H_2 permeance and increased the diffusional resistance of the H_2 selective layer.

Figure 22a shows the dependence of the leak as a function of time during the high temperature testing of membranes N_02, N_03 and N_09. The He flux of N_02 and N_03 increased in a fairly linear fashion. The linear increase of the membrane leak has been attributed to pinhole formation caused by the incoherent sintering of Pd clusters, which occurred over the entire membrane surface and had a growth rate at 500ºC of $9.1*10^{-5}$ $m^3/(m^2*h)/h$ [37]. The He leak growth rates for N_03 and N_02 were $7*10^{-6}$ and $3*10^{-6}$ $m^3/(m^2*h)/h$ respectively making the growth rate of N_02 and N_03 more than an order of magnitude less than the rate reported previously for pure Pd membranes. Indeed, the leak growth rates at 500°C of N_02 and N_03 were even slightly less than the growth rates measured at 450°C for pure Pd membranes [37].

Since the majority of the membranes tested by Guazzone and Ma [37] were pure Pd, it appeared that the presence of Cu increased the leak stability of N_02 and N_03.

[*] N_08 was not tested at 500ºC

The small He leak growth rates seen in N_02 and N_03 could be due to the fact that the solubility of hydrogen in Pd/Cu alloys decreased with Cu content [38]. Since the He leak growth was faster in a H_2 atmosphere than in a He atmosphere [36, 39], less H_2 dissolved in the lattice could have decreased the leak growth.

It should also be noted that N_03 was tested for 530 hours and N_02 was tested for 450 hours while they were being characterized before the temperature was raised to 500°C. The total testing time when the last He leak was measured was 1900 hours for N_03 and 1650 hours for N_02. The ideal H_2/He separation factors at the conclusion of the testing period were 320 and 350 for N_02 and N_03 respectively (shown in Figure 22b).

The He flux growth of N_09 followed a different pattern than that of N_02 and N_03. The He leak was barely detectable for roughly 800 hours at 500°C, and did not show a steady increase. The initial stability was due to the method of fabrication. Annealing the electroless deposited Pd layer of N_09 at 550ºC caused the Pd grains to sinter and form pores in the layer as the surface tension of the grains approached equilibrium at a high temperature. After removing part of the annealed layer by mechanical treatment, re-plating, and repeating the process, the heat-treated layers would not form through-through pinholes but rather each layer would form pinholes which would not be connected to the pinholes of the adjacent heat-treated layer thereby stymieing the leak growth.

However, at 800 hours a leak appeared which was relatively large in comparison to the He leaks of N_02 and N_03 at the same testing time. Contrary to the slow, steady increase seen with N_02 and N_03, the large leak of N_09 appeared suddenly. It is believed that the sudden appearance of the leak in N_09 was caused by defects in the area of the weld between the non-porous and porous parts of the support. During fabrication, it was found that He was still flowing through the area of the weld even though the rest of the membrane was dense. Repeated platings of just the weld area were required in order to make N_09 dense at room temperature, but did not prevent the leak from opening up in that area at high temperatures. The final ideal H_2/He separation factor for N_09 was 620 at 500ºC.

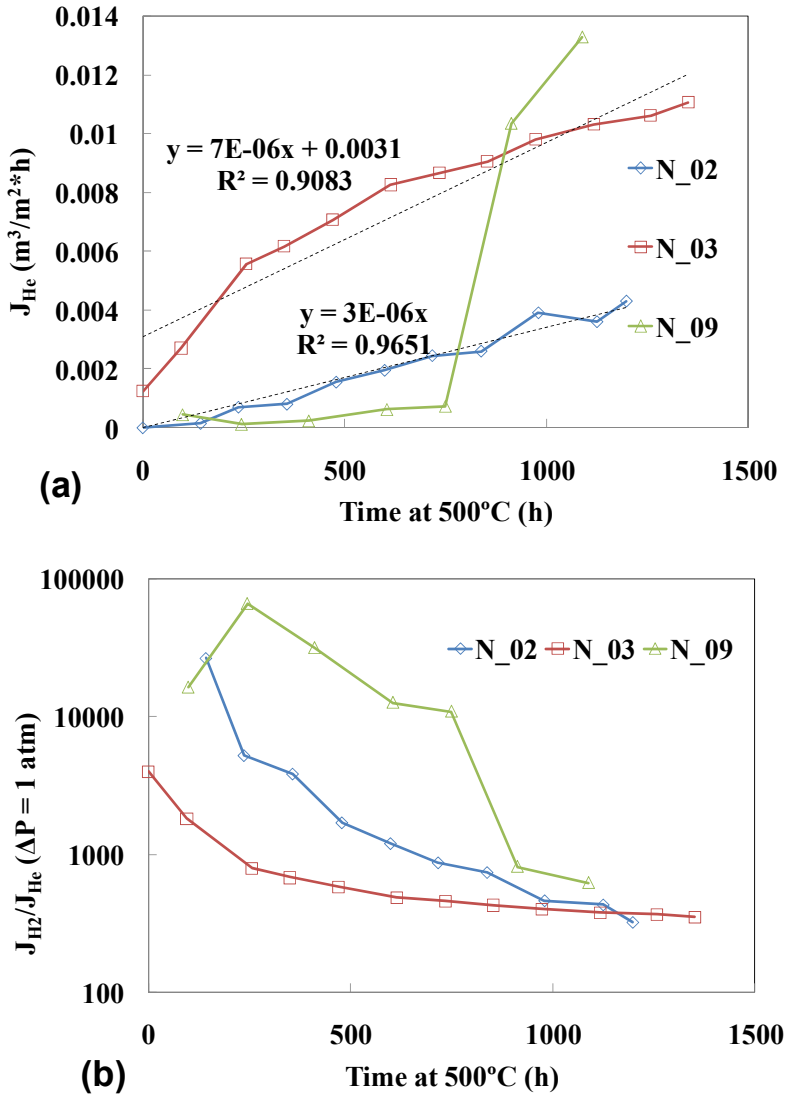

Figure 22. (a) He flux as a function of time and (b) ideal H_2/He separation factor as a function of time during the long-term testing at 500°C.

Pd/Cu membrane testing in H_2S

Figure 23 shows the percent of permeance decline and recovery as a function of time at 450ºC during testing with 42.7 ppm H_2S/H_2 and the subsequent recovery in pure H_2. The y-axis shows the relative permeance where F is the H_2 permeance and F_0 is the H_2 permeance at 450ºC before the introduction of the H_2S/H_2 mixture. Membrane N_03 was exposed to 42.7 ppm H_2S/H_2 for 2 hours, and then pure H_2 was reintroduced to recover the hydrogen permeance until a stable value was reached. The effect of H_2S poisoning on the He leak was examined by monitoring the He leak flux before each poisoning experiment and after each recovery in pure H_2. All measurements were performed at ΔP = 1 bar (P_{feed} = 2 bar, $P_{permeate}$ = 1 bar).

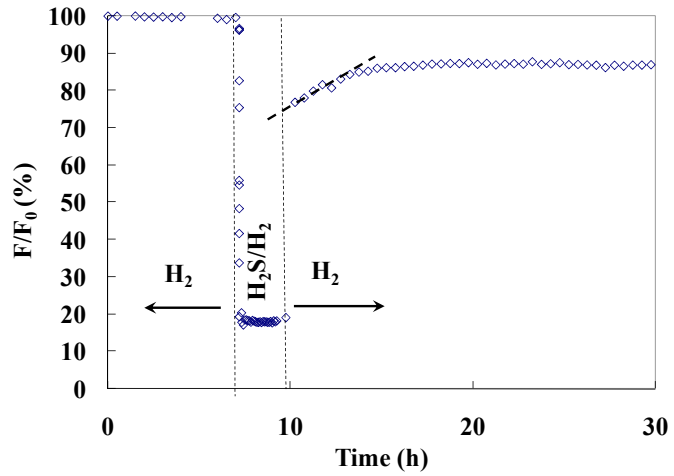

Figure 23. A sample of a poisoning test run for N_03 in 42.7 ppm H_2S/H_2, and the recovery in pure H_2 at 450ºC.

As seen in Figure 23, the permeance of N_03 dropped sharply by approximately 80% within the first few minutes of the exposure to the H_2S/H_2 mixture. The permeance decline occurred instantaneously, and for the duration of 2 hours of poisoning, the permeance did not change. The permeance decline was caused by surface sulfide formation where sulfur blocked H_2 adsorption sites with the surface sulfide most likely being a palladium sulfide. The sulfur adsorption caused the segregation of Pd atoms to

the surface of Pd/Cu alloys to form a pure Pd layer on the topmost atomic layer of Pd/Cu alloys which consequently formed palladium sulfide [31].

Assuming that the poisoning was purely a surface phenomenon, the magnitude of the decline would have indicated that 80% of the H_2 adsorption sites were blocked for N_03, reducing the effective area for H_2 adsorption and dissociation. The bulk sulfide formation either caused the hydrogen permeance to have a continuous decline during poisoning as the sulfide layer formed and thickened [40] or caused the hydrogen permeance to increase while accompanied by an increase in the flux of non-permeable gases as the sulfide ruptures the membrane [4]. Since both the permeance and the ideal H_2/He separation factor for N_03 remained relatively constant during poisoning, the permeance decline appeared to be a result of the surface sulfide formation.

N_02 and N_03 were exposed to 42.7 ppm H_2S/H_2 for 2 hours at several temperatures. N_02 was tested twice at 450 and 400°C (in that order) and N_03 was tested twice at 500, 450, 400 and 350°C (in that order). The permeance decline of N_02 at 450ºC was similar in both magnitude and manner to that of N_03 at 450ºC, but was difficult to measure accurately because the flow of the permeate was small relative to the range of the mass flow meter after the prior permeance loss caused by the intermetallic diffusion.

The permeance recovery of the membranes occurred in three stages as shown in Figure 23. The first stage was marked by an instantaneous permeance increase starting from F/F_0 = 20% upon the introduction of pure H_2, indicating that the adsorbed sulfur combined with H_2 and desorbed from the surface. The second stage was linear (marked by the dashed line in Figure 23) which was at a slower rate than the first stage and lasted between 3 – 10 hours. The third stage was characterized by a very slow increase lasting between 50 - 200 hours. The first stage involved the greatest amount of hydrogen permeance recovered with the percent recovery varying between 50% (at 350ºC) and 85% (at 500ºC). The linear stage recovered roughly an additional 10% of the permeance, and the third stage recovered the least amount of permeance which varied between 5 – 10%.

The three stages of recovery probably corresponded to the changing binding energy of sulfur at the adsorption sites with sulfur coverage. According to previous

theoretical work [41], the binding energy of sulfur to the FCC sites of the Pd(1 1 1) surface decreased from 5.07 to 3.29 eV/atom at 0.11 and 1.0 ML (monolayers) respectively, meaning that the strength of the bond decreased as the surface coverage increased. A similar trend was seen with the HCP (hexagonal close packed) surface adsorption sites and with the tetragonal and octahedral subsurface adsorption sites as the sulfur coverage increased [41, 42]. This phenomenon was also seen with sulfur adsorption on Ni and Pt where the heat of adsorption increased with increasing sulfur coverage. The change in the rate of the permeance decrease would correspond to the increasing binding energy (heat of adsorption becoming less negative) of sulfur to Pd as the surface coverage decreased due to sulfur desorption [43].

In addition, the binding energy of sulfur to an adsorption site changes depending on the location of the site and alloy composition. Alfonso *et al.* [44] calculated the binding energies for the adsorption sites on the Pd(1 1 1), Cu(1 1 1), $PdCu_3$(1 1 1), Pd_3Cu(1 1 1) and PdCu(1 1 0) surfaces and found that the greatest difference in the binding energy between the most energetically favorable sites of the surfaces was 0.42 eV, showing a differing bond strength of sulfur to alloyed surfaces of different compositions. In addition, the PdCu(1 1 0) surface had a difference of 0.22 eV between the sulfur adsorption sites, showing differing bond strengths for different adsorption sites on the same surface. The sharp increase in permeance upon the reintroduction of H_2 would be from sulfur desorbing from the least energetically favorable sites (lowest binding energy). The linear stage of recovery would be from sites which were more energetically favorable and the last stage of recovery from sites which were the most energetically favorable.

Even though the last stage of recovery was lengthy in time, not all of the permeance could be recovered. At 450ºC, 95% of the hydrogen permeance of N_03 was recovered after poisoning, showing that at these conditions, part of the sulfur could not be desorbed and irreversible surface sulfides had formed. It was unlikely that bulk sulfide formation was the cause of the irreversible poisoning since bulk sulfides had previously caused a continuous permeance decline during poisoning [40], contrary to the unchanged permeance of N_03 during exposure. Since the process of sulfur desorbing from the membrane surface would increase the binding energy of the remaining adsorbed sulfur

atoms and increase the heat of adsorption for the remaining adsorbed sulfur due to a lessening in repellant forces between the adsorbed sulfur atoms during desorption [42], the irreversible poisoning could have been caused by adsorbed sulfur atoms which had very high binding energies. Also, it was found that the sub-surface sulfur adsorption became energetically favorable after 0.5 ML of sulfur was adsorbed on the Pd(1 1 1) surface [42]. Once sulfur was present in the subsurface of Pd, desorption would take longer and might possibly be irreversible.

Irreversible and reversible H_2S poisoning has been seen with many catalysts [43]. Work with Pt/Al_2O_3 [45] showed that the amount of irreversibly adsorbed sulfur remained constant at 500ºC while the amount of reversibly adsorbed sulfur increased with increasing H_2S concentration in H_2. Horanyi and Ritzmayer [46] have identified irreversible sulfur poisoning within a monolayer of sulfur coverage on Pt as PtS, while reversible sulfur poisoning was identified as PtS_2. It was possible that the formation of more than one surface sulfide resulted in the irreversible poisoning of the Pd/Cu membranes.

The sudden drop in permeance upon the introduction of the H_2S/H_2 mixture with no further decrease during the two hours of exposure was observed at each of the temperatures tested. The only difference between each temperature tested was the magnitude of the permeance loss.

As seen in Figure 24 (y-axis on the left), there was a slight increase in the amount of permeance lost during exposure to the H_2S mixture with decreasing temperature. Similar to the recovery at 450ºC, the permeance recovery at 350, 400 and 500ºC occurred in three stages. The fact that the only differences between the recovery curves at each temperature were the rate and magnitude of each stage indicated that the poisoning and recovery mechanisms were the same for the range of temperatures in this work. Figure 24 shows the values of the final percent recovery (y-axis on the right) as a function of temperature. The percent permeance of N_03 during poisoning and the percent permeance after recovery slightly increased with temperature, showing that the amount of irreversible poisoning increased with decreasing temperature.

Figure 25 shows the amount of time required for the hydrogen permeance to stabilize during recovery in pure H_2 as a function of temperature. While recovery times

were short (roughly 20 hours) at 500ºC, the total time needed for the permeance to stabilize in pure H_2 greatly increased at lower temperatures. In addition, the rate of recovery of the linear stage increased with increasing temperature. Indeed, membrane regeneration at higher temperatures would be more reasonable in an industrial setting should a membrane become exposed to larger quantities of H_2S.

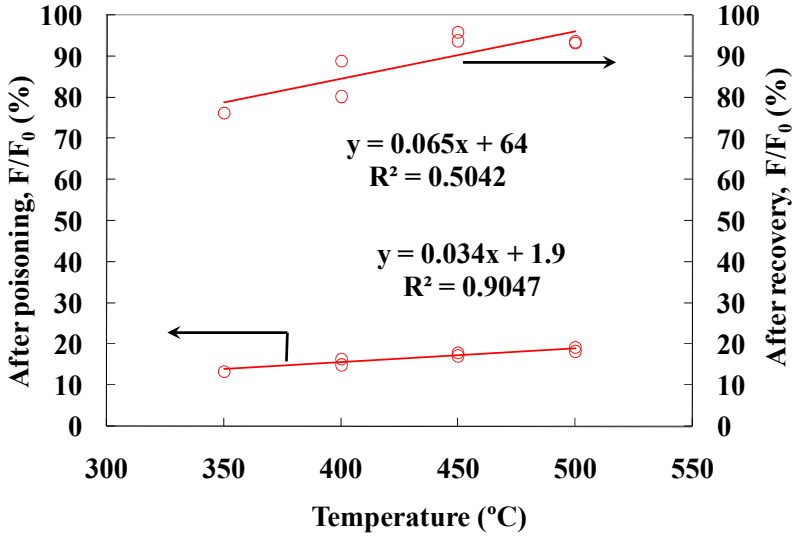

Figure 24. Percent of hydrogen permeance during exposure to 42.7 ppm H_2S/H_2 and percent of hydrogen permeance recovery after exposure to pure H_2 as a function of temperature for N_03.

The dissociative chemisorption of H_2S on metals is an exothermic reaction:

$$H_2S + M \leftrightarrow S - M + H_2 \quad \Delta H_{ads} < 0$$

and increasing the temperature of the system would shift the equilibrium of the reaction towards the reactants, resulting both in less H2S chemisorption during poisoning and more H2S desorption during recovery. Assuming that the poisoning was due primarily to sulfur adsorption on the membrane surface, higher temperatures would result in more overall tolerance. The increased rate of the permeance recovery with temperature seen in Figure 25 would be a result of the increased H2S desorption rate but the decreasing

amount of irreversible poisoning with increasing temperature would be due to the exothermic nature of H2S adsorption.

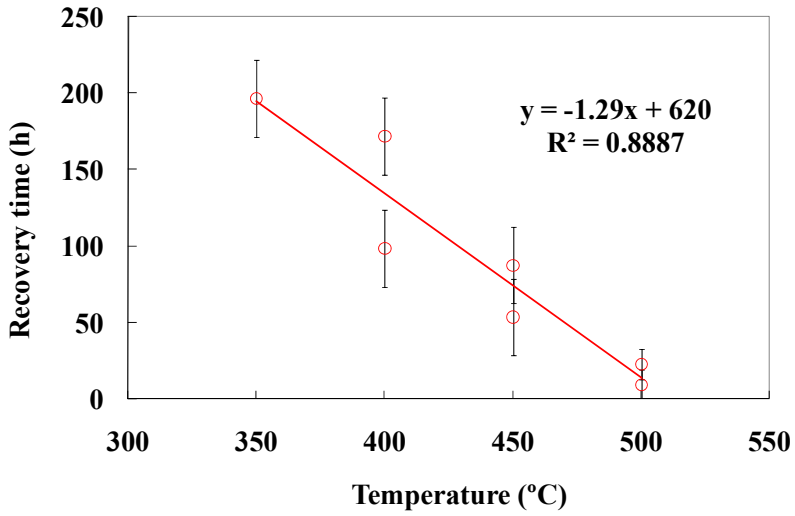

Figure 25. Recovery time as a function of temperature for N_03.

Figure 26 shows the permeance decline and recovery for membrane N_08 which was exposed to 54.2 ppm H_2S/H_2 for 125 hours at 450ºC. The permeance dropped instantaneously and did not change throughout the lengthy exposure to the H_2S/H_2 mixture. The magnitude of the drop was 80% of the original permeance at 450ºC, which was similar to the permeance drop that N_03 experienced at 450ºC. However, the period of recovery lasted over 500 hours, which was much longer than the 95 hours needed after the 2 hour exposure of N_03 at 450ºC seen in Figure 25. Moreover, only 65% of the permeance of N_08 was recovered in comparison to the 95% that was recovered with N_03 at 450ºC.

The longer period of recovery coupled with the decreasing amount of permeance recovered showed that the irreversibility of the membrane poisoning increased with H_2S exposure time. If the irreversible poisoning was caused by irreversibly adsorbed sulfur, either at binding sites with very high binding energies or in subsurface adsorption sites, the amount of sulfur at these sites would gradually increase with increased exposure time. Since increasing the amount of sulfur on the surface decreased the bond strength of the adsorbed sulfur [41], it would appear that it was the amount of subsurface adsorbed sulfur

which increased with exposure time, thereby increasing the irreversibility of the membrane poisoning.

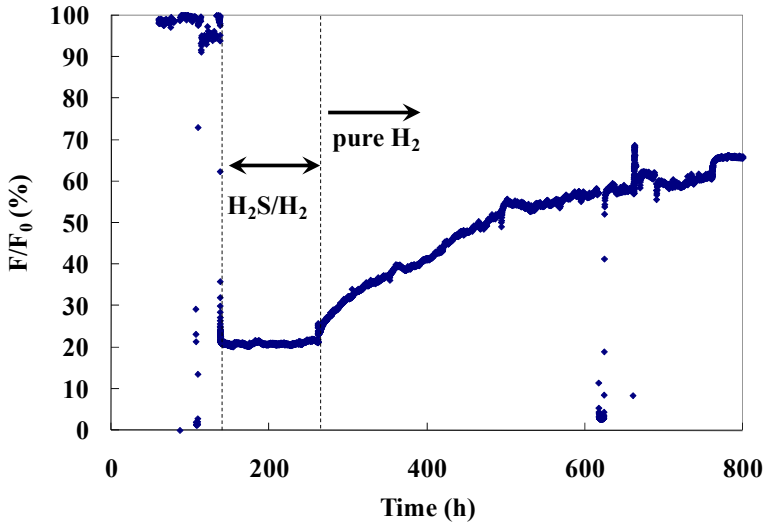

Figure 26. Permeance decline and recovery for N_08 for 125 hours of exposure to 54.2 ppm H_2S/H_2 at 450ºC.

The activation energy of hydrogen permeation of N_08 after the permeance recovery was 13.8 kJ/mol. The fact that the activation energy did not significantly change before (15.0 kJ/mol, shown in Figure 21) and after the H_2S testing indicated that the irreversible sulfur poisoning did not significantly change the hydrogen transport mechanism, even though the irreversibly adsorbed sulfur decreased the permeance. In addition, the negligible change in the activation energy indicated that the irreversible poisoning caused a decrease in the effective membrane area for the H_2 adsorption and did not cause the formation of bulk sulfides.

Following the experiments shown in Figure 24 and Figure 25, N_03 was tested in 54.8 ppm H_2S/H_2 for 8, 29, 50, 94 and 59 hours (in that order) at 450ºC with the permeance recovery in pure H_2 monitored in between each poisoning experiment. The effect of H_2S poisoning on the selectivity was examined by measuring the He leak before and after each exposure to the H_2S/H_2 mixture.

Figure 27 shows the final value of the permeance recovery as a function of cumulative exposure time to the H_2S/H_2 mixture (not including the recovery time in pure

H_2). After exposure to the H_2S/H_2 mixture for 2 and 8 hours, the percent recovery was 85%, only slightly lower than the percent recovery which was measured at 450ºC during the previous experiments shown in Figure 24. However, after a cumulative exposure time of 250 hours, the recovery dropped to 60%. The decline in the total permeance recovery with time proved that not only was the H_2S poisoning mechanism irreversible at these conditions, but also that the extent of the irreversible poisoning increased with time. Previous studies have concluded that the extent of H_2S poisoning of Pd and Pd alloy membranes was dependent upon the H_2S concentration and temperature [5, 7] but not upon the time of exposure. However, permeance recovery experiments were not performed in these studies.

The results of the permeance recovery of N_08 were superimposed on the results from N_03 in Figure 27. The percent recovery of N_08 after one lengthy exposure to the H_2S/H_2 mixture fell only slightly below the curve for N_03 which had several recovery periods in between each exposure to the H_2S/H_2 mixture, showing that the irreversible poisoning was solely dependent on the total amount of poisoning time.

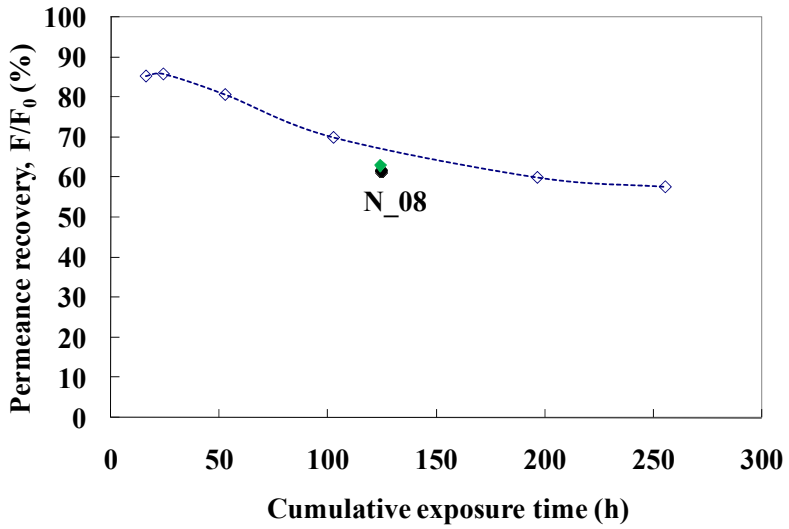

Figure 27. Total permeance recovery as a function of cumulative exposure time to the H_2S/H_2 mixture for membrane N_03 at 450ºC. The results of N_08 were superimposed on the graph for comparison. The line is for guiding the eye.

Figure 28a and Figure 28b respectively show the He leak and ideal H_2/He separation factor as a function of time for membrane N_03 while N_03 was being characterized in pure H_2 and during the series of H_2S testing and permeance recoveries. The progression of the He leak over time during the long-term testing of N_03 shown in Figure 28a shows a contrast in the trend before and after the H_2S testing. During the long-term characterization in pure H_2, the He leak of N_03 increased and the ideal H_2/He separation factor decreased, shown in Figure 28b. After the poisoning and recovery experiments began, the He leak remained relatively stable for 1500 hours, oscillating between 0.8 – 1 sccm, and then decreased drastically to 0.13 sccm after an additional 500 hours. The leak oscillated between 0.13 – 0.3 sccm for the next 2000 hours of testing at 450ºC, and did not show a steady increase.

Not only did the leak stop increasing with the onset of the H_2S experiments, but the leak decreased to values that were measured towards the beginning of the characterization. However, the ideal H_2/He separation factor decreased at times even though the He leak lessened because the permeance of N_03 did not recover to the original value after the H_2S poisoning. Even so, the ideal H_2/He separation factor at 450°C at the beginning of the H_2S testing was 83 and increased to 540 as the H_2S testing progressed over a period of 1800 hours, despite the fact that the permeance decreased.

Similar to the results of N_03, the leak of N_08 increased at 450ºC from 0.1 to 1.2 sccm over a period of 300 hours and the ideal H_2/He separation factor decreased from 1770 to 220 before the H_2S testing. After the H_2S testing began, the He leak decreased from 1.2 to 1 sccm over a period of 800 hours at 450ºC. Likewise, the leak of N_02 exhibited a clear upward trend during the long-term testing in H_2 at 500ºC. After the poisoning and recovery experiments began, the He leak decreased and the ideal H_2/He separation factor increased until the membrane became dense again, while still being tested. N_02 continued to be dense 200 hours later.

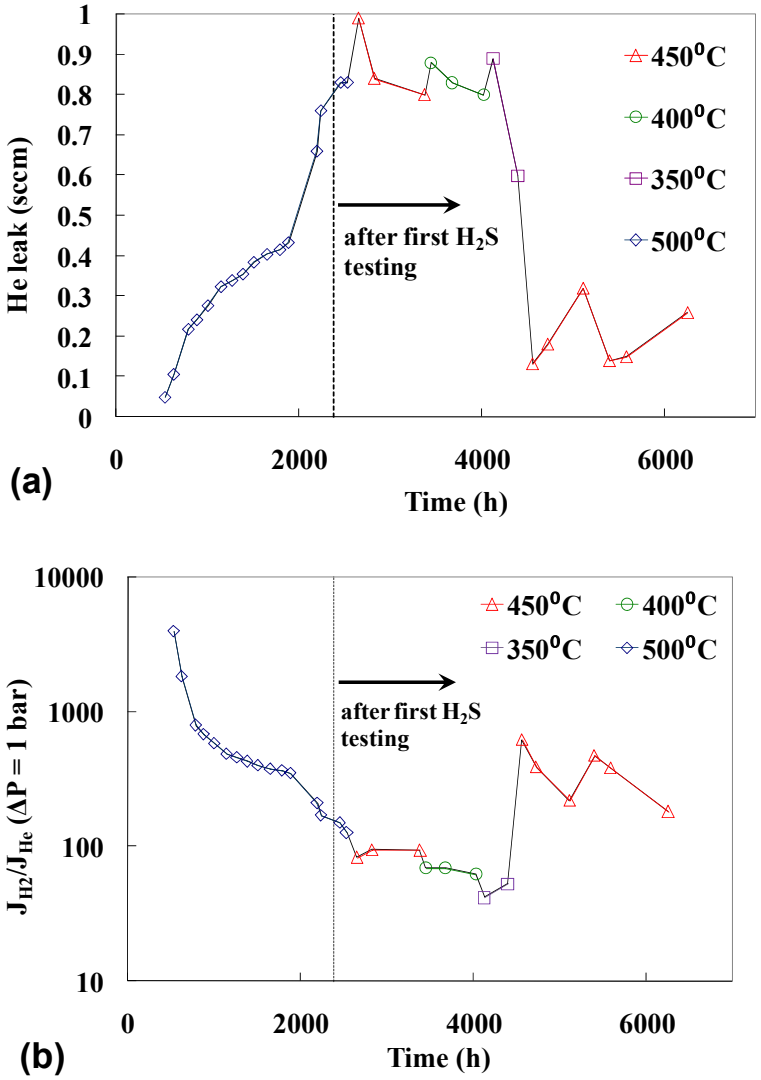

Figure 28. (a) He leak as a function of time for N_03. (b) Ideal H_2/He separation factor as a function of time for N_03. The lines are for guiding the eye.

Exposing electroless deposited Pd and Pd alloy membranes, which have not been fabricated to hinder leak development as with N_09, to elevated temperatures caused leaks to develop over time due to grain coarsening as grain boundaries migrated to equilibrate the surface tensions and reduced the total energy of defects within the Pd lattice. Saini [39] observed that after annealing at 500ºC in both H_2 and He atmospheres, the grains of electroless deposited Pd grew larger. The grain growth would continue until

reaching a static equilibrium where the surface tensions of the adjoining grain boundaries were equal. Guazzone *et al.* [47] observed that microstrains and stresses in the deposit released upon heating caused pinhole formation and growth. Indeed, past research [37,39,47] indicated that the He leak of electroless deposited Pd membranes increased over the time period of the membrane characterization.

Also, according to the dusty gas flow model [48], the flux of non-permeable gases should increase with decreasing temperature. The work of Mardilovich *et al.* [18] showed the increase of the He leak of Pd membranes with decreasing temperature both computationally and experimentally. However, Figure 28a shows that the He leak of N_03 decreased from 0.99 sccm at 450ºC to 0.6 sccm at 350ºC. Furthermore, N_02 had a He leak of 0.2 sccm at 500ºC and eventually became dense during testing at 400ºC.

Since either a small change or a reduction was seen in the He leak after the initiation of the H_2S testing and a decrease in the He leak was observed with a decrease in temperature, it could be concluded that the exposure to the H_2S/H_2 mixture not only prevented the He leak growth but even decreased the leak at times. The reason for the unusual effect that H_2S had on the leak growth could be due to sulfur segregation in the grain boundaries of the membrane. Non-permeable gases could only permeate through grain boundaries, cracks, defects, and pinholes in the membrane layer. It was precisely to these areas that impurities would segregate with sulfur being no exception. Indeed, sulfur was detected by EDS in the grain boundaries of Pd membranes tested with gas mixtures containing H_2S [49] and the phenomenon of sulfur segregation in grain boundaries has also been investigated in Fe [50]. If sulfur segregated to the grain boundaries and defects, it would reduce the area of the openings of pathways for non-permeable gases if not blocking them completely.

Furthermore, hydrogen would also be hindered from passing through the pathways between the defects and grain boundaries. A portion of the permeance that was not recovered with N_03 and N_08 would also be partially due to the blockage of pathways.

Figure 29a and Figure 29b respectively show the cross sectional micrographs of N_02 and N_03. A Cu gradient can clearly be seen in both membranes indicating that a homogeneous alloy had not formed even after the long-term testing at 500ºC. The Cu as

detected by EDS extended 6 μm into the Pd layer of N_02 and 5 μm into the Pd layer of N_03. The Cu gradient of N_02 was sharper than that of N_03 due to the higher Cu content of the membrane (see Table 2). However, the Cu penetration into both Pd layers had similar lengths and the Cu gradient enabled only part of the Pd/Cu membranes to have a high Cu content in the FCC region. The result of which would be a membrane with a higher permeance than a homogeneous Pd/Cu membrane of the same surface composition in the FCC phase [35]. In order to increase the hydrogen permeance of the membranes, less Cu could be added so that the Pd/Cu layer would be thinner.

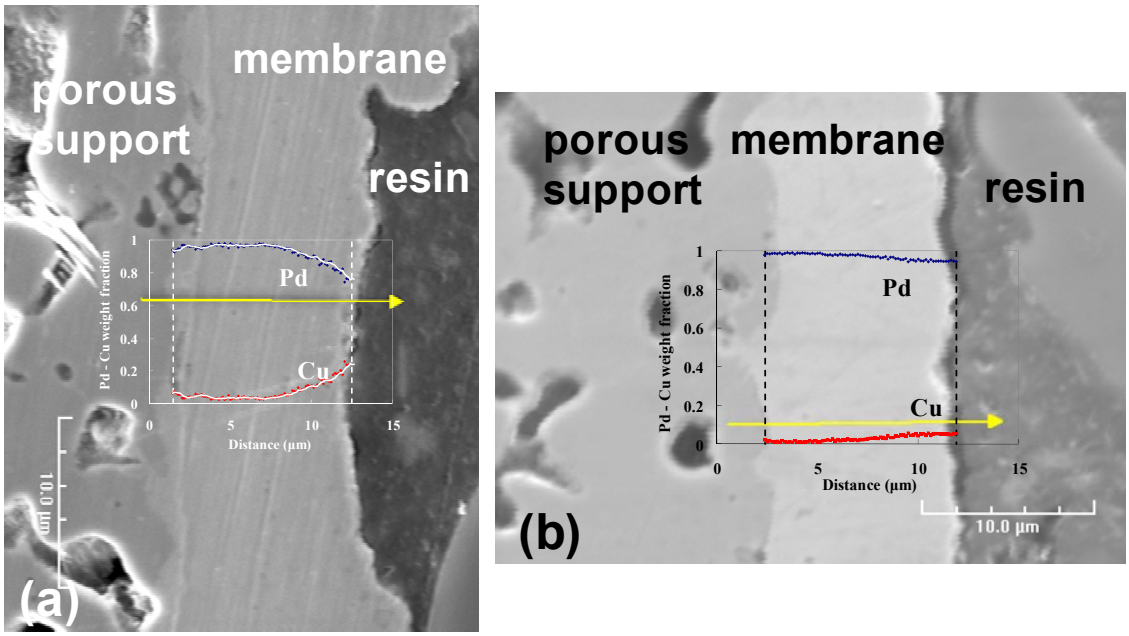

Figure 29. SEI cross sectional micrographs and the corresponding EDS line scans of (a) N_02 and (b) N_03.

Figure 30a and Figure 30b respectively show the surfaces of N_02 and N_03 after testing. No evidence of bulk sulfide formation in the morphology of the Pd/Cu deposit could be seen on N_02, which was exposed to the H_2S/H_2 mixture for a total of 8 hours or N_03, which was exposed to the H_2S/H_2 mixture for a total of 250 hours. The

morphology of the membrane surfaces was similar to that of Pd/Cu deposits fabricated by electroless deposition and annealed in H_2 or He atmospheres [36].

The EDS analysis was not able to detect the presence of sulfur on either membrane surface. However, with a penetration depth of 0.2 – 0.8 μm for EDS, the adsorbed sulfur which caused the irreversible poisoning would be undetectable by this method of analysis. The surface Cu content ranged from 10 – 30 wt% for N_02 and the from 10 – 20 wt% for N_03 confirming that the top layers of the Pd/Cu membranes were indeed in the more sulfur tolerant FCC region of the Pd/Cu phase diagram. However, the composition of the top atomic layer could have a much higher Cu content. Surface studies have shown that heat treated Pd/Cu alloys formed a top atomic layer which had a Cu composition more conducive to the BCC phase [51].

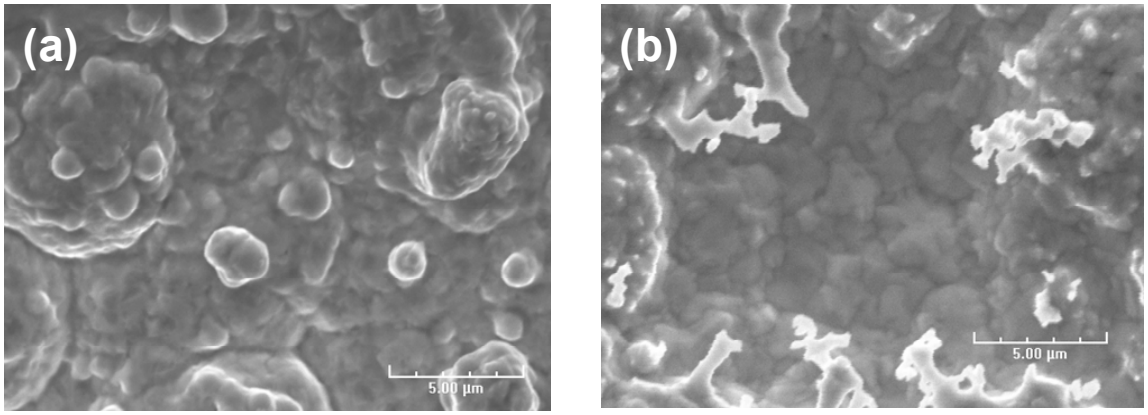

Figure 30. SEI micrographs of the surfaces of (a) N_02 and (b) N_03.

In addition, the EDS analysis showed that the surface compositions were not uniform. This non-uniformity in surface composition might have contributed to the changing rate of hydrogen permeance recovery (seen in Figure 23) due to the difference in binding energy of sulfur adsorption sites on Pd/Cu alloy surfaces of varying compositions [44].

HTXRD studies of Pd/Cu alloys

To investigate the Pd/Cu alloying process, HTXRD was used to characterize the Pd – Cu phase transformations *in-situ* in a H_2 atmosphere. Coupons were oxidized at 800ºC for 12 hours and then plated with approximately 13.0 μm Pd and 1.7 μm Cu for a total bi-layer composition of 13 wt% Cu. A vacuum was applied while heating the samples to 250ºC at a rate of 50ºC/min. At 250ºC, a pure H_2 atmosphere was introduced at a pressure of 1 atm and the temperature was increased to the final annealing temperature at a rate of 50ºC/min. The samples were annealed at 500, 550 and 600ºC.

Figure 31 shows the XRD patterns as a function of time for the coupon annealed at 500ºC in H_2. The first pattern shows the peaks of the (1 1 1) plane for both Pd and Cu at room temperature. The second pattern was taken at 500ºC and shows the peak shift of both the Pd (1 1 1) and Cu (1 1 1) planes to a lower value of 2Θ due to the thermal expansion of the lattice. Also, the peak representing the (1 1 0) plane of the β phase (BCC) of the Pd/Cu alloy appeared next to the Cu (1 1 1) peak, showing that the interdiffusion of Pd and Cu was very fast and that the alloy formation had already began upon reaching the testing temperature. The trail to the left of the β (1 1 0) peak showed the Cu rich α (FCC) phase (1 1 1) peak forming. The width of the peak attested to the concentration gradient within the Cu rich α phase. As time progressed, the Cu (1 1 1) and Cu rich α (1 1 1) peaks disappeared, the Pd (1 1 1) and β (1 1 0) peaks became smaller and the Pd rich α (1 1 1) peak increased in size.

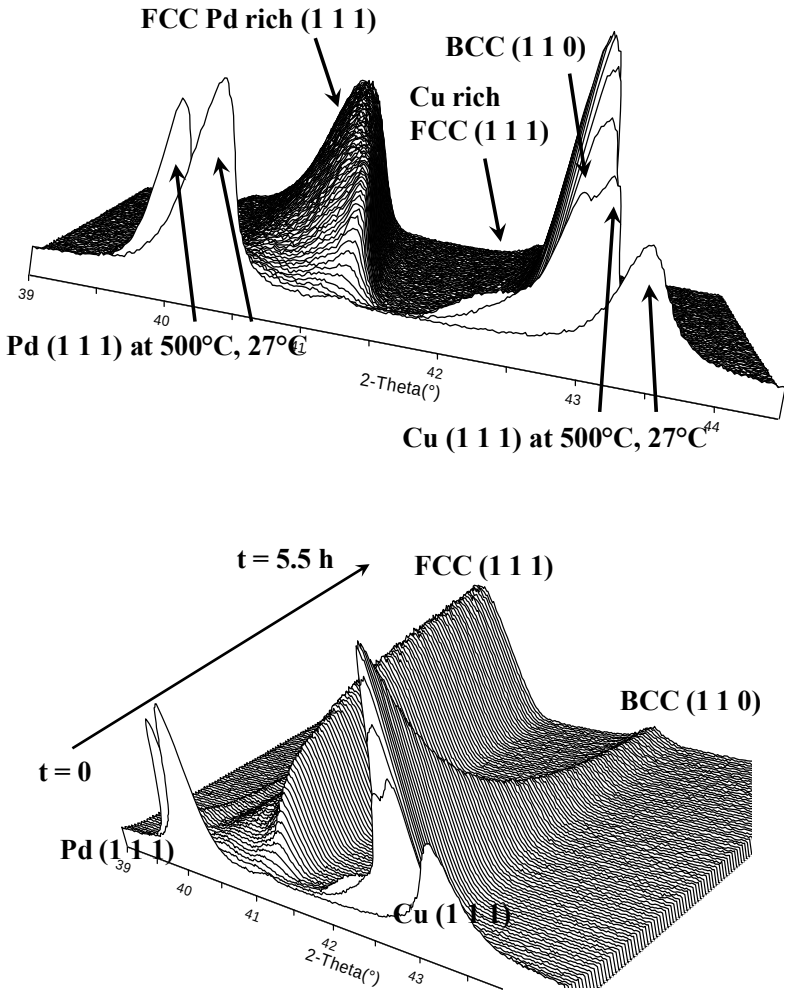

Figure 31. XRD patterns of the Pd/Cu coupon annealed at 500ºC as a function of time.

Figure 32 shows the progression of the annealing as the phase changes on the Pd-Cu phase diagram as represented by the arrow. At 500ºC, a maximum of five phases may be present, and these phases were indeed seen as represented by their peaks in the XRD patterns in Figure 31. A schematic of the annealing process is shown in Figure 33. Before the annealing process began, the only phases present were from the bi-layers of Cu and Pd. The diffusion of Cu brought on by heating caused five phases to form with the phases the most rich in Cu towards the surface.

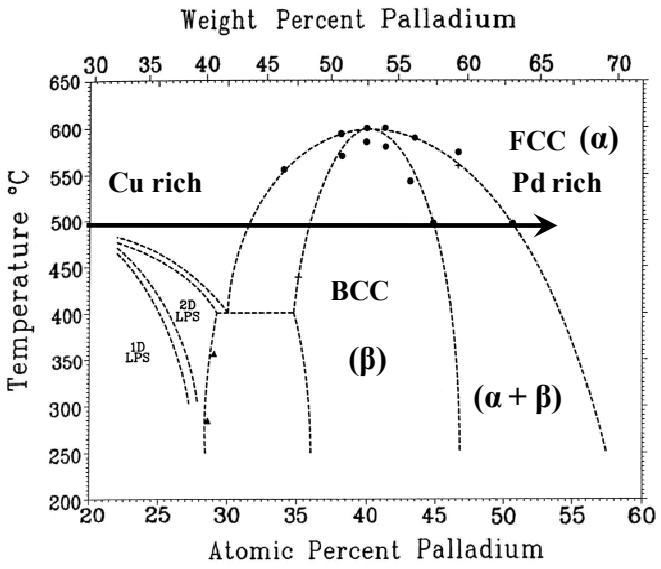

Figure 32. Annealing process superimposed on the Pd-Cu phase diagram [8].

As more Cu diffused into the Pd layer, the more Cu rich phases disappeared and the only phases which remained were the Pd rich α, β and pure Pd phases. Further interdiffusion caused the interface between the β and Pd rich α phases to move towards the surface of the deposit and the interface between the Pd rich α and pure Pd phases to move towards the support (see Figure 33). If enough time were to pass, the Pd and β phases would eventually disappear leaving the Pd/Cu layer a homogeneous alloy entirely in the Pd rich α phase with a Cu concentration of 13 wt%.

Figure 34a shows the weight fraction for all of the phases as a function of time for the sample annealed at 500ºC. The pure Cu phase dropped off quickly at the onset of the annealing while the pure Pd phase gradually decreased. Contrary to the pure Cu and Pd phases which only decreased or the Pd rich α phase which only increased, the Cu rich α and β phases both had maxima. The Cu rich α phase increased in wt% until roughly 100 minutes had passed and then the wt% started to decrease until it could not be detected anymore. Similarly, the β phase increased in wt% until a maximum was reached at 500 minutes. The maximum appeared because the Cu rich α and β phases were interim alloy which formed on the way to forming the Pd rich α phase, as shown in the phase diagram in Figure 32 and schematically in Figure 33.

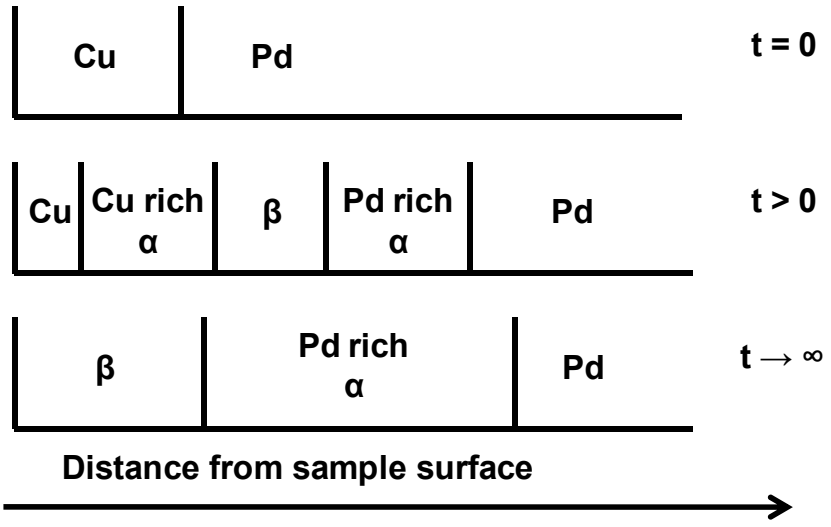

Figure 33. Progression of phase transformation with time.

The diffusion and consequently the rate of phase transformation significantly slowed down with time. In Figure 34a, the pure Pd composition decreased from 18 wt% to 5 wt% in the first 1000 minutes, and then decreased another 1 – 2 wt% over the next 2000 minutes. In Figure 34b, the sample annealed at 550ºC showed that the pure Pd phase was undetectable after 1000 minutes, and in Figure 34c, the sample annealed at 600ºC showed that the pure Pd phase was undetectable after only 300 minutes.

The decrease in the rate of the phase change was due in part to a lessening of driving force as the concentration gradient of Cu in the sample became less steep and also in part to the changing of the increasing barrier to diffusion as the sample alloyed. The Cu-Pd interdiffusion coefficient varied by two orders of magnitude depending on the alloy composition [52]. The value was highest at Cu compositions of roughly 70 wt% and lowest at 0 wt%. Cu had a lower Tamman temperature than Pd (405ºC and 640ºC respectively) and therefore became mobile due to thermal vibrations at lower temperatures than Pd. The result was that Cu diffused into the Pd very quickly but as more Cu diffused into the Pd, more Pd would have to diffuse into the Cu from deeper within the bi-layer where the interdiffusion coefficient would be smaller and the driving force much less.

It should be noted that the penetration depth of the XRD did not encompass the entire depth of the Pd/Cu bi-layer, and the phases detected were limited to those present in the penetration depth shown in Figure 35 which ranged from 5.5 to 8.5 μm depending on the Cu concentration. However, the pure Pd phase present within the penetration depth of the coupons annealed at 550 and 600ºC disappeared while the amount of pure Pd phase present in the coupon annealed at 500ºC decreased very slowly between 1000 – 3000 minutes so that the amount appeared to not change at all.

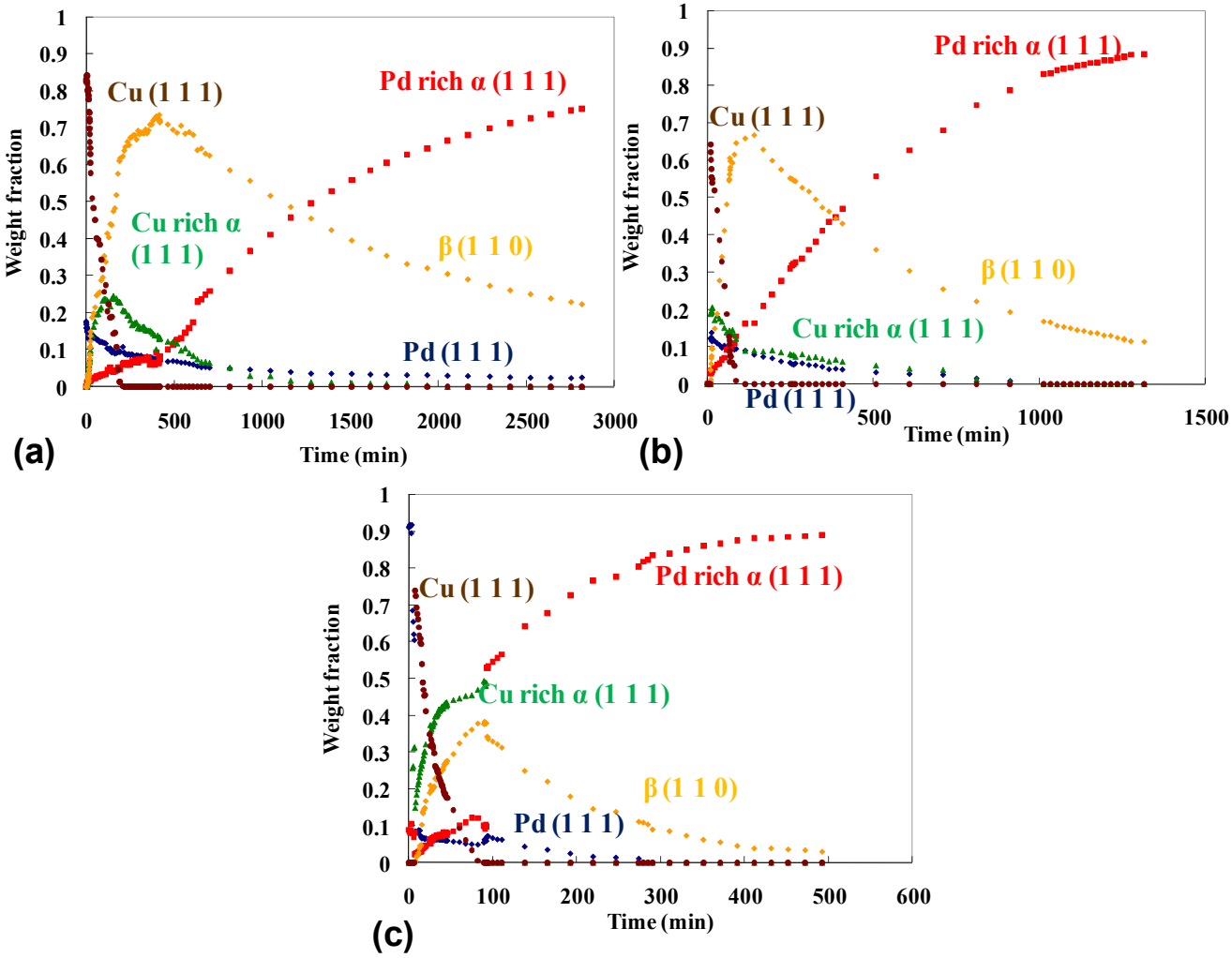

Figure 34. Weight fraction as a function of time for the coupons annealed in H_2 at (a) 500°C, (b) 550°C, and (c) 600°C.

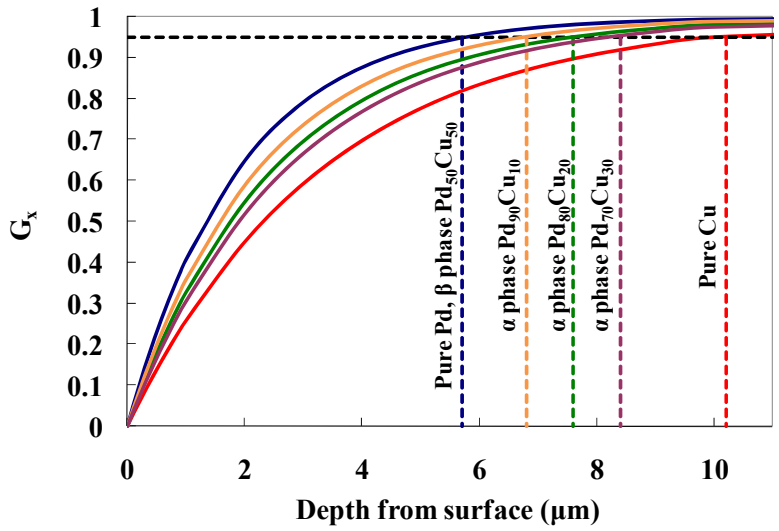

Figure 35. Fraction of the diffracted intensity (G_x) which was contributed by a surface layer of depth x for Pd, Cu and Pd/Cu alloys from the (1 1 1) plane of the FCC lattice structure and the (1 1 0) plane of the BCC lattice structure. Penetration depth shown with dotted lines, taken from $G_x = 0.95$.

As the Cu penetrated farther into the Pd layer, more heat and more time was necessary to allow the Cu to diffuse farther into the layer. At 550 and 600ºC, there was enough thermal energy to increase the diffusivity so that the Pd phase would disappear from the penetration depth. At 500ºC, there was not enough thermal energy to cause the Cu to penetrate farther into the layer, which would explain why the Pd/Cu coupons (Figure 18a and Figure 18b) heated for 5 and 10 hours at 500ºC in H_2 had Cu gradients which were similar to the Cu gradients seen with membranes N_02 and N_03 (Figure 29a and Figure 29b) which were tested at 500ºC in H_2 for several thousand hours. In both cases, the Cu penetrated roughly 4 – 7 µm into the Pd layer.

The slowing down of the diffusion process and consequently the phase transformation between the Pd rich α phase and the β phase is shown in Figure 36a and Figure 36b respectively. At higher temperatures, less of the β phase and more of the Pd

rich α phase was present towards the end of the annealing. In addition, the maximum of the progression of the β phase weight fraction with time decreased with increasing temperature. At 500ºC, the maximum was at roughly 75 wt%, at 550ºC the maximum was at 68% and at 600ºC the maximum was at 40 wt%. The decrease was due to the shape of the phase diagram, shown in Figure 33. The miscibility gap where the β phase formed decreased in width with increasing temperature, resulting in less of the β phase forming at higher temperatures.

The disappearance of the β phase never occurred, even after the lengthy annealing time at 500ºC, or the high annealing temperature at 600°C. Due to the direction of the Cu diffusion, the remaining β phase (the less sulfur-resistant phase) would be on the surface of the sample and in the case of the membrane, exposed to the feed stream. Even though the total concentration of the Pd/Cu bi-layers was roughly 13 wt%, which would place the layer in the Pd rich α phase portion of the Pd-Cu phase diagram at the membrane operating temperatures. The annealing did not suffice to cause the surface of the membrane to be in the Pd rich α phase. Consequently, it was possible that portions of the surfaces, if not the entirety of the surfaces, of the membranes tested in this work were in the less sulfur resistant β phase even though the surface concentrations as detected by EDS were not conducive to the β phase.

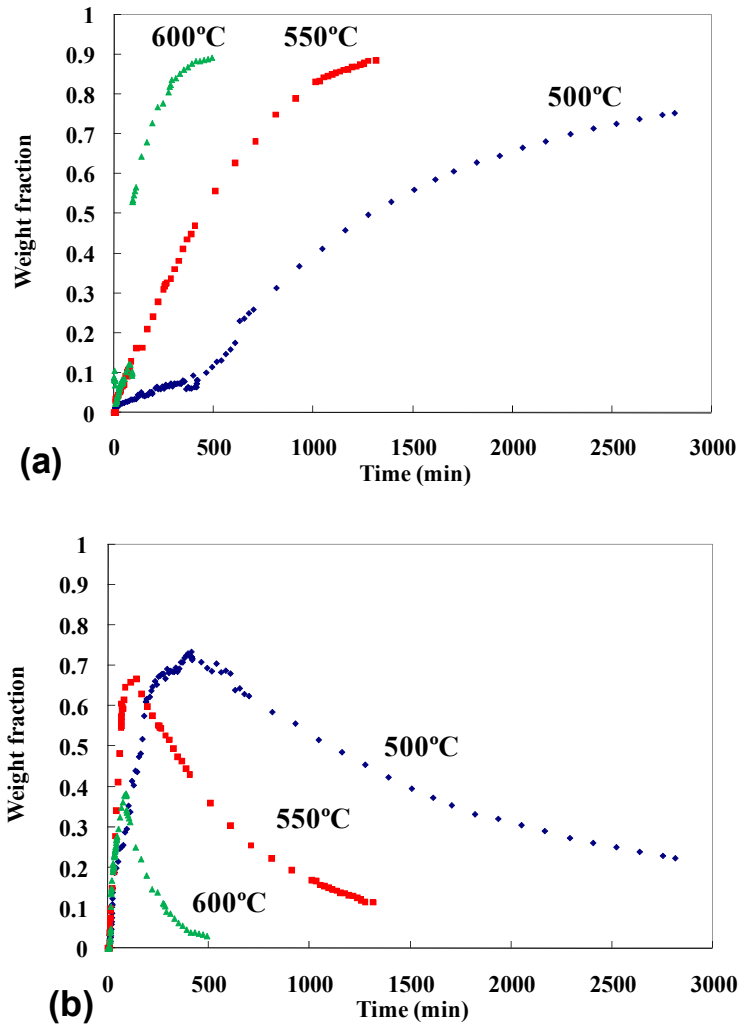

Figure 36. Weight fraction as a function of time for the (a) α phase and the (b) β phase.

Pd/Au studies

Au galvanic displacement plating on Pd

The Pd surface condition was found to be important for the Au displacement plating, and proper pre-treatment of Pd prior to the Au displacement plating could result in more Au deposition. Figure 37 shows the Au content detected by EDS after the displacement plating of the samples that were pre-immersed in three different solutions, 0.01 M HCl, acetone, and water. The pre-immersion of the Pd samples in the 0.01 M HCl solution for 3 minutes showed the most Au deposition compared to those pre-immersed in water or acetone for the same time. The results suggested that the organic and oxide contaminants on the Pd surface could prohibit the displacement reaction, and pre-treating the Pd with acid to remove the contaminants resulted in a better Au displacement reaction.

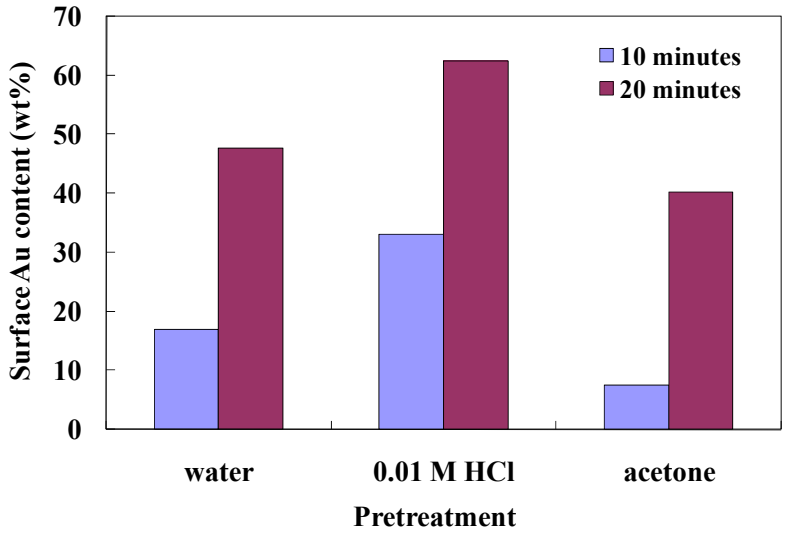

Figure 37. Effect of three pretreatments (i.e. water, 0.01 M HCl, and acetone) on the amount of Au deposited by displacement plating.

Further examination of the effect of pre-treatment with acid on the Au displacement plating showed that higher HCl concentrations (as high as 1 M) and longer immersion time (as long as 3 minutes) in the HCl solution resulted in more Au

deposition, as shown in Figure 38 and Figure 39, which were the ratio of the peaks of the XRD patterns to that of the Pd (1 1 1) peak.

The effect of plating bath conditions, including Au^{3+} concentration, pH, and temperature on the plated Au content was investigated. Figure 40 shows that the Au deposition increased as the Au^{3+} concentration and plating time were increased, as evidenced by the Au content detected by EDS. Furthermore, higher Au^{3+} concentrations not only resulted in more Au deposition but also resulted in a higher deposition rate (the higher slope in Figure 40). Figure 41 shows the effect of the Au^{3+} concentrations on the deposited Au amount. As shown in Figure 41, the deposited Au amount increased as the Au^{3+} concentration was increased but approached asymptotically to a constant value of 85 wt% when the Au^{3+} concentration was greater than 9 mM.

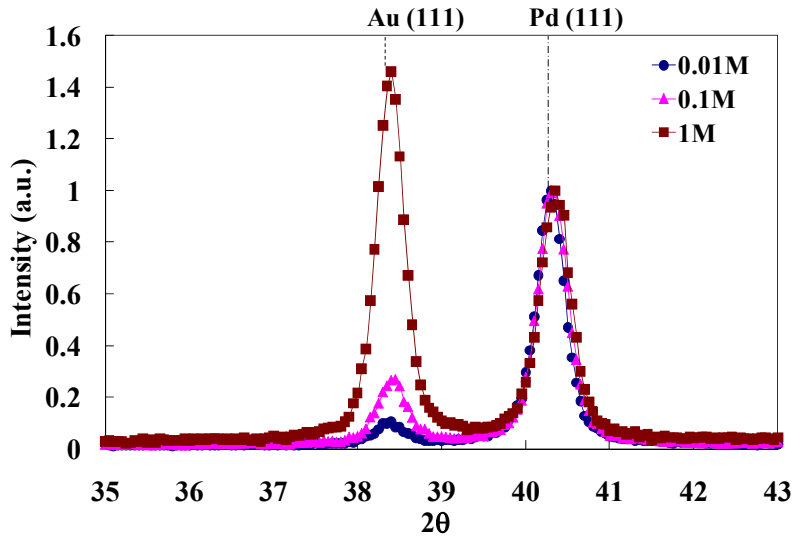

Figure 38. Effect of concentration of pretreatment acid on the amount of Au deposited by displacement plating.

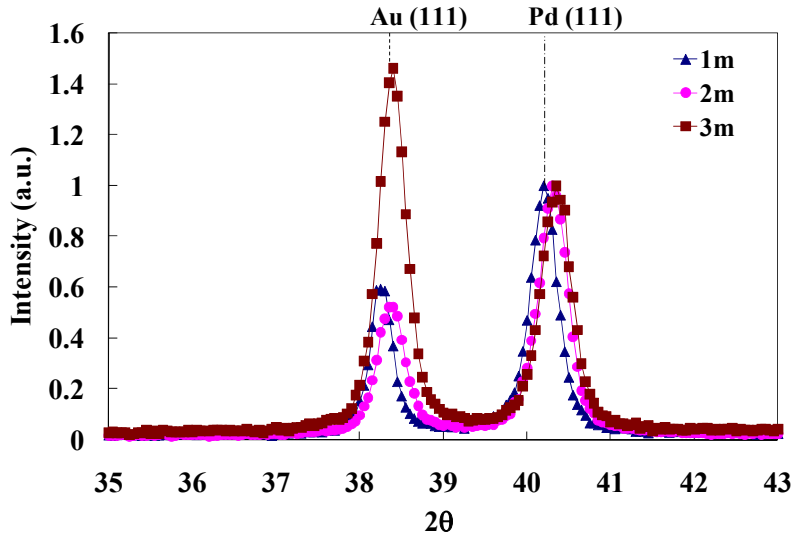

Figure 39. Effect of pretreatment time in acid on the amount of Au deposited by displacement plating.

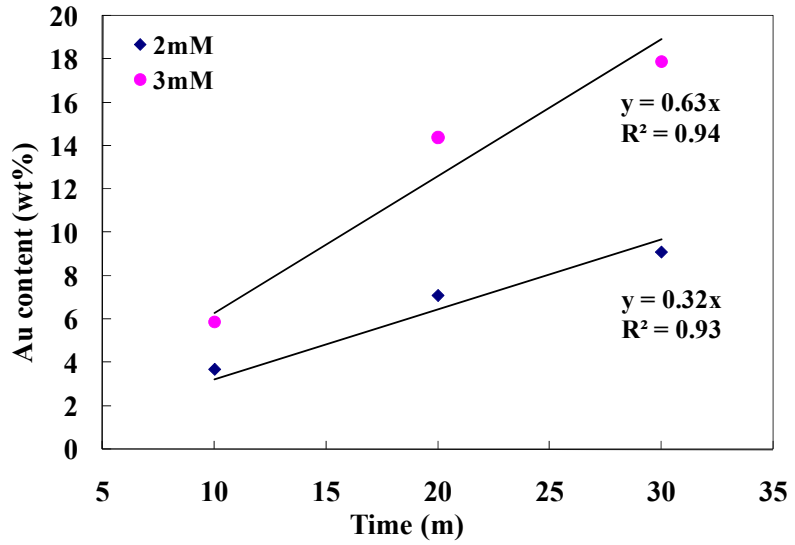

Figure 40. Effect of Au^{3+} concentration and time on the amount of Au deposited by displacement plating.

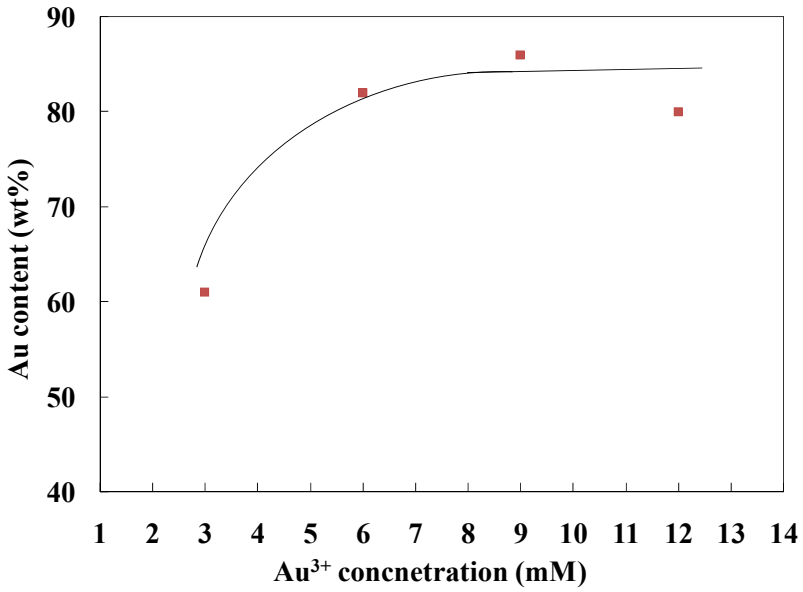

Figure 41. Effect of Au^{3+} concentration on the amount of Au deposited by displacement plating (in the higher Au^{3+} concentration range). The line is for guiding the eye.

Figure 42 shows the Au plating rate as a function of pH. The original pH value of the $Na_2Au(Cl)_4{\cdot}2H_2O$ solution was about 3, and could be altered by adding HCl or NaOH solution. The result showed that the plating rate increased as the pH decreased, as evidenced by both EDS and XRD. Since the mechanism of the displacement plating involved both the reduction of the Au ions and the oxidation of the surface Pd atoms, the lower pH environment resulted in a higher metal oxidation rate and thereby a higher Au plating rate.

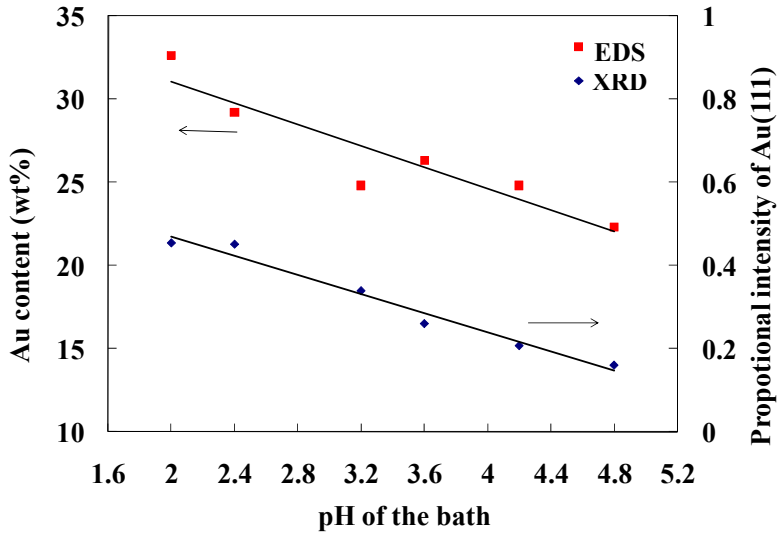

Figure 42. Effect of bath pH on the amount of Au deposited by displacement plating. The lines are for guiding the eye.

Figure 43 shows the temperature effect on the Au displacement plating. EDS analysis yielded that higher temperatures (as high as 60°C) resulted in more Au deposition at a fixed time. This was due to the fact that metals also tended to be oxidized faster at higher temperatures in addition to in higher acidity.

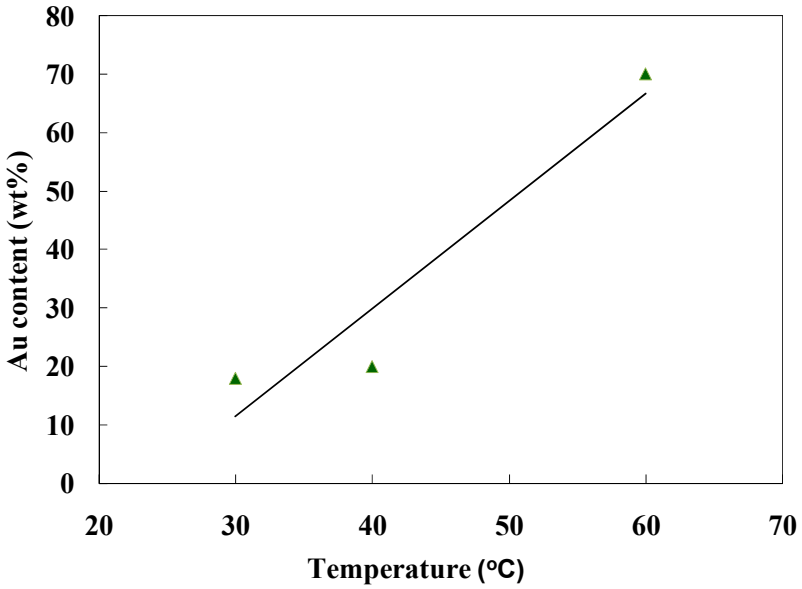

Figure 43. Effect of bath temperature on the amount of Au deposited by displacement plating. The line is for guiding the eye.

The effect of bath agitation on the Au deposit morphology was investigated, and the results are shown in Figure 44. Figure 44 (a) and (c) show the micrographs of the Au deposit without bath agitation, while Figure 44 (b) and (d) show the micrographs of the Au deposit with a stirring rate of 200 rpm. Figure 44 (a) and (b) represented a lower Au content of about 6 – 7 wt%, while (b) and (d) showed a higher Au content of about 36 – 40 wt% on the surface. At both low and high Au contents, the Au deposit without bath agitation was not uniform and the particle size of the Au deposit varied. In contrast, the morphology of the Au deposit which resulted from a bath stirred at a rate of 200 rpm was more uniform, and the Au layer consisted of roughly equal-sized fine particles which covered all over the Pd surface. The diffusional mass transfer resistance in the bath was minimized by stirring while plating and more nuclei were deposited which resulted in a more even growth.

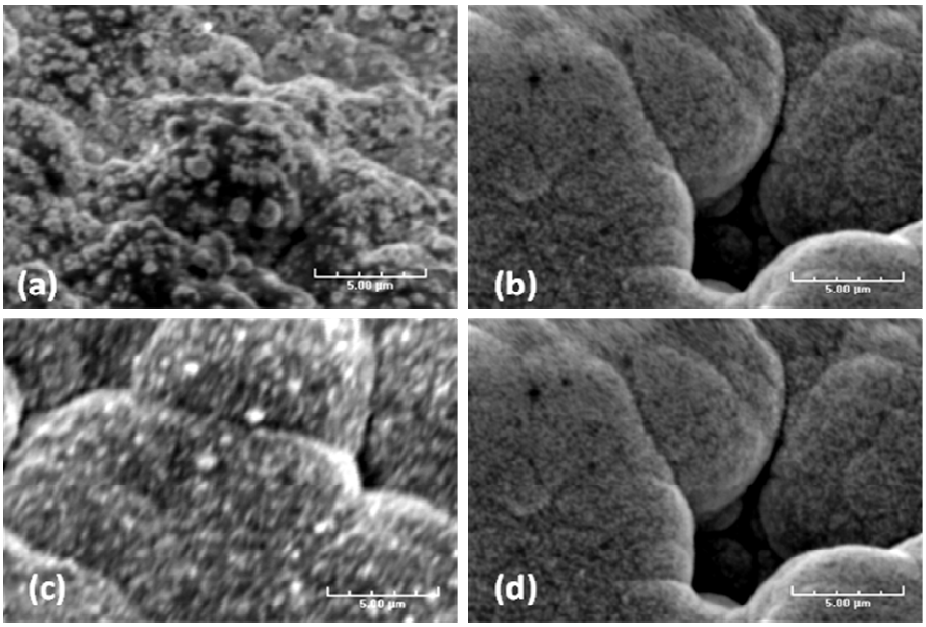

Figure 44. SEM micrographs (5 kX) of the Au deposit of (a) 7 wt% Au, without bath agitation, (b) 6 wt% Au, bath stirring at 200 rpm, (c) 40 wt% Au, without bath agitation, and (d) 36 wt% Au, bath stirring at 200 rpm.

Figure 45 shows the surface morphology of the Au deposit with different stirring speeds from 0 to 600 rpm. The surface Au content of these samples was nearly the same

(40 – 55 wt%) after the fixed plating time of 20 minutes, indicating that the deposited Au amount and the plating rate were not significantly affected by the stirring. The large grain size and non-uniform coverage of Au deposits were easily observed on the samples with a stirring speed equal to or lower than 100 rpm. Therefore, 100 rpm was not sufficient to eliminate the diffusional mass transfer resistance of Au ions in the bath. In contrast, when the stirring speed was equal to or higher than 200 rpm a finer, more uniform Au deposit was observed, indicating that most of the diffusional mass transfer resistance in the bath was minimized at a speed equal to or higher than 200 rpm.

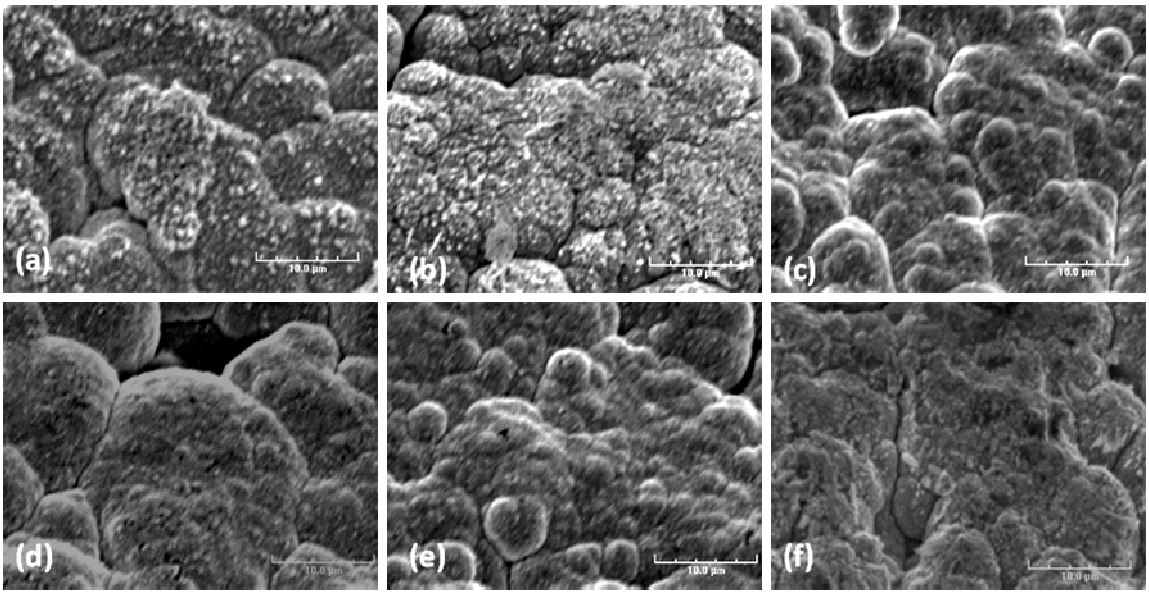

Figure 45. SEM micrographs (3 kX) of the Au deposit (a) without bath agitation, (b) with bath stirring at 100 rpm, (c) with bath stirring at 200 rpm, (d) with bath stirring at 400 rpm, (e) with bath stirring at 500 rpm , and (f) with bath stirring at 600 rpm.

Pd/Au alloy formation

The annealing study was performed by heating the Au deposited Pd coupons in a furnace at different temperatures from 12 to 96 hours in H_2 to study the effect of temperature and time on the formation of Pd/Au alloys. SEM including EDS and XRD analyses were performed to study the surface morphology, composition and the crystal phase change after the annealing.

Figure 46 are the X-ray diffraction patterns of the Pd/Au bi-layers before and after annealing for 12 hours in H_2 at temperatures of 250°C, 400°C, 450°C, 500°C, and 550°C. Before annealing, distinct peaks representing FCC phase Au and Pd from plane (1 1 1), (2 0 0), (2 2 0) to plane (3 1 1) at 2θ of 38.45°, 44.75°, 65.05°, 78.05° , and at 2θ of 40.35°, 47.05°, 68.55°, 82.5° can be easily observed. After annealing, the resultant XRD patterns showed that the degree of the Au/Pd inter-diffusion and alloy formation increased as the annealing temperature was increased, as evidenced by the growth of the FCC alloy peak in between the Pd and Au FCC peaks and the disappearance of the Au peaks. Above 400°C, the pattern clearly showed Pd/Au alloy peaks from plane (1 1 1) to plane (3 1 1). However, a distinct Pd peak was still visible at 500ºC, indicating that the bi-layers had not homogenized within the penetration depth of the XRD. For the pattern representing the sample annealed at 550°C, single alloy peaks were observed indicating more complete inter-diffusion and a thicker Pd/Au alloy layer. However, the asymmetrical peak shape, especially in the higher planes, appeared to show that the incomplete alloy formation still existed. Finally, by comparing the Pd peaks before and after annealing, a narrower peak shape was found for the latter implying that the Pd grains grew and the grain size increased during the annealing.

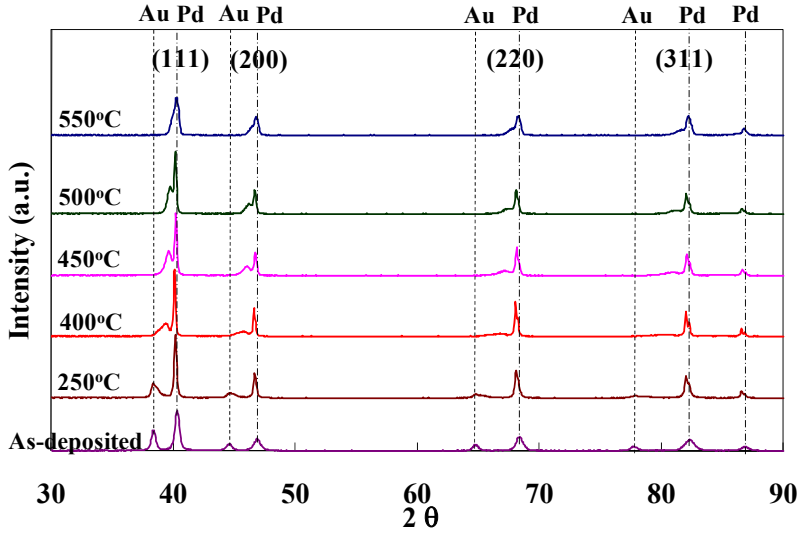

Figure 46. Temperature effect of formation of the Pd/Au alloy for 12 h.

Figure 47 shows the X-ray diffraction patterns of the Pd/Au samples annealed at 500°C in H_2 from 12 to 96 hours. It clearly shows that the degree of Pd/Au diffusion and alloy formation increased as the annealing time increased at the fixed temperature by observing the evolution of the alloying peaks with increasing time. The sample annealed for 48 hours showed the peaks of a single alloy phase, and more symmetrical peaks of the alloy could be observed in the sample annealed for 96 hours, indicating the highly homogenized Pd/Au alloy phase.

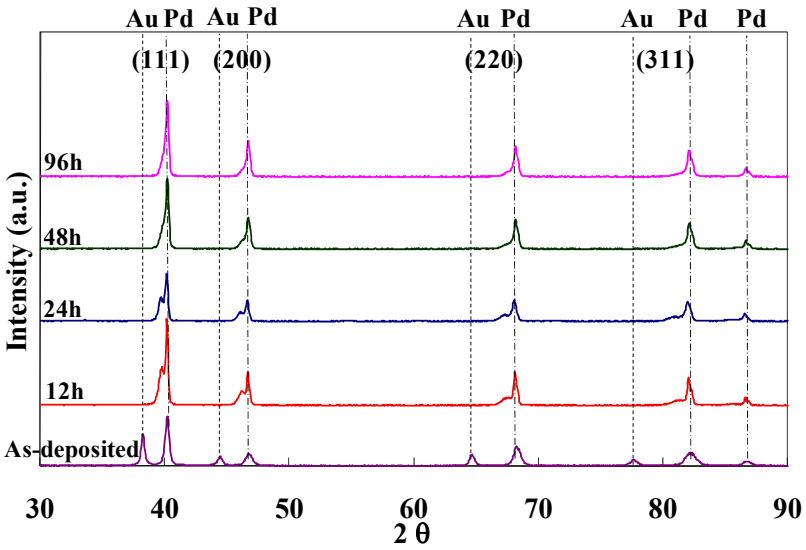

Figure 47. Time effect of formation of the Pd/Au alloy at 500°C.

Figure 48 shows the surface Au content evolution during the annealing process at different temperatures. From the plot, the surface Au weight percentage dropped the most in the first 12 hours at all temperatures indicating that most of the diffusion occurred in this period. In addition, the final surface Au content varied with temperature. Lower annealing temperatures resulted in higher Au weight percentages on the surface indicating that less diffusion occurred and that the alloy formation was less complete, which was in agreement with the XRD results. Figure 49 is the surface Au content after 96 hours of annealing as a function of temperature. As seen in Figure 48, the final surface Au content decreased as the annealing temperature was increased, indicating the increasing inter-diffusion between Pd and Au at higher temperatures. Furthermore, the surface Au content was leveled off at temperatures above 500°C, indicating that the

annealing temperature of 500°C was sufficient to form a homogenous Pd/Au alloy with sufficient Pd/Au inter-diffusion.

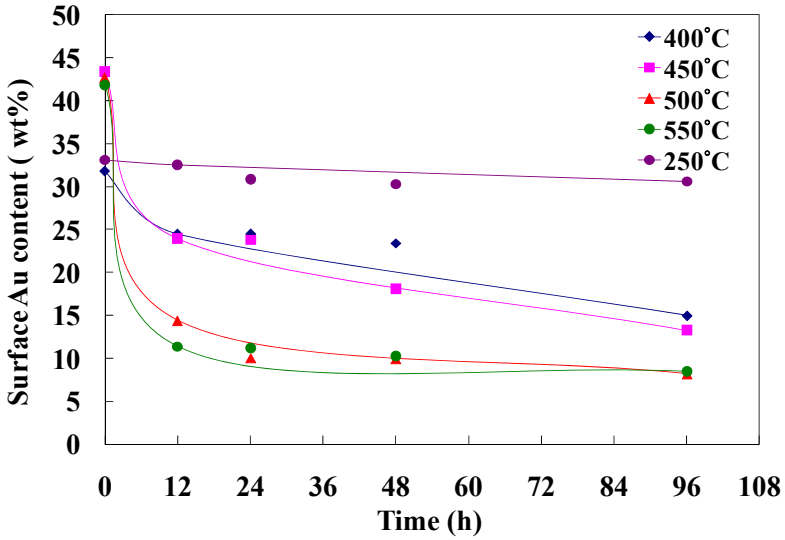

Figure 48. Effect of annealing time and temperature on the surface Au content. The lines are for guiding the eye.

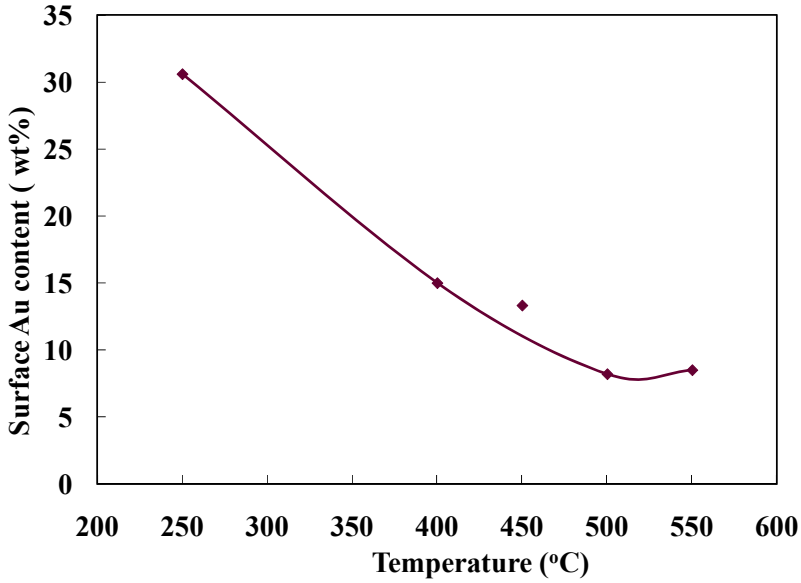

Figure 49. Effect of annealing temperature on the surface Au content. The line is for guiding the eye.

Figure 50 shows the SEM micrographs of the sample surfaces after annealing for 96 hours at different temperatures. The sample before annealing showed numerous small grains on the surface. After annealing, the degree of morphology change increased as the temperature was increased. The surface morphologies of the samples annealed below 450^{o}C showed only minor changes with a slightly larger grain size, while the samples annealed above 500^{o}C showed siginificant rounder and more flat grain shapes with several pinholes on the surface. The result indicated that intense growth and coarsening occurred during annealing process at temperatures above 500^{o}C.

Figure 51 shows the morphologies of the samples annealed at 500^{o}C for different time periods. The results show that the morphology changed as the annealing time was increased. The grains on the surface were larger and rounder as the annealing time increased, and all grains were coarsened together resulting in a flat surface with several pinholes after 96 hours of annealing.

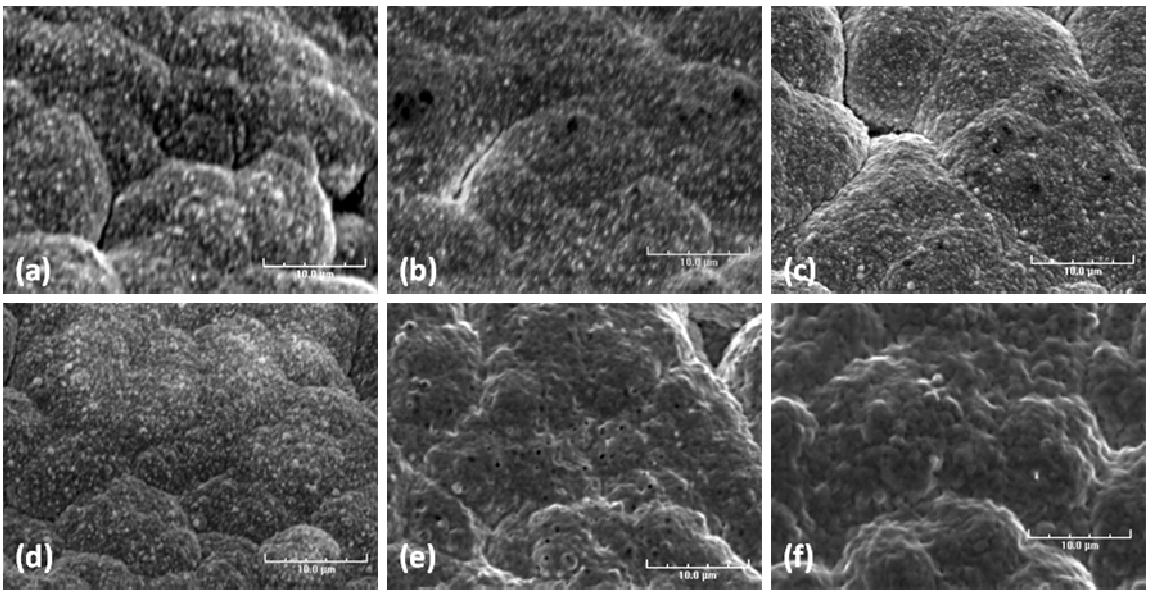

Figure 50. SEM micrographs (3 kX) of the annealed Pd/Au bi-layers for 96 hours at (a) as-deposited, (b) 250^{o}C, (c) 400^{o}C, (d) 450^{o}C, (e) 500^{o}C, and (f) 550^{o}C.

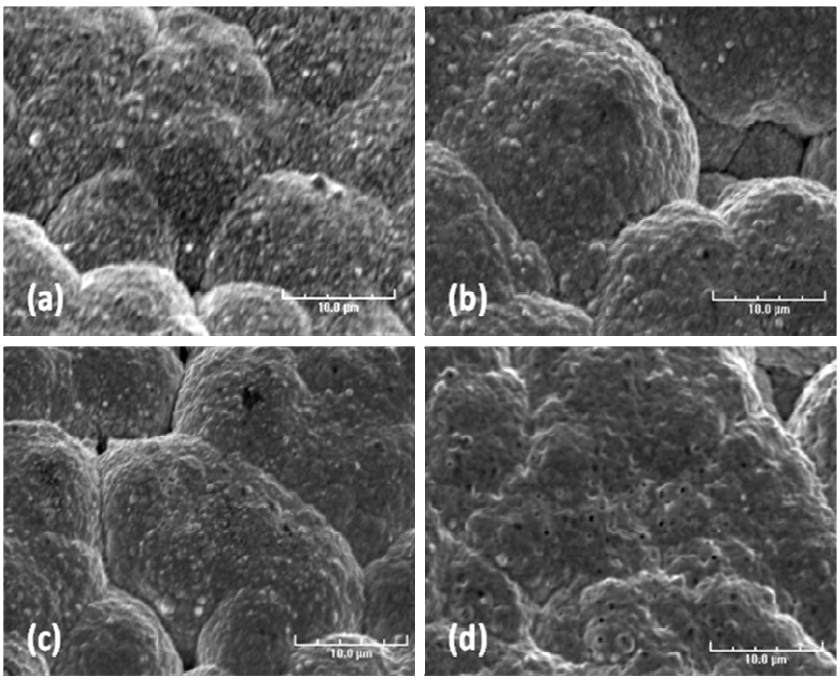

Figure 51. SEM micrographs (3 kX) of the annealed Pd/Au bi-layers at 500^{o}C for (a) as-deposited, (b) 24 hours, (c) 48 hours, and (d) 96 hours.

Figure 52 shows the cross sectional SEM micrographs coupled with EDS line scans of the samples annealed at 450^{o}C and 500^{o}C for 96 hours. The line scan results showed the diffusion of Au into the Pd layer. The higher Au content observed in the concentration gradient in the sample after annealing at 450^{o}C than that observed at 500^{o}C once again suggested the higher degree of Pd-Au inter-diffusion at higher temperatures.

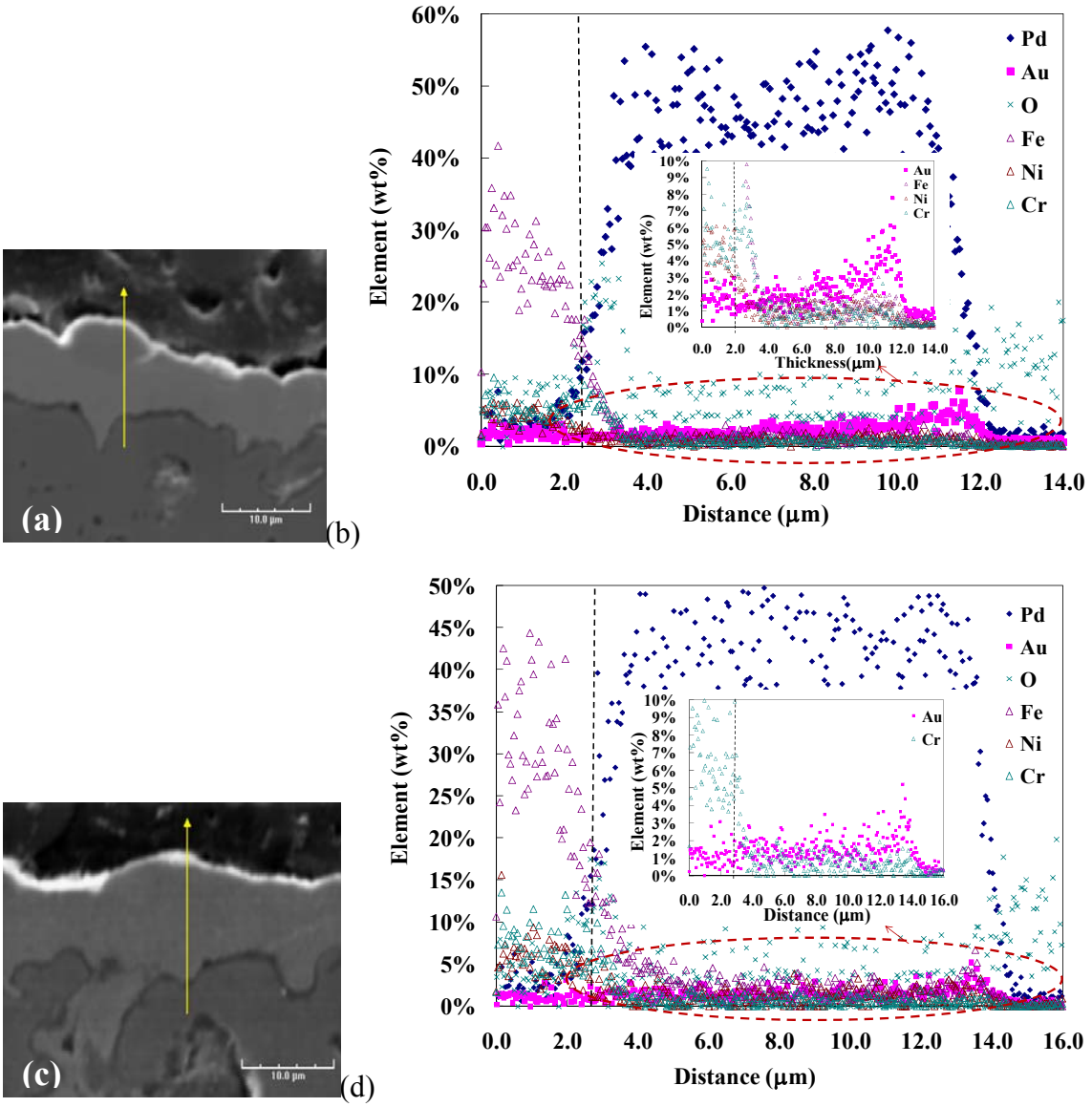

Figure 52. Cross sectional SEM micrographs (3 kX) of Pd/Au bi-layers annealed for 96 hours at (a) 450°C and the corresponding line scan (b); (c) 500°C and the corresponding line scan (d) (The dotted line in the line scans represent the interface between the selective layer and oxidized support).

Pd/Au membrane fabrication and characterization

Two Pd/Au membranes, C_03 and C_05, were prepared for characterization. The details of the preparation are summarized in Table 3**.** Figure 53 shows the appearances of C_03 and C_05 after the final Au deposition.

Table 3. Pd/Au membranes investigated.

membrane	intermetallic diffusion barrier	grading	membrane thickness (μm)	bath agitation?	Au wt%
C_03	Calcination 10 hours at 550 ºC	Al_2O_3 slurry	17.5	no	3 - 5
C-05	oxidized 12 h at 700°C	Al_2O_3 slurry, Pd/Ag barrier	16.4	200 rpm	5 - 8

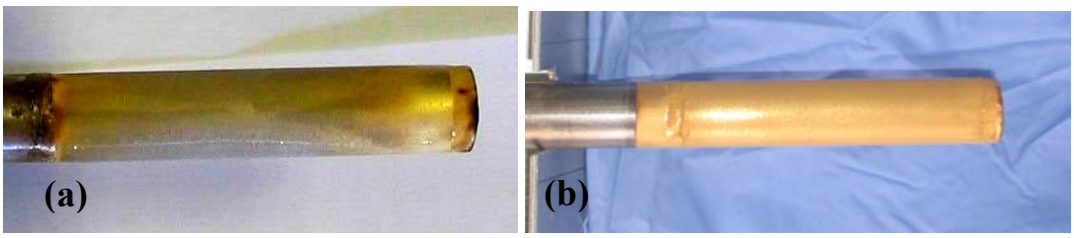

Figure 53. Appearances of (a) C_03, and (b) C_05.

Figure 54 shows the H_2 flux as a function of the difference of the square root of the high and low pressure for C_03 at temperature of 250 - 400°C according to Sieverts' equation. A linear regression was used to calculate the permeance of C_03 which was 13.6 $m^3/(m^2*h*atm^{0.5})$ at 250°C and increased as temperature increased to 31.5 $m^3/(m^2*h*atm^{0.5})$ at 400°C. Similarly, Figure 55 shows the Sieverts' plot for the temperature range of 250 – 450°C for C_05. The permeance of C_05 was 22.3 $m^3/(m^2*h*atm^{0.5})$ at 250°C and increased to 41.2 $m^3/(m^2*h*atm^{0.5})$ at 450°C.

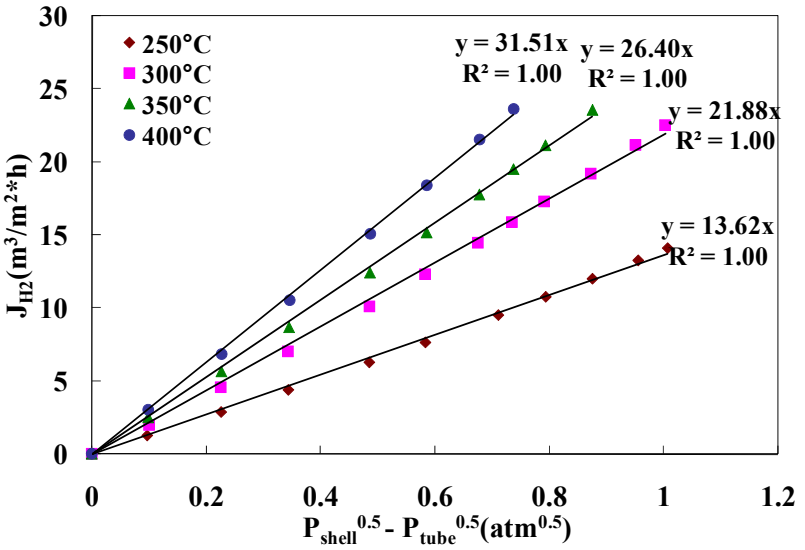

Figure 54. Sieverts' plot of C_03 at temperature of 250°C to 400°C.

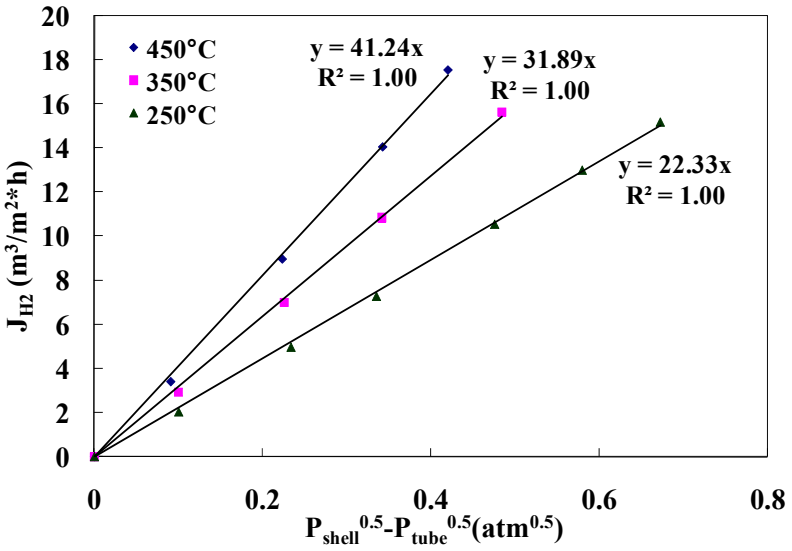

Figure 55. Sieverts' plot of C_05 at temperature of 250°C to 450°C.

Figure 56 and Figure 57 show the Arrhenius dependence of the H_2 permeance on temperature for C_03 and C_05 respectively. For the purpose of comparison, Figure 56 and Figure 57 also included the calculated permeance for pure Pd films of the same thickness and the measured values adjusted for the effect of mass transfer resistance of the support and grading layers. The mass transfer resistance of the support only slightly

affected the permeance of the deposited layers of C_03 and C_05 (the support resistance accounted for about 12% of the total resistance for C_03 at 400°C and 11% for C_05 at 450°C respectively). The figures show that the permeances of C_03 and C_05 were much higher than those of pure Pd films of the same thickness. The permeance of C_03 was about 50% higher than that of a pure Pd foil, while the permeance of C_05 was about 60% to 100% higher than that of a Pd foil if the mass transfer effects caused by the supports were considered. Grayznov [11] reported that the hydrogen permeance of the Pd/Au alloys with 5 - 20 wt% Au were twice of those of pure Pd foils at 500°C. The lower permeance of the Pd/Au layer of C_03 might be due to the lower Au content (less than 5 wt%) in the membrane. Furthermore, the activation energies for the H_2 permeation of C_03 and C_05 determined by the Arrhenius equation were lower than that of the freestanding Pd films, as expected from the higher values of permeance for Pd/Au alloys. Table 4 summarized the permeance data and activation energies of C_03 and C_05.

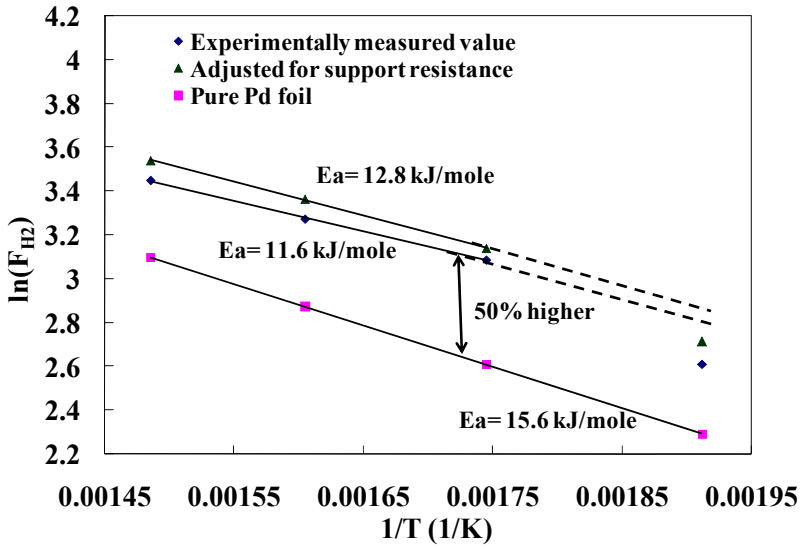

Figure 56. Arrhenius dependence of the H_2 permeance on temperature for C_03.

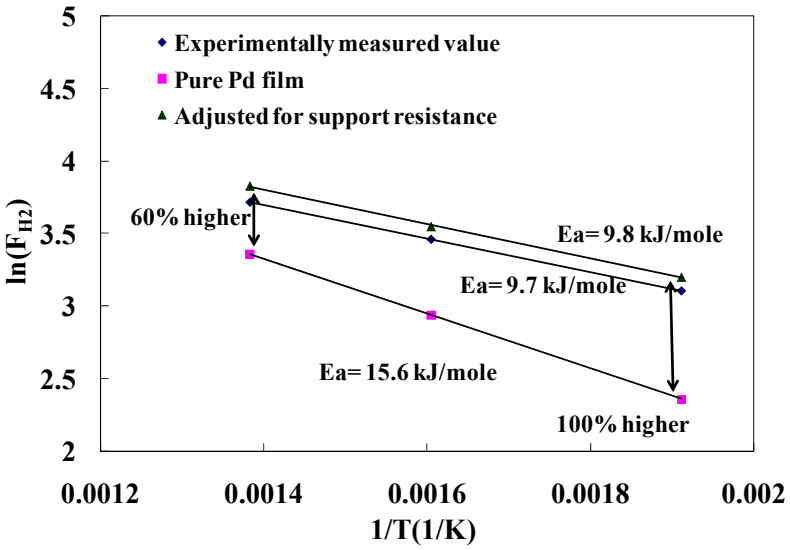

Figure 57. Arrhenius dependence of the H_2 permeance on temperature for C_05.

The higher H_2 permeances and lower activation energies of the Pd/Au membranes were believed to be the result of the Pd/Au alloy formation. In addition, a higher permeance was seen in C_05 which had a higher Au content.

Table 4. Permeance data for C_03 and C_05.

membrane	F_{H2} at 250°C ($m^3/m^2*bar^{0.5}*h$)	F_{H2} at 350°C ($m^3/m^2*bar^{0.5}*h$)	F_{H2} at 400°C ($m^3/m^2*bar^{0.5}*h$)	F_{H2} at 450°C ($m^3/m^2*bar^{0.5}*h$)	Ea (kJ/mol)
C_03	13.1	25.5	30.8	-	12.7
C_05	22.3	31.9	-	41.2	9.8
Pd foil (16.4 μm thick)	10.6	18.9	-	28.8	15.6

Figure 58 shows the long term testing of C_03. The permeance was relatively stable for about 1000 hours for temperatures up to 400°C indicating the high thermal stability of the membrane structure. No intermetallic diffusion occurred during the long term testing at the elevated temperatures. Similar stability tests were also performed on

C_05, and the result is shown in Figure 59. A stable permeance without any decline was found in C_05 after 450 hours of testing for temperatures up to 450°C.

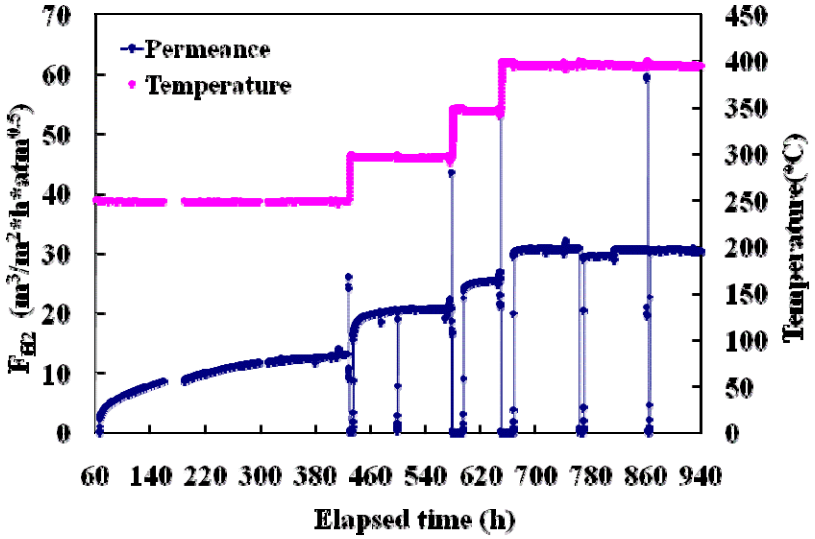

Figure 58. H_2 permeance history of C_03 at elevated temperatures.

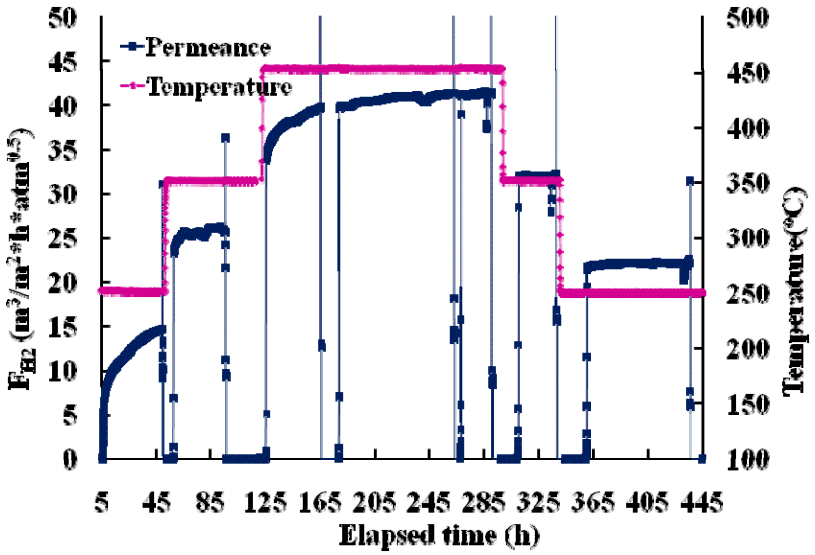

Figure 59. H_2 permeance history of C_05 at elevated temperatures.

Figure 60 and Figure 61 show the He leak flow rate and ideal H_2/He separation factors of C_03 and C_05 as a function of time and temperature for the duration of the testing periods. Although both C_03 and C_05 showed long term thermal stability within

the membrane structure without intermetallic diffusion between the H_2 selective layer and the support as stated earlier, small He leaks developed with increasing time and temperature due to the grain growth of the selective layers. In addition, after 200 hours at 450ºC, the He leak increased with decreasing temperature in the case of C_05 (as shown in Figure 61) because the permeance of non-permeable gases through cracks and defects was inversely dependent on temperature, as described by the dusty gas flow model.

The ideal H_2/He separation factor of both membranes increased with temperature during the first half of testing due to the increase in the permeance from the Pd/Au alloy formation, even though the He leak continued to increase. However, the stable permeance of C_05 at 450ºC coupled with the increasing He leak caused a decrease in the ideal H_2/He separation factor over time during the latter half of the testing.

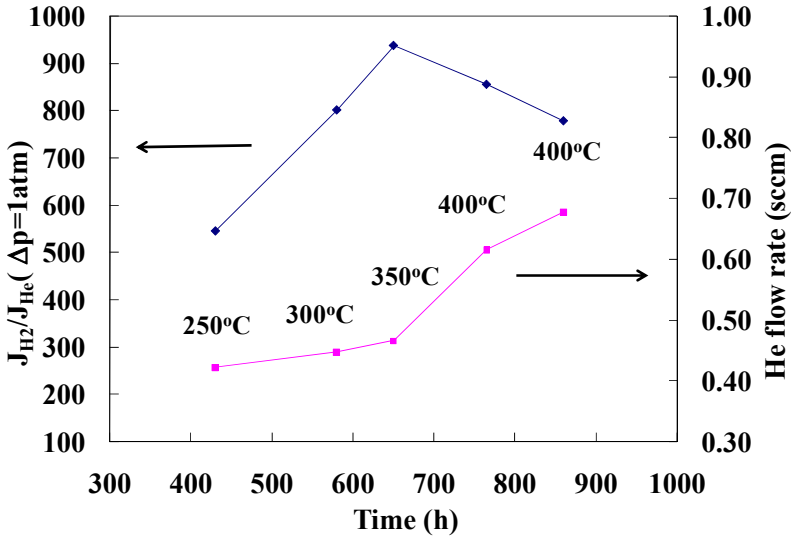

Figure 60. He flow rate and ideal H_2/He separation factor as a function of time and temperature of C_03. The lines are for guiding the eye.

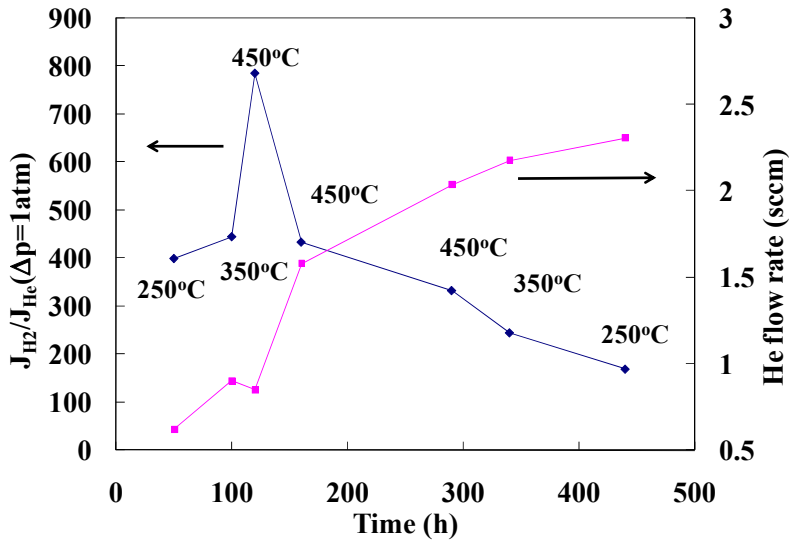

Figure 61. He flow rate and ideal H_2/He separation factor as a function of time and temperature of C_05. The lines are for guiding the eye.

Pd/Au membrane testing in H_2S

The Pd/Au alloy membrane, C_04 was prepared identically to C_05, and characterized in pure H_2 and He at the temperatures of 250°C to 550°C prior to the sulfur poisoning tests for over 2000 hours. C_04 was re-deposited with Pd and Au and re-characterized twice before the H_2S characterization. The thickness of C_04 was estimated to be 18 μm with roughly 10 wt% Au content. C_04 showed a steady state hydrogen permeance of 1.2 $m^3/(m^2*h*atm^{0.5})$ at 250°C and increased to 6.5 $m^3/(m^2*h*atm^{0.5})$ at 500°C with an activation energy for H_2 permeation of 13.1 kJ/mol. The unreasonably low H_2 permeance observed on C_04 was considered to be caused by contaminations during the fabrication, which needed to be further confirmed with SEM, EDS and XRD. A stable ideal H_2/He separation factor of 100 with a He leak rate of 0.55 ml/min at 400°C was observed after the long period of characterization.

The gas permeation characterization in the presence of 54.8 ppm H_2S was then performed on C_04, and the resultant H_2 permeation history before and after the H_2S exposure is shown in Figure 62. The result showed that the H_2 permeance also dropped sharply right after the H_2S introduction (the period after the first dashed line shown in

Figure 62). However, the permeance reached a steady state value within a few minutes without continuing to decline. The result suggested only one dominant poisoning mechanism occurring on the Pd/Au alloy membrane, which was the rapid surface adsorption and blocking of the sites for hydrogen dissociation.

Furthermore, the H_2 permeance could be recovered to some extent when re-introducing the pure H_2 to C_04 at the same temperature (the period after the second dashed line shown in Figure 62), indicating that the sulfur effect on C_04 was reversible to some extent. Moreover, Figure 63 shows that after further recovering at 500°C in pure H_2, the final H_2 permeance of C_04 at 400°C was 97% of the original permeance at 400°C. The almost full recovery suggested that the poisoning effect on Pd/Au alloy membrane was reversible and the higher recovery rate could be obtained at higher temperatures due to the desorption of the H_2S molecules.

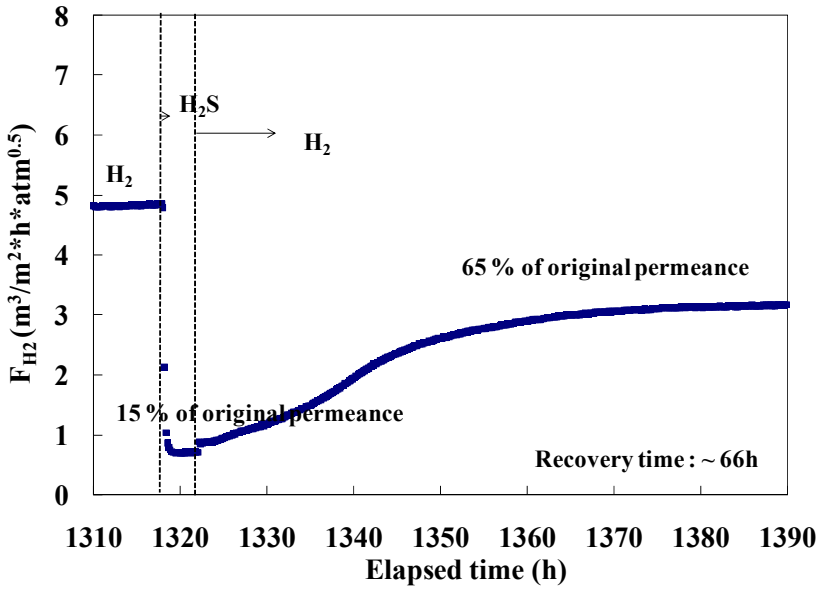

Figure 62. Effect of H_2S on H_2 permeance at 400°C of C_04.

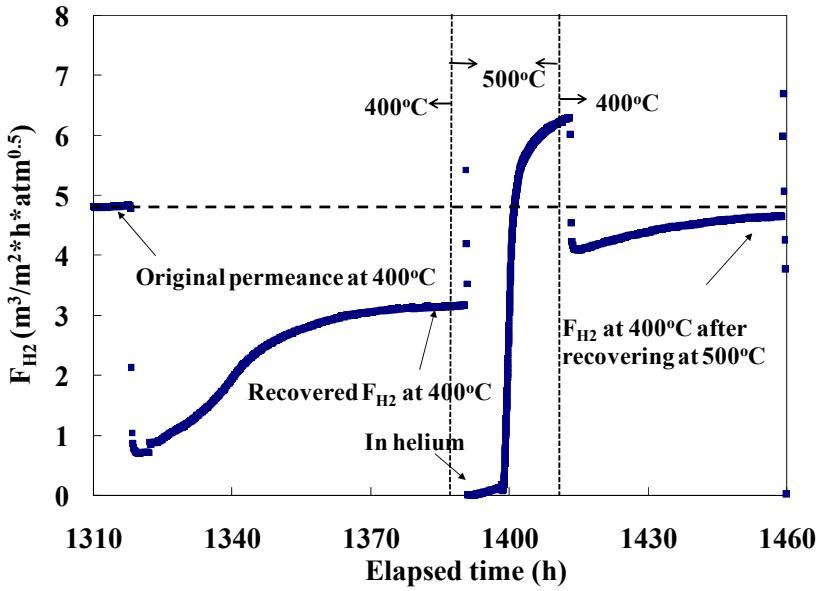

Figure 63. Permeance recovery of C_04 after recovering at 500°C.

The same poisoning/recovering tests have also been performed on C_04 at other temperatures. Figure 64 shows that the percentage of permeance decline during the H_2S exposure decreased as the temperature was increased, from 88% at 350°C, 85% at 400°C, 74% at 450°C, to 60% at 500°C. The extent of recovered permeance increased as the temperature was increased from 43% of the original value at 350°C, 65% at 400°C, 74% at 450°C, and ~100% at 500°C. The results suggested that the higher desorption rate of the H_2S molecules at higher temperatures resulted in less sulfur adsorption on the membrane surface, resulting in less sulfur poisoning effect on the membrane at higher temperatures.

By comparing the result with that of the Pd/Cu membranes discussed in Section 3.2.3, the permeance change during the poisoning and recovery of the Pd/Au membrane appeared to show a stronger temperature dependence than the Pd/Cu membrane. Each poisoning/recovery characterization of the Pd/Au membrane was conducted after the permeance was almost fully recovered at 500°C from the previous poisoning test, while the Pd/Cu membrane was characterized without a full recovery at higher temperatures between each exposure. As a result, the temperature effect of the Pd/Cu membrane might include the accumulated effect of the previously adsorbed H_2S, accounting for the difference between the results of the Pd/Cu and the Pd/Au membranes.

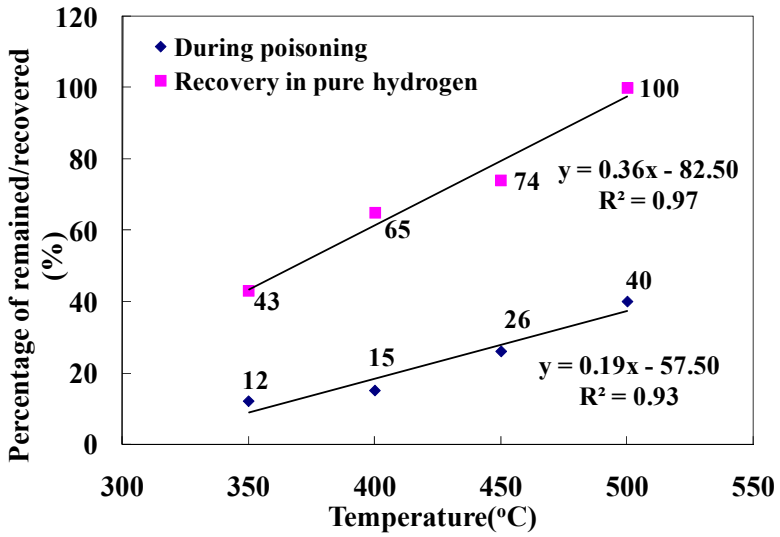

Figure 64. Temperature effect on H_2 permeance remained and recovered.

In Figure 62, three stages of the permeance recovery were observed consisting of instantaneous, linear, and slower (non-linear) recovery, similar to the three stages observed with the Pd/Cu alloy membranes discussed in Section 3.2.3. Among the three stages, the linear stage of permeance recovery was the most interesting because most of the permeance was recovered during this stage. Figure 65 summarized the linear recovery rate for the temperatures of 400°C to 500°C and the result clearly showed the faster permeance recovery at higher temperatures (the higher slopes in the plot). The recovery of H_2 permeance was due to the desorption of H_2S and the faster H_2 permeance recovery at higher temperatures represented higher H_2S desorption rate. From the linear desorption rate obtained at different temperatures, the activation energy of desorption was estimated to be 71 kJ/mol by the use of the Arrhenius relation, which suggested the partial physical and partial chemical adsorption of H_2S. Figure 66 shows the He leak flow rate at 500°C through the entire H_2S characterization period, which showed no significant increase (the He leak even decreased) after the sulfur exposures over a long testing time, indicating that the structure of the Pd/Au alloy membrane remained nearly unchanged after the H_2S exposures. The He leak flow rate in Pd/Cu membranes discussed in Section 3.2.3 also decreased after the long term characterization in H_2S, which was believed to be the result of sulfur segregation to the grain boundaries in the Pd/Cu layers.

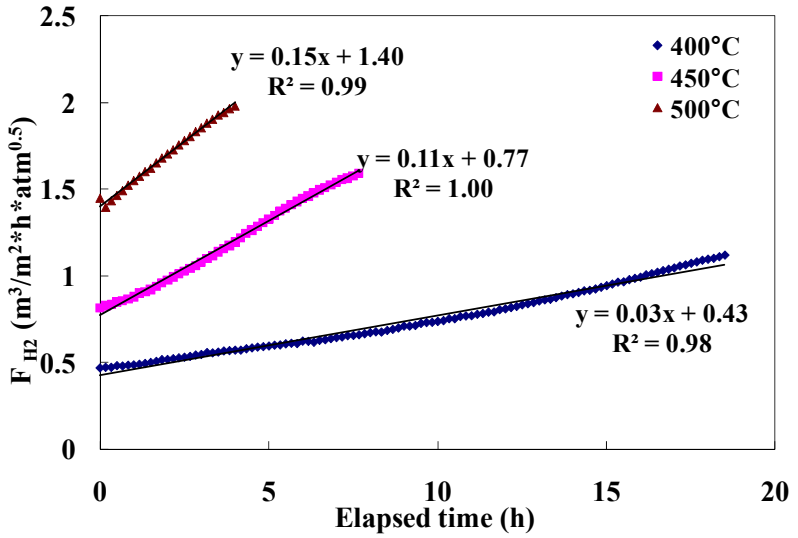

Figure 65. Linear H_2 permeance increase during the recovery.

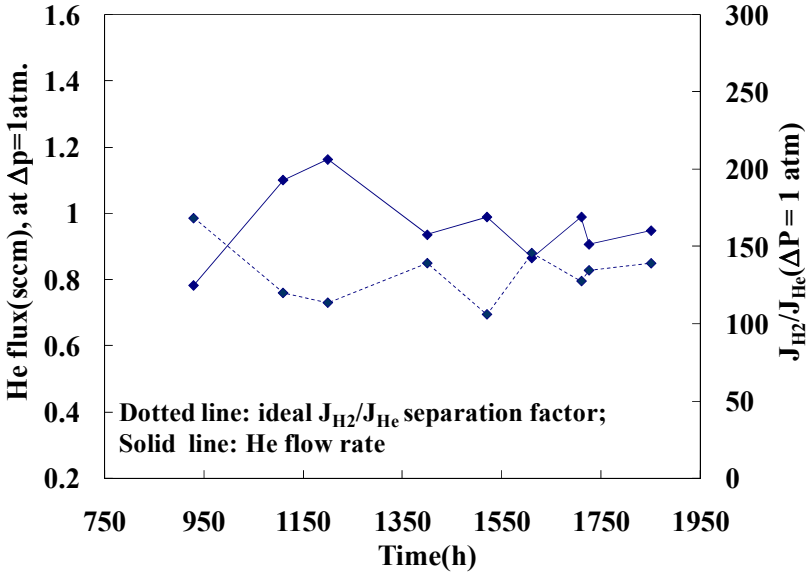

Figure 66. He flow rate and ideal H_2/He separation factor history of C_04 at 500°C during the entire H_2S characterization period. The lines are for guiding the eye.

Further characterization of the effect of H_2S exposure time on the permeation characteristics of C_04 was also carried out and the result was plotted in Figure 67. The H_2 permeance relative to its original value prior to each H_2S exposure was used in the plot. C_04 was exposed to a 54.8 ppm H_2S/H_2 gas mixture at 400°C for 4, 8, 12, and 24

hours. Each H_2S exposure was performed after the H_2 permeance had been recovered to almost 100% at 500°C, thereby preventing an increase in the irreversible poisoning with time as seen with the Pd/Cu membranes which were not recovered at 500°C between each exposure to H_2S. The result showed that the exposure time did not affect the percentage of permeance decline during the exposure. However, the recovery rate (the slopes in Figure 67) in pure H_2 afterwards was slower after longer exposure times, and the time required to reach the stable permeance at the same exposure temperature was longer.

Similar phenomena were also observed on the Pd/Cu membranes discussed in Section 3.2.3. The Pd/Cu membrane exposed to a 54.2 ppm H_2S/H_2 gas mixture at 450°C for 125 hours showed the same permeance decline of about 80% compared to the Pd/Cu membrane exposed to a H_2S/H_2 gas mixture of the same concentration at the same temperature for only 2 hours. Furthermore, increasing recovery time and less recovered permeance were also observed with the Pd/Cu membrane after longer exposure times. Longer recovery time and less recovered permeance observed on the Pd/Au membrane after longer exposure time without attempting recovery at higher temperatures (e.g., 500°C might be the irreversible poisoning part on the membranes increased as the exposure time was increased as discussed in Section 3.2.3. Kulprathipanja *et al.* [5] concluded from the poisoning results of the Pd/Cu membranes with 50 – 300 ppm H_2S/H_2 feeds that the degree of poisoning and the permeance decline depended on H_2S concentration but not exposure time, which was in agreement with the results of both Pd/Cu and Pd/Au membranes described in the present study. However, Kulprathipanja *et al.* did not further examine the effect of exposure time on permeance recovery. Finally, higher permeance recoveries of the Pd/Au membrane in shorter times in comparison to the Pd/Cu membranes were observed, which was possibly due to longer exposure times (up to 250 hours) of the Pd/Cu membrane and recovering the permeance of the Pd/Au membrane at 500°C prior to each characterization.

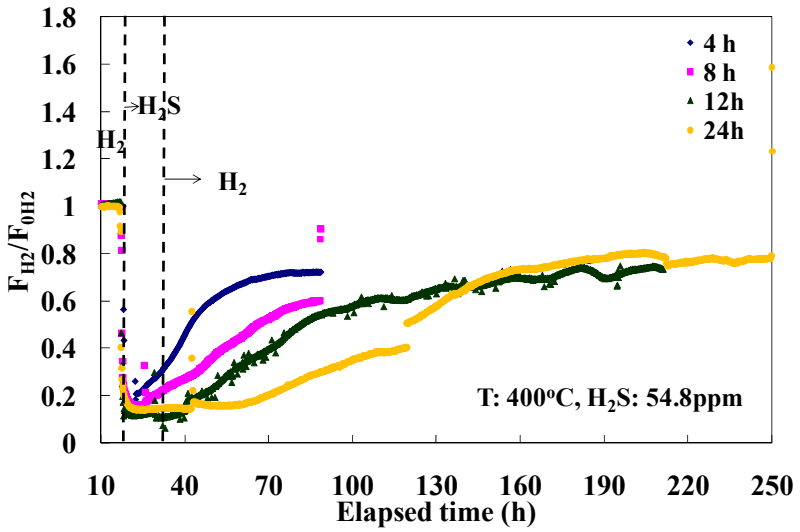

Figure 67. Time effect on H_2S poisoning of C_04 at 400°C.

Figure 68 shows the Arrhenius dependence of the H_2 permeance on temperature for C_04 before and after the H_2S characterization for over 3000 hours (accumulated time in H_2S exposure was over 72 hours). The result showed that the H_2 permeance decreased slightly after the H_2S exposure for a long period of time from 6.1 $m^3/(m^2*h*atm^{0.5})$ to 5.3 $m^3/(m^2*h*atm^{0.5})$ at 450°C. In addition, the activation energy for hydrogen permeation increased from 13.1 kJ/mol to 15 kJ/mol. The slight decrease of the hydrogen permeance coupled with the slight increase of the activation energy indicated the minor property change of C_04 after the H_2S exposures, which was believed to be due to minor irreversible interactions on the surface between the adsorbed sulfur and the Pd/Au alloy. The increase of the activation energy for hydrogen permeation might have been caused by an increase in the energy barrier for hydrogen dissociative adsorption on the Pd/Au alloy surface which was caused by the adsorbed sulfur atoms. Wilke and Scheffler [53] have performed theoretical calculations showing that the hydrogen dissociation path on the Pd surface was non-activated (no activation energy barrier), and would become an activated process when sulfur atoms were adsorbed on Pd surface.

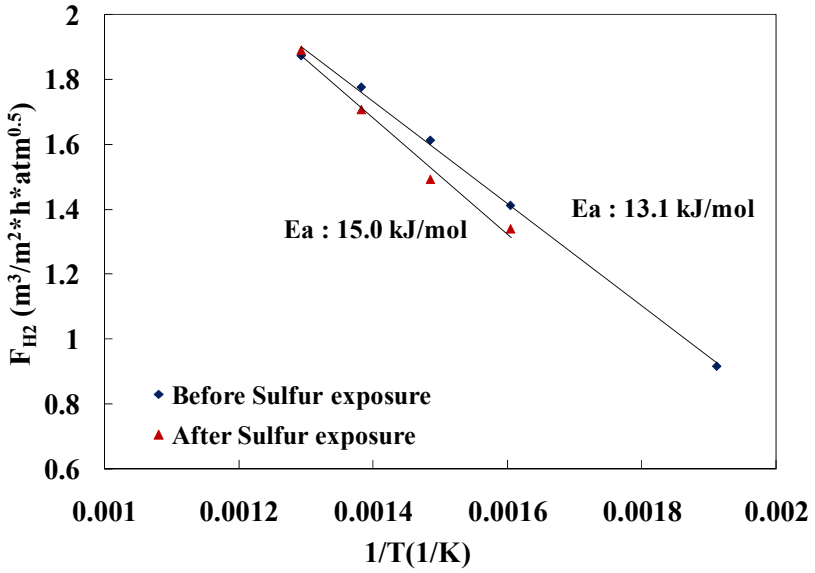

Figure 68. Activation energy for H_2 permeation of C_04 before and after the H_2S exposures.

Conclusions

Pure Pd

Exposure to 50 ppm H_2S/H_2 mixtures at lower temperatures caused bulk sulfides to form on the pure Pd coupons while higher temperatures only caused the dissociative chemisorption of H_2S to form surface sulfides with the Pd.

The lattice rearrangement from the Pd to the bulk sulfide caused drastic morphology changes which would cause irreparable damage to a membrane. Indeed, the permeance decline of the Pd membrane during exposure to the H_2S/H_2 mixture was completely irreversible and the Pd layer lost the selective properties due to bulk sulfide formation rendering the membrane useless.

While longer exposure times and higher H_2S concentrations resulted in higher degree of sulfidation, the dissociative chemisorption of H_2S on the Pd decreased at higher temperatures due to the exothermic nature of H_2S adsorption.

Pd/Cu

The Pd/Cu membranes were tested over a period of several thousand hours between the temperatures of 250 - 500ºC with many cycles between H_2 and He atmospheres. With the exception of the membrane with the 0.5 μm Ru intermetallic diffusion barrier, the H_2 permeance of the membranes was stable for the duration of the long-term testing period.

The exposure of the membranes to 45 – 55 ppm H_2S/H_2 resulted in a significant decrease in hydrogen permeation due to sulfur adsorbing on the membrane surface. Contrary to the results from the pure Pd studies, the hydrogen permeance could be mostly regenerated in pure H_2 with the amount recovered and the rate of recovery increasing with increasing

temperature due to the exothermic nature of H_2S adsorption and the increasing rate of desorption with temperature.

The irreversible poisoning was due to irreducible surface sulfides which reduced the effective membrane area for hydrogen adsorption. The amount of the irreducible surface sulfides increased with increasing exposure time and decreasing temperature.

Throughout the testing period, the Pd/Cu membranes retained their selective properties. The He leak of the Pd/Cu membranes oscillated and even decreased over time following the initiation of the H_2S testing, most likely due to sulfur segregating to grain boundaries and defects and reducing the area of the pathway for non-permeable gases.

Annealing times and temperatures may not have been sufficient to have the surface of the membranes in the Pd rich α phase and less Cu should be used, both to increase the permeance and to increase the sulfur resistance.

In the event of 50 ppm H_2S/H_2 reaching the Pd/Cu membranes, the membranes would not necessitate replacement, and might only suffer a minor loss in permeance depending on the length of exposure. Flushing the membrane with pure H_2 at high temperatures would regenerate the majority of the permeance.

Pd/Au

Pre-treating the Pd surface with 0.1 M HCl, increasing the acidity and temperature of the displacement bath and increasing the concentration of $NaAu(Cl)_4 \cdot 2H_2O$ resulted in a faster displacement rate and higher Au content in the Pd/Au bi-layer.

Stirring the Au displacement bath resulted in a more uniform deposition morphology on the Pd layer, but the displacement rate did not appear to be affected by the stirring as long as the rate is equal to or greater than 200 rpm.

Higher annealing temperature and longer time resulted in more complete Pd/Au inter-diffusion and alloy formation. Annealing temperature of 500^{o}C coupled with annealing time of 48 hours were sufficient to yield homogeneous Pd/Au alloy with the Au content of 10 wt%.

The H_2 permeances of both C_03 and C_05 were stable during the testing periods of 1000 and 450 hours respectively and the ideal selectivity were 780 at 400ºC and 350 at 450ºC, respectively. The permeance of the Pd/Au membranes was between 50 - 100% higher and the activation energies lower than those of freestanding Pd films of the same thickness at the temperatures tested. The increased permeance and lower activation energies were believed to be due to the formation of a Pd/Au alloy.

The Pd/Au membrane showed high resistance to the H_2S exposure although an almost instantaneous sharp decline of the H_2 permeance was observed. No significant morphology changes and no new phase formation were observed after the H_2S exposure in the entire testing temperature range for as long as 96 hours up to 200 ppm H_2S.

C_04, the Pd/Au alloy membrane, showed one step of sharp permeance decline and recovery was possible after the re-introduction of pure H_2. The percentages of permeance recovered in pure H_2 after the H_2S exposure and the percentages of permeance remained during the H_2S exposure were higher at higher temperatures. Longer H_2S exposure time did not increase the decline of permeance but slowed down the permeance recovery rate. The helium leak flow and activation energy for hydrogen permeation after the H_2S exposures did not increase significantly indicating only slight change of C_04 property after the loge tern H_2S exposures.

Future work

The following work is recommended:

- Further understanding of the interactions between H_2S and Pd/Cu and Pd/Au membranes and the recovery mechanism by XPS.

- Deposition of a smaller amount of Cu for new Pd/Cu membranes to ensure no β phase present on the surface.

- Variation of the Au content of Pd/Au membranes to investigate the effect of Au content on H_2 permeance and H_2S tolerance.

- Testing of Pd/Cu and Pd/Au membranes with varying H_2S concentration (in the concentration range below 50 ppm) to determine the existence of an upper bound of H_2S concentration below which the poison effect is negligible.

- Investigation of the effect of plating bath agitation on Cu deposition to fabricate a more uniform surface and to obtain optimize plating conditions.

- Investigation of the annealing process of Pd/Au alloys by High Temperature X-Ray Diffraction (HTXRD) to provide a better understanding of the membrane synthesis.

Acknowledgements

The work with XPS made use of the Shared Experimental Facilities supported by the MRSEC Program of the National Science Foundation under award number DMR 02-13282.

The work with HTXRD was sponsored by the Assistant Secretary for Energy Efficiency and Renewable Energy, Vehicle Technologies Program, as part of the High Temperature Materials Laboratory User Program, Oak Ridge National Laboratory, managed by UT-Battelle, LLC, for the U.S. Department of Energy under contact #DE-AC05-00OR22725.

A portion of the work with HTXRD was conducted at Oak Ridge National Laboratory's Center for Nanophase Materials Sciences.

References

[1] R. Bredesen, K. Jordal, and O. Bolland. High-temperature membranes in power generation with CO_2 capture. Chem. Eng. Process, 43 (2004) 1129.

[2] D.L. McKinley, W. Nitro, Metal alloy for hydrogen separation and purification, US Patent 3,350,845, 1967.

[3] M.V. Mundschau, X. Xie, C.R. Evenson, and A.F. Sammells. Dense inorganic membranes for production of hydrogen from methane and coal with carbon dioxide sequestration. Catal. Today, 118 (2006) 12.

[4] M. Kajiwara, S. Uemiya, and T. Kojima. Stability and hydrogen permeation behavior of supported platinum membranes in presence of hydrogen sulfide. Int. J. Hydrogen Energy, 24 (1999) 839.

[5] A. Kulprathipanja, G.O. Alptekin, J.L. Falconer, and J.D. Way. Pd and Pd-Cu membranes: inhibition of H_2 permeation by H_2S. J. Membr. Sci., 254 (2005) 49.

[6] S. Uemiya, N. Sato, H. Ando, Y. Kude, T. Matsuda, and E. Kikuchi. Separation of hydrogen through palladium thin film supported on a porous glass tube. J. Membr. Sci., 56 (1991) 303.

[7] B.D. Morreale, M.V. Ciocco, B.H. Howard, R.P. Killmeyer, A.V. Cugini, and R.M. Enick. Effect of hydrogen-sulfide on the hydrogen permeance of palladium-copper alloys at elevated temperatures. J. Membr. Sci., 241 (2004) 219.

[8] P.R. Subramanian, D.E. Laughlin. Cu-Pd (copper-palladium). J. Phase Equilib., 12 (1991) 231.

[9] D.L. McKinley, W. Nitro, Method for hydrogen separation and purification, US Patent 3,247,648, 1966.

[10] A.G. Knapton. Palladium alloys for hydrogen diffusion membranes. Platinum Met. Rev., 21 (1977) 44.

[11] V. Gryaznov. Metal-containing membranes for the production of ultrapure hydrogen and the recovery of hydrogen isotopes. Sep. Purif. Methods, 29 (2000) 171.

[12] Y.H. Ma, B.C. Akis, M.E. Ayturk, F. Guazzone, E.E. Engwall, and I.P. Mardilovich. Characterization of intermetallic diffusion barrier and alloy formation for Pd/Cu and Pd/Ag porous stainless steel composite membranes. Ind. Eng. Chem. Res., 43 (2004) 2936.

[13] A. Sieverts, E. Jurisch, and A. Metz. Solubility of hydrogen in the solid alloys of palladium with gold, silver and platinum. Z.Anorg.Allg.Chem.; Zeitschrift fuer Anorganische und Allgemeine Chemie, 92 (1915) 322.

[14] J.D. Way, M. Scheffler, and P. Thoen, Sulfur-resistance composite metal membranes, US Patent Application 20080038567, 2008.

[15] Y.H. Ma, P.P. Mardilovich, and Y. She, Hydrogen gas-extraction module and method of fabrication, US Patent 6,152,987, 2000.

[16] M.E. Ayturk, I.P. Mardilovich, E.E. Engwall, and Y.H. Ma. Synthesis of composite Pd-porous stainless steel (PSS) membranes with a Pd/Ag intermetallic diffusion barrier. J. Membr. Sci., 285 (2006) 385.

[17] Y.H. Ma, I.P. Mardilovich, and E.E. Engwall, Composite gas separation modules having intermediate porous metal layers, US Patent 7,175,694, 2007.

[18] P.P. Mardilovich, Y. She, Y.H. Ma, and M. Rei. Defect-free palladium membranes on porous stainless-steel support. AIChE J., 44 (1998) 310.

[19] Y.H. Ma, I.P. Mardilovich, and E.E. Engwall. Thin composite palladium and palladium/alloy membranes for hydrogen separation. Ann. N. Y. Acad. Sci., 984 (2003) 346.

[20] M.F. El-Shazly, K. Baker. High build electroless gold processes. AES Electroless Plat. Symp., 1st, 20 (1982) 23.

[21] E.A. Parker, Immersion Solutions, in F.H. Reid and W. Goldie (Ed.), Gold Plating Technology, Scotland, Electrochemical Publications Limited, 1974.

[22] Y. Okinaka, Electroless Solutions, in F.H. Reid and W. Goldie (Ed.), Gold Plating Technology, Scotland, Electrochemical Publications Limited, 1974.

[23] N. Fairbanks, A. Carrick, The Casa Cookbook, Acolyte Science, 2005.

[24] B.D. Cullity, S.R. Stock, Elements of X-ray Diffraction, New Jersey, USA, Prentice Hall, 2001.

[25] Y. Matsumoto, M. Soma, T. Onishi, and K. Tamaru. State of sulfur on the palladium surface studied by Auger electron spectroscopy, electron energy loss spectroscopy, ultraviolet photoelectron spectroscopy, and x-ray photoelectron spectroscopy. J. Chem. Soc., Faraday Trans. 1, 76 (1980) 1122.

[26] K. Endo, H. Ohno, K. Matsuda, and S. Asakura. Electrochemical and surface studies on the passivity of a dental Pd-based casting alloy in alkaline sulphide solution. Corros. Sci., 45 (2003) 1491.

[27] B.P. Chaplin, J.R. Shapley, and C.J. Werth. Regeneration of Sulfur-Fouled Bimetallic Pd-Based Catalysts. Environ. Sci. Technol., 41 (2007) 5491.

[28] C.H. Bartholomew, P.K. Agrawal, and J.R. Katzer. Sulfur poisoning of metals. Adv. Catal., 31 (1982) 135.

[29] J.R. Taylor. Phase relationships and thermodynamic properties of the palladium-sulfur system. Metall. Trans. B, 16B (1985) 143.

[30] O. Iyoha, R. Enick, R. Killmeyer, and B. Morreale. The influence of hydrogen sulfide-to-hydrogen partial pressure ratio on the sulfidization of Pd and 70 mol.% Pd-Cu membranes. J. Membr. Sci., 305 (2007) 77.

[31] J.B. Miller, B.D. Morreale, and A.J. Gellman. The effect of adsorbed sulfur on surface segregation in a polycrystalline $Pd_{70}Cu_{30}$ alloy. Surf. Sci., 602 (2008) 1819.

[32] K. Niwa, T. Yokokawa, and T. Isoya. Equilibriums in the PdS-H_2-Pd_4S-H_2S and Pd_4S-H_2-Pd-H_2S systems. Bull. Chem. Soc. Jpn., 35 (1962) 1543.

[33] J. Oudar. Sulphur-metal interactions. Mat. Sci. Eng., 42 (1980) 101.

[34] Edlund J., Pledger A. Thermolysis of hydrogen sulfide in a metal membrane reactor. Applied Catalysis A: General, 96 (1993) 110.

[35] D.L. McKinley, W. Nitro, Method for hydrogen separation and purification, US Patent 3,439,474, 1969.

[36] F. Guazzone, Engineering of substrate surface for the synthesis of ultra-thin composite palladium and palladium-copper membranes for hydrogen separation. Ph D Thesis, Worcester Polytechnic Institute, 2006.

[37] F. Guazzone, Y.H. Ma. Leak growth mechanism in composite Pd membranes prepared by the electroless deposition method. AIChE J., 54 (2008) 487.

[38] P. Kamakoti, B.D. Morreale, M.V. Ciocco, B.H. Howard, R.P. Killmeyer, A.V. Cugini, et al. Prediction of Hydrogen Flux Through Sulfur-Tolerant Binary Alloy Membranes. Science, 307 (2005) 569.

[39] A. Saini, An investigation of the cause of leak formation in palladium composite membranes, MS Thesis, Worcester Polytechnic Institute, 2006.

[40] B.D. Morreale, B.H. Howard, O. Iyoha, R.M. Enick, C. Ling, and D.S. Sholl. Experimental and computational prediction of the hydrogen transport properties of Pd_4S. Ind. Eng. Chem. Res., 46 (2007) 6313.

[41] D.R. Alfonso. First-principles study of sulfur overlayers on Pd(1 1 1) surface. Surf. Sci., 596 (2005) 229.

[42] D.R. Alfonso. Initial incorporation of sulfur into the Pd(1 1 1) surface: A theoretical study. Surf. Sci., 600 (2006) 4508.

[43] J. Barbier, E. Lamy-Pitara, P. Marecot, J.P. Boitiaux, J. Cosyns, and F. Verna. Role of sulfur in catalytic hydrogenation reactions. Adv. Catal., 37 (1990) 279.

[44] D.R. Alfonso, A.V. Cugini, and D.S. Sholl. Density functional theory studies of sulfur binding on Pd, Cu and Ag and their alloys. Surf. Sci., 546 (2003) 12.

[45] J. Barbier, P. Marecot, L. Tifouti, M. Guenin, and R. Frety. Thioresistance of supported metal catalysts: structure sensitivity of hydrogen sulfide adsorption on platinum/alumina, iridium/alumina, and platinum-iridium/alumina catalysts. Appl. Catal., 19 (1985) 375.

[46] G. Horanyi, E.M. Rizmayer. Radiotracer study of the adsorption of hydrogen sulfide by a platinized platinum electrode. J. Electroanal. Chem. Interfacial Electrochem., 206 (1986) 297.

[47] F. Guazzone, E.A. Payzant, S.A. Speakman, and Y.H. Ma. Microstrains and Stresses Analysis in Electroless Deposited Thin Pd Films. Ind. Eng. Chem. Res., 45 (2006) 8145.

[48] E.A. Mason, A.P. Malinauskas, Chemical Engineering Monographs, Vol. 17: Gas Transport in Porous Media: The Dusty-Gas Model. Amsterdam, Elsevier, 1983.

[49] O. Iyoha, R. Enick, R. Killmeyer, B. Howard, M. Ciocco, and B. Morreale. H_2 production from simulated coal syngas containing H_2S in multi-tubular Pd and 80wt% Pd-20wt% Cu membrane reactors at 1173K. J. Membr. Sci., 306 (2007) 103.

[50] N.G. Ainslie, R.E. Hoffman, and A.U. Seybolt. Sulfur segregation at α-iron grain boundaries--I. Acta Metallurgica, 8 (1960) 523.

[51] J.B. Miller, C. Matranga, and A.J. Gellman. Surface segregation in a polycrystalline $Pd_{70}Cu_{30}$ alloy hydrogen purification membrane. Surf. Sci., 602 (2008) 375.

[52] D.B. Butrymowicz, J.R. Manning, and M.E. Read. Diffusion in copper and copper alloys. Part IV. Diffusion in systems involving elements of Group VIII. J. Phys. Chem. Ref. Data, 5 (1976) 103.

[53] S. Wilke, M. Scheffler. Poisoning of Pd(100) for the dissociation of H_2: a theoretical study of co-adsorption of hydrogen and sulfur. Surf. Sci., 329 (1995) L605.